Ollscoil na hÉireann, Corcaigh

National University of Ireland, Cork

An Enhanced Angular Range Analysis workflow with multibeam backscatter for wider industrial impact and uptake of INFOMAR data

Thesis presented by

Cara Brennan, BSc. (Hons)

0009-0006-0408-6835

for the degree of

Master of Research

University College Cork

Department of Geography

Head of Department: Dr. Kieran Hickey

Supervisor(s): Dr. Aaron Lim, Dr. Gerard Summers, and Dr. Larissa Macedo Cruz de Oliveira

2025

Table of Contents

List of Figures

List of Tables

List of Abbreviations

GSI	Geological Survey Ireland
INFOMAR	Integrated Mapping for the Sustainable Development of Ireland's Marine Resource
SBES	Single-Beam Echosounder
MBES	Multi-Beam Echosounder
GEBCO	General Bathymetric Chart of the Oceans
MAREANO	Marine Areal Database for Norwegian Coasts and Sea Areas
INSS	Irish National Seabed Survey
GDG	Gavin and Doherty Geosolutions
UNCLOS	United Nations Convention on the Law of the Sea
ORE	Offshore Renewable Energy
RE	Renewable Energy
EU	European Union
GW	Gigawatt
DECC	Department of Climate, Energy and the Environment
SC-DMAP	South Coast Designated Maritime Area Plan
ADCP	Acoustic Doppler Current Profiler
SSS	Side-Scan Sonar
USBL	Ultra-short Baseline
SBL	Short Baseline
UXO	Unexploded Ordnance
AVG	Angle-Varying Gain
ARA	Angular Range Analysis

ARC	Angular Response Curve
SVM	Support Vector Machine
KNN	K-Nearest Neighbours
DT	Decision Tree
PBIA	Pixel-Based Image Analysis
OBIA	Object-Based Image Analysis
ML	Machine Learning
QTC	Quester Tangent Corporation
eARA	enhanced Angular Range Analysis
PSA	Particle Size Analysis
FMGT	Fledermaus Geocoder Toolbox
ROV	Remotely Operated Vehicle
SIS	Seafloor Information Systems
QPS	Quality Positioning Services
BPC	Beam Pattern Correction
PEM	Pratt Evaluation Metric
HD	Hausdorff Distance
JI	Jaccard Index
AR	Angular Response
iHAC	Interpolated Hyper-Angular Cube
sHAC	Synthetic Hyper-Angular Cube
BPI	Benthic Position Index
OW	Offshore Wind
MI	Machine Learning

UTM	Universal Transverse Mercator
IHO	International Hydrographic Organisation
DEM	Digital Elevation Model
BTM	Benthic Terrain Modeler
TPI	Topographic Position Index
VRM	Vector Ruggedness Measure
AOI	Area of Interest
DoD	DEM of Difference
LAT	Lowest Astronomical Tide
VORF	Vertical Offshore Reference Frame
ISS	Irish Ice Sheet
CAPEX	Capital Expenditure
OWT	Offshore Wind Turbine

Acknowledgements

Words cannot fully express my gratitude to everyone who has supported me over the past two years and beyond. Without your encouragement, guidance and kindness, this thesis would not have been possible.

To my supervisory team, Dr Aaron Lim, Dr Ger Summers, and Dr Larissa Macedo de Oliveira, words cannot express my gratitude to you all. Aaron, thank you for your time, patience, and sharing your extensive knowledge on everything marine geoscience related over the past three years. Without your support and encouragement, I would not be pursuing this masters, submitting this thesis, nor found a career I love, and for that I am forever grateful. Ger and Larissa, thank you for the countless hours you have spent, reading the roughest of drafts, replying to my emails no matter the time of day, answering my every question despite how silly they seemed, and for sharing your extensive knowledge. I have shared some amazing adventures with you that I will remember forever.

I would like to thank everyone in the Earth and Ocean Labs groups, Irene, Kevin, Corie, Bonnie, Franck, Dom and everyone in the geography research office. I couldn't have any better work colleagues or friends over the past two years to share a laugh, ideas, memorable offshore adventures, or even a rollie. I am grateful for sharing this journey with you. I would be remiss in not mentioning all of the Department of Geography staff who have never been anything but friendly and kind, especially Ray for entrusting me with your first years, providing me an opportunity to not only teach, but learn. Mary, thank you for your time with the many technical issues I have experienced along the way.

I would also like to thank all of the crew, scientists, and everyone involved in the cruises onboard the RV *Tom Crean* and RV *Celtic Explorer*, Smart Sea School, and in Belize over the past two years. Thank you for your kindness, for generously sharing your extensive knowledge and experience. I am especially grateful to Mark Coughlan for giving me to opportunity to contribute to and for bringing me on my first offshore survey, an experience I will never forget.

I would also like to thank the GSI for funding this research and giving me an opportunity to pursue something I am passionate about. Thank you to the Marine Institute and INFOMAR, and to all of the crews and people involved in providing and collecting the data used in this research, without the endless hours you have spent, this research would not have been possible. I would also like to thank Dave Hardy of the GSI who sat on the steering committee for this research, you have provided invaluable feedback which has helped this research.

I would like to express my deepest gratitude to my girlfriend Gretta, your support has been unrelentless throughout this experience. I am extremely grateful for the hours you have spent listening to me practice for conferences, supporting me when I was stressed, for always believing in me, and providing the best emotional support dog, Ted. I'm extremely grateful for all my friends, you have made this experience so much more enjoyable. Ally, your daily visits have provided a constant source of laughter, mutual abuse, and much needed therapy. Both I and Cork will miss your presence. I cannot forget my all of housemates throughout the past 24 months, Amy, Bev, Katylyn, Becca, Sophia, Emma, Kayla and Sadie, thank you. An honourable mention to Amy, Bev and Katylyn you've been there since the start, thank you for being my practice audience, your keen interest in the "backsplatter", and making Bandon Road a better place.

Finally, to my family, especially my parents Noel and Teresa, Pat, my brother Sean, and my grandparents, John and Peggy. Mam, not only have you supported me over the past two years but the twenty-two prior to that, you have always been there for me no matter what I needed, and I will never be able to repay you, thank you. To my brother Sean, thank you for your unwavering support, proof-reading my work and for always showing an genuine interest in my research.

Thank you,
Cara

Declaration

This is to certify that the work I am submitting is my own and has not been submitted for another degree, either at University College Cork or elsewhere. All external references and sources are clearly acknowledged and identified within the contents. I have read and understood the regulations of University College Cork concerning plagiarism.

Signed

Cara Brennan, author

Signed

Dr. Aaron Lim,

Dr. Gerard Summers and Dr. Larissa Macedo Cruz de Oliveira

Abstract

The climate crisis, EU energy targets, along with the need for energy security are driving increased demand for renewable energy (RE). Given the constraints associated with onshore RE, there has been a push for offshore renewable energy (ORE), leading to intense geophysical and geotechnical investigations in marine environments. In Ireland, at the forefront of this is the South Coast Designated Maritime Area Plan (SC-DMAP), which proposes four ORE sites off Ireland's south coast as part of a plan-led marine spatial planning approach.

The demand for subsea infrastructure highlights the need for accurate, repeated seabed characterisation. Initiatives such as Seabed 2030 and national mapping programmes such as INFOMAR (Ireland) and MAREANO (Norway) have given way to vast quantities of data. Yet, freely available INFOMAR datasets for ORE development remain underutilised. Moreover, existing seabed characterisation methodologies are often fragmented, bespoke, and time-consuming, thereby underlining the need for scalable, repeatable approaches to support large-scale mapping programmes.

Acoustic backscatter strength plays a crucial role in seabed characterisation, as backscatter intensity varies, in part due to sediment composition, enabling grain size estimations from acoustic returns. Traditionally, image-based backscatter processing has dominated seabed characterisation workflows. Signal-based approaches such as Angular Range Analysis (ARA) are gaining traction due to their robust characterisation. However, the latter is constrained by its low spatial accuracy, hindering its widespread use. While various attempts have been made to address this, many remain complex, resource-intensive and lack scalability. Therefore, requiring methods that are efficient, adaptable, and applicable under varying conditions.

Moreover, a holistic understanding of seabed conditions in the Irish portion of the Celtic Sea is required to de-risk ORE development in the region, yet research on seabed dynamics, bedform mobility and seabed stability, in the context of ORE in this region, remain limited.

Firstly, I aim to develop a more spatially comprehensive workflow for grain-size estimation utilising ARA. To address this, the high spatial accuracy of multibeam backscatter data is integrated with the high-fidelity sediment characterisation derived from ARA, through object-based image analysis (OBIA), to derive enhanced Angular Range Analysis (eARA). Applied to four sites with ranging depths, operating frequencies, sonars, and varying environments offshore Ireland, utilising freely available INFOMAR data. I investigate the influence of various geophysical characteristics, sediment sedimentological parameters and sediment sampling strategies to understand the influence of these parameters on the error of our grain size estimation.

Secondly, building upon the previous aim, I aim to investigate the seabed dynamics and geological constraints at the proposed Tonn Nua ORE site and evaluate the implications for ORE. To address this, the latter methodology is applied to Tonn Nua, a proposed ORE site in the SC-DAMP. Here, high-resolution, time-lapse bathymetry datasets, grain size information via eARA and various theoretical formulae are employed to understand the spatio-temporal seabed change and investigate the hydrodynamics within Tonn Nua.

Results addressing the first aim indicate strong correlations between observed and estimated grain size (Spearman's ρ up to 0.75, $p<0.01$), overall accuracies up to 96.15% ($k=0.84$) and improved spatial accuracies compared to traditional ARA.

Results addressing the second objective indicate that at the Tonn Nua Site, sandwaves are relatively stable, migrating at an average of 0.25 and 0.26 m yr^{-1}, between 2007 - 2024 and 2013 - 2024, respectively. Additionally, results demonstrate an average residual current of 41 cm s^{-1}, flowing NE - SW, is consistent with legacy measurements and bedform derived estimates. Moreover, providing evidence of mobile sediment, seabed scour, sandwaves and potential bedrock outcrops, that may influence ORE development.

Overall the results presented in this thesis, demonstrate the capacity of eARA as a robust and spatially accurate sediment grain-size estimator, therebyproviding a scalable and low-cost seafloor characterization approach, applicable to large-scale governmentalprogrammes such as INFOMAR and MAREANO. By applying this methodology to a proposed ORE site, this research further illustrates the applicability of this methodology to ORE development, acting as a preliminary assessment of sediment grain size, seabed dynamics, and seabed stability. The constraints identified in this research at the Tonn Nua site provide critical baseline information to ensure the safe development and longevity of offshore subsea structures at this site.

Chapter 1: Introduction

1.1 Development of Offshore Renewable Energy in Ireland

The future of global energy sources has been questioned as a result of the growing urgency of climate change issues, along with the need for economic stability and energy security (Hassan et al., 2024). Renewable energy by means of solar, hydro, geothermal, biomass, and wind is pivotal to address these challenges (Hassan et al., 2024). In terms of wind power, the development of onshore wind is constrained by factors including a lack of suitable locations (Martinez and Iglesias, 2022). Despite Ireland's vast resource of offshore renewable energy (ORE) (Dinh et al., 2021), it is failing to capitalise on its ORE resources (Cummins and McKeogh, 2020). Consequently, resulting in a failure to meet European Union (EU) energy targets, which are the main drivers behind the development of both offshore and onshore wind energy (Cummins and McKeogh, 2020). The Irish government has proposed a centralised plan-led approach to deliver 5 gigawatts (GW) of offshore wind capacity by 2030 and 37 GW by 2050 (Cummins and McKeogh, 2020; DECC, 2024; Esmaeili et al., 2024). Consequently, the South Coast Designated Maritime Area Plan (SC-DMAP) has been announced, identifying four key potential ORE maritime areas off the southeast coast of Ireland (DECC, 2024). Therefore, reliable high-resolution marine data is an essential prerequisite to provide essential knowledge on the marine environment, thereby identifying potential geohazards and constraints to the development of ORE. Subsequently, datasets acquired by the Integrated Mapping for the Sustainable Development of Ireland's Marine Resource (INFOMAR) programme offer a preliminary source of information regarding potential ORE sites in Ireland and to provide initial seabed assessments, accordingly, reducing costs for future ORE developments and aiding the site selection process.

1.2 Seabed Mapping

The world's oceans cover 71% of the earth's surface (Wölfl et al., 2019), and despite years of mapping efforts, at present, only 27.3% of the world's ocean floor has been mapped, according to Seabed 2030 ("Seabed 2030 announces millions of square kilometers of new seafloor data on World Hydrography Day," 2025). It is therefore acknowledged that our understanding of the seafloor is relatively limited (Mayer et al., 2018a). To address this, the General Bathymetric Chart of the Oceans (GEBCO) and the Nippon Foundation launched the Seabed 2030 Project, aiming to map the entirety of the world's ocean floor by 2030 (Jakobsson et al., 2020; Mayer et al., 2018a). Concurrently, the Decade of Ocean Science for Sustainable Development (2021–2030) was announced in 2017, emphasizing the need for ocean observation and research, promoting sustainable ocean management (Wölfl et al., 2019). Along with global mapping initiatives, regional and national mapping initiatives have progressed our understanding of the seafloor, such as the Florida Seafloor Mapping Initiative, Norway's Marine Areal Database for Norwegian Coasts and Sea Areas (MAREANO), and INFOMAR. The latter, combined with its predecessor, the Irish National Seabed Survey (INSS), has almost mapped the entirety of Ireland's 700,000 km^2 maritime area since 2000, creating a vast database of over 20-years' worth of hydrographic and geophysical data (O'Toole et al., 2022). The utilisation of publicly available INFOMAR datasets has the potential to considerably reduce marine traffic, reduce noise in the marine environment, and limit the known effects that geophysical surveys have on marine mammals (Hildebrand, 2004). Thereby, reducing the carbon footprint associated with the acquisition of marine datasets. Despite the advantageous nature of the INFOMAR database, many restrictions hinder the widespread industrial use of this vast wealth of data, which was highlighted by Peters et al. (2019) and Gavin & Doherty Geosolutions (GDG) (2021). GDG (2021) identified issues related to the resolution and overlap of MBES datasets, particularly in the context of sediment mobility assessments and for later phases of ORE developments. This issue is further exacerbated by an ineffective use of publicly available data obtained by the INFOMAR programme.

As for the question of why we map the seafloor, it is well recognised that knowledge of the seafloor through acoustic seabed mapping is important for a wide range of applications as highlighted in Wölfl et al. (2019), such as safety of navigation; establishing limits of the extended continental shelf under the United Nations Convention on Law of the Sea (UNCLOS) for military and defence applications; marine conservation; locating wreckages (e.g. flight MH370); development of offshore infrastructure; and marine geohazards.

1.3 Acoustic Seabed Mapping Techniques

Marine remote sensing plays a crucial role as it aids our understanding of the marine environment (Huang et al., 2013) in a less intrusive, more efficient and cost-effective manner than of geotechnical surveying (Brown et al., 2011). *In situ* technologies offer an efficient localised description of the seafloor, yet have limited coverage, compared to acoustic remote sensing techniques (Schimel et al., 2010). Marine remote sensing is typically carried out through shipborne or towed acoustic systems, typically with side-scan sonar (SSS), SBES and MBES (Schimel et al., 2010), along with emerging technologies such as interferometric synthetic aperture sonar (InSAS). While, SBESs comprise of a single acoustic beam and offer a relatively cost-effective method for seabed mapping. However, SBESs offer limited coverage compared to MBES, ensonifying only a limited area of the seafloor (Landero Figueroa et al., 2021). Whereas, MBES cover a wide swath area and the ability to acquire high-resolution datasets (Landero Figueroa et al., 2021). The principles of both echosounders remain relatively similar; however, unlike traditional SBES, MBESs gather multiple soundings across the ship's track simultaneously, forming multiple orthogonal beams in a fan-like configuration, collecting oblique soundings, compared to downward (Beaudoin, 2010). A series of transmit and receive beams are formed in the transducer hardware, measuring the depth of the seafloor in discrete angular increments across the swath (Hughes Clarke et al., 1996; Hopkins, 2007). Various operating frequencies are used for MBES system, depending on seafloor depth, low frequencies are used for deeper waters (e.g., 12 kHz for up to 10,000 m deep in some cases), while higher frequencies are used for shallower waters (Hopkins, 2007).

1.4 Multibeam Backscatter

Multibeam Echosounders offer a cost-effective technique to accurately map the seafloor and are capable of mapping vast areas at high resolutions while providing bathymetric and backscatter data (Hamilton and Parnum, 2011). Thus, this potential has been widely exploited for a variety of purposes from benthic habitat mapping (McGonigle et al., 2009; Hossain, 2019); bedform migration analysis (Van Dijk and Kleinhans, 2005; Van Landeghem et al., 2012; Creane et al., 2022); sediment distribution mapping (Fonseca et al., 2009; Santos et al., 2018); and geohazard/constraint mapping (Schneider Von Deimling et al., 2013; Casas et al., 2016; Downing et al., 2025).

In recent years, there has been a growing interest within the research community in the development of novel methods to remotely characterise seabed properties using MBES backscatter data (Lucieer et al., 2018). Backscatter intensity is a measure of the acoustic energy that is returned toward the transmitter by acoustic reflection and scattering, from within the sediment known as volume scattering and at the sediment water interface (Jackson et al. 1986; Goff et al. 2004; Ferrini and Flood 2006; De Falco et al. 2010). Backscatter intensity is dependent on the acoustic frequency, angle of incidence and seabed composition (Jackson and Richardson, 2007; Gaida et al., 2018). As mentioned by Gaida et al.(2018), the dependence of backscatter strength on acoustic frequency arises from three primary factors: (i) the interaction between seabed roughness and the acoustic wavelength, (ii) the dominant scattering regime, which depends in particle size and acoustic wavelength (i.e. Rayleigh, geometric or transitional), and (iii) volume scattering, which depends on signal penetration into the seabed. In terms of scattering regime, this is in part due to the relationship between grain size and acoustic wavelength.

When sediment grain sizes are smaller or in the same magnitude as the acoustic wavelength, backscattering strength is typically well understood, and backscatter strength increases with increasing grain size (Eleftherakis et al., 2014). However, when the grain size exceeds the acoustic wavelength, this is not the case (Eleftherakis et al., 2014). Instead, with increased acoustic frequency, the sediment cannot be described as a continuous medium, thereby individual grains are considered discrete scatterers (Gaida et al., 2019b). In the Rayleigh scattering regime, this can be described as when the roughness elements (e.g., grain size) are smaller than the acoustic wavelength (Buscombe et al., 2017), whereas in the Geometric regime, the roughness elements are larger than the acoustic wavelength. Transitional scattering regimes may occur in heterogeneous beds comprised of mixed materials (such as silt, sand, gravels and boulders), thereby scattering is transitional between regimes (Buscombe et al., 2014) and is difficult to differentiate. For example, Urick, (1983) demonstrated that at 400 kHz with an acoustic wavelength of 3 mm, fine sediments such as mud and sand will fall within the Rayleigh scattering regime and produce weak incoherent echoes, whereas coarser sediments such as gravel and rock lie within the geometric regime, producing strong coherent echoes. Consequently, as mentioned by Buscombe et al.,(2014), frequency dependent scattering behaviour can be exploited for acoustic sediment classification. Several studies in both field (e.g. (Jackson et al., 1986a; Gaida et al., 2018; Brown et al., 2019)) and tank (e.g. (Ivakin and Sessarego, 2007)) environments have demonstrated the frequency dependent aspect of backscatter intensity, with finer sediments often displaying a higher sensitivity to varying frequency than coarser sediments (Gaida et al., 2018).

Additionally, a lack of standardisation between backscatter data is prevalent with inconsistencies in data acquisition, processing and classification, especially driven by differences between MBES systems produced by different manufacturers, introducing ambiguity to these data highlighted in 2015 by the Backscatter Working Group (Lamarche and Lurton, 2018). Angle-varying gain (AVG) corrections are applied to the backscatter intensity data, removing their angular dependence in order to normalise the backscatter intensity and produce backscatter mosaics (Huang et al., 2013; Lamarche and Lurton, 2018; Misiuk and Brown, 2022). The latter removes an intrinsic property of the seafloor, hindering the robust characterisation of seafloor sediments (Misiuk and Brown, 2022). Consequently, resulting in user bias as the backscatter normalization is not an accurate representation of the distribution of backscatter intensity across an area (Huang et al., 2013). Moreover, this issue can be solved with the effective use of automated classification of the data based on the backscatter signal, mitigating user bias. While image-based backscatter processing methods have previously dominated in the literature, signal-based approaches such as angular range analysis (ARA) are becoming increasingly available due to their consistent and robust sediment classification (Hughes Clarke, 1994a; Rzhanov et al., 2012).

The variation of backscatter strength as a result of grazing angleis an inherent seafloor property (Fonseca and Mayer, 2007). This information is lost during traditional backscatter processing, as a result of AVG normalisation to produce a backscatter mosaic to show a consistent grey level for the same type of seafloor regardless of the angle of insonification (Fonseca and Mayer, 2007). Therefore, ARA preserves both the angular response (AR) and uses the entire backscatter time-series (Fonseca and Mayer, 2007). ARA, originally developed at the University of New Hampshire at the Centre for Coastal and Ocean Mapping, based on and similar to amplitude-versus-offset (AVO) analysis, a seismic reflection method used in the oil and gas industry (Fonseca et al., 2005). A set of thirty consecutive acoustic pulses are stacked into two distinct seafloor patches, either side of the swath (port and starboard), reducing speckle noise (Fonseca et al., 2005; Fonseca and Mayer, 2007), although limited to half the swatch of the sonar. The stacked backscatter response is divided into discrete angular regimes; near (with incident angles of 65° to 90°), far (35° to 65°) and the outer ranges (5° to 35°) (Fonseca et al., 2005; Fonseca and Mayer, 2007). Seabed properties are determined by the inversion based on a composite roughness model (Jackson et al., 1986b), originally developed for operating frequencies of <100 kHz. The inversion of the model is done by iteratively adjusting the model to the observed angular response curve (ARC), constrained by the equations published by Hamilton (1974). Moreover, given the constraint of spatial resolution, limited to half the swath of the sonar, heterogeneous bottom types may not be accurately characterised (Rzhanov et al., 2012). Therefore, ARA should be conducted in homogeneous areas of seafloor (Alevizos and Greinert, 2018). Nonetheless, several studies have successfully applied ARA despite spatial resolution and operating frequency constraints. For instance, ARA has been applied to data acquired at operating frequencies >100 kHz (Fonseca et al., 2005; McGonigle and Collier, 2014a; Alevizos and Greinert, 2018; Santos et al., 2018) and in heterogeneous, highly dynamic environments (Santos et al., 2018). In addition, several studies have endeavoured to overcome these limitations, Fonseca et al. (2009) proposing to aggregate sounds by homogeneous seabed types; Che Hasan et al. (2012, 2014) built on this approach through the segmentation of the backscatter mosaic into image-objects, which were used as a framework to group soundings; Parnum (2007) prosed to derive an “angular cube” interpolating discrete incidence angles; Huang et al. (2014) proposing to achieve this through producing multiple backscatter mosaics using different angles for the AVG correction; and Alevizos and Greinert (2018), who compared both approaches.

1.5 Automated Classification Techniques

The development of objective and repeatable methods of acoustic data interpretation lags behind our ability to collect high-quality acoustic data (Diesing et al., 2014). As volumes of data increase, there is an urgent need for standardised, repeatable and scalable methods that can only be replicated by automated methods (Ierodiaconou et al., 2018a). Recently, automated methods are becoming increasingly common in comparison to manual approaches, given their ability to extract information in a more subjective, time and cost-efficient, and repeatable manner than that of manual interpretation (Ierodiaconou et al., 2018a). As mentioned by Diesing et al. (2016), classification approaches can be grouped in a variety of ways. Lu and Weng (2007) group classification approaches by i) supervised or unsupervised, ii) parametric or non-parametric, iii) hard or soft, and iv) unit of analysis (e.g., pixel, sub-pixel or image-object). Considering class i), unsupervised methods attempt to find regularities in unclassified data, usually involving clustering the data into a predefined number of groups. However, a common issue is determining the optimum number of groups (Stephens and Diesing, 2014). Unsupervised techniques have been used for seabed characterisation and benthic habitat mapping, such as ISODATA (Li et al., 2017) and k-means (Diesing et al., 2020; McGonigle et al., 2009). Supervised techniques are algorithms that learn to extract patterns from datasets to predict a class (Stephens and Diesing, 2014). Supervised techniques have been utilised for seabed characterisation and benthic habitat mapping and include models such as random forest (Hasan et al., 2012; Diesing et al., 2014; Stephens and Diesing, 2014; Diesing et al., 2020); support vector machine (SVM) (Diesing and Stephens, 2015a; Hasan et al., 2012), K-nearest neighbour (KNN)(Diesing and Stephens, 2015b); and decision tree (DT) (Che Hasan et al., 2012). Moreover, classifications can also be defined using the basic unit of analysis.

Two broad approaches are commonly used for supervised or unsupervised classification of acoustic data, pixel-based image analysis (PBIA) classification and object-based image analysis (OBIA). Several studies have compared both approaches individually or combined. Ierodiaconou et al. (2018) compared PBIA and OBIA based approaches for benthic habitat mapping, with a combination of both approaches offering the best results, and OBIA approaches displaying higher accuracies than PBIA. Stone et al. (2024)

compared both approaches for mapping coral reefs, with PBIA approaches offering superior results, albeit using drone datasets. Diesing et al. (2020) compared five methods for predicting substrate classes, with all methods producing relatively similar results. Diesing et al. (2014) compared several methods of mapping seabed sediments using manual, geostatistical, OBIA and machine learning (ML) approaches. However, the latter reported no statistically significant differences between the approaches, therefore not singling out a "best performing" method.

Traditionally, PBIA classification approaches have been used in marine remote sensing research. However, these methods are poorly suited to the high-resolution datasets (metre to sub-centimetre resolution) provided by acoustic remote sensing technologies (Castilla and Hay, 2008). Moreover, with increased resolution, the pixel may be smaller than the feature of interest (Blaschke et al., 2014). Therefore, incorporating whole features rather than individual pixels in isolation is advantageous in terms of class discrimination when classifying data at these finer resolutions (Ierodiaconou et al., 2018a). In addition, PBIA approaches are more susceptible to "salt and pepper" artefacts which lead to misclassification, resulting in errors in the classification (Che Hasan et al., 2012; Ierodiaconou et al., 2018a).

Contrastingly, the OBIA approach groups together homogeneous pixels, based on spatial and spectral properties, into meaningful image-objects, maximising the between-object heterogeneity and the intra-object homogeneity (Blaschke, 2010). Thus, the basic unit of analysis is image-objects rather than individual pixels (Castilla and Hay, 2008; Blaschke, 2010). OBIA also offers many advantages compared to PBIA approaches, including the ability to calculate summary statistics for each segment (Ierodiaconou et al., 2018a); image-objects are inherently linked to specific scales of features in the environment (Phinn et al., 2012); image-objects also provide an opportunity to extract additional information, providing ancillary information of seafloor properties (Ierodiaconou et al., 2018a); and reduce common backscatter artefacts such as speckle and nadir noise (Ierodiaconou et al., 2018a). This method of classification has been successfully applied in marine habitat mapping (Ierodiaconou et al., 2018a); mapping of cold water corals (Conti et al., 2019); geomorphological classifications (Summers et al., 2021, 2022, 2023); and seabed characterisation (Diesing et al., 2014; Janowski et al., 2018; Diesing et al., 2020). OBIA consists of two main steps, segmentation and classification, with the former being the most critical step (Blaschke, 2010; Hossain and Chen, 2019). Manual segmentation techniques are often time-consuming, constrained by user bias, unstandardised, and unfeasible for large-scale mapping. Therefore, automatic segmentation algorithms offer a solution to these issues and are becoming increasingly common in marine research. A review by Hossain and Chen (2019) summarised different segmentation algorithms, segmentation parameters and software, highlighting the challenges and benefits of each. However, many of these segmentation techniques require trial and error to iteratively select parameters to find an idealised segmentation, as they can result in under- or over-segmentation (Che Hasan et al., 2012).

Two algorithms have been commonly used in previous marine OBIA studies, multi-resolution segmentation (Benz et al., 2004) and mean-shift segmentation (Comaniciu and Meer, 2002). The latter algorithm was successfully employed by Che Hasan et al. (2012) to group pixels with similar characteristics in backscatter imagery. Mean shift segmentation is based on non-parametric feature space analysis, using a kernel density estimation (Comaniciu and Meer, 2002). This algorithm requires adjustment of three parameters, spectral detail (based on attribute values), spatial detail (weighting based on proximity), and minimum segment size (Misiuk and Brown, 2022) to ensure correct delineation of acoustic facies.

1.6 Marine Geohazards and Constraints

Marine geohazards or constraints can result from both natural and anthropogenic factors. Keer and Cardinell (1981) described geohazards as higher risk features, as their potential for damage cannot be eliminated, whereas constraints were considered lower risk as their impact can be mitigated or prevented by engineering solutions. Marine geohazards and constraints pose a threat to several offshore industries, particularly for engineering design, planning, and installation of offshore infrastructure (Camargo et al., 2019). When identifying marine geohazards and constraints, both the seafloor surface and subsurface must be considered (Camargo et al., 2019). However, for the purpose of this review, only hazards or constraints that occur on the seafloor surface are considered. Several examples of natural seafloor surface geohazards and constraints include seabed scour, sandwaves and migrating bedforms, mobile sediments, and bedrock outcrops.

Although migrating bedforms, active sandwaves and mobile sediments have often been considered as geohazards due to their potential threat to offshore infrastructure (Jiang et al., 2023; Kopp et al., 2021), this review refers to all potential geohazards and constraints collectively as constraints, given the varying terminology used in literature. Seabed scour is a naturally occurring phenomenon, resulting from the presence of natural features such as bedrock or anthropogenic obstacles such as pilings, foundations and shipwrecks (Quinn and Smyth, 2018). When an object such as wind energy foundations are installed on the seafloor, this increases the hydrodynamic field locally, increasing sediment transport and erosion processes (Whitehouse et al., 2011). This results in a well-established engineering concern as it may compromise the structural stability of the installation (Whitehouse et al., 2011). Sandwaves are transverse seabed bedforms, forming perpendicular to the prevailing current direction under current velocities of 0.3 to 0.75 m s^{-1} (Stow et al., 2009). The growth and migration of these features present hazards to navigation (Ashley, 1990); influence the bed design level of a structure (Whitehouse et al., 2000); undermine foundations; expose pipelines or cables, increasing the risk of damage and free-spanning in cables or pipelines (Németh et al., 2002); or, in contrast may lead to the overburial of cables or pipelines (Besio et al., 2003; Camargo et al., 2019; Emeana et al., 2016; Whitehouse et al., 2000). The presence of sandwaves may also be indicative of the presence of mobile sediment (Whitehouse et al., 2000), which may also lead to scour (Whitehouse et al., 2011). In addition, bedrock outcrops and variable bedrock levels pose a viable threat to the development of offshore infrastructure such as demonstrated at the Celtic Array project, which was subsequently cancelled (Coughlan et al., 2020a), as exposed bedrock forms a surface that is difficult to pile (Mellett et al., 2015). Therefore, a comprehensive understanding of sediments, bedform migration patterns, and the position and variable level of bedrock outcrop is critical to the development of ORE (Mellett et al., 2015).

1.7 Seabed stability and Seabed dynamics

Increased marine economic activities such as offshore renewables and the blue economy underline the need for a comprehensive understanding of sediment dynamics and the mechanisms responsible (Auguste et al., 2021). Bedload transport via bedform migration can occur under mean, wave current, or combined wave current conditions (Coughlan et al., 2021; Lichtman et al., 2018). The distribution of sediment along continental shelves reflects the balance between the supply of sediment and the reworking of sediments over millennia by the prevailing hydrodynamic regime (Whitehouse et al., 2011). Seabed erosion and sediment transport, including the movement of bedforms, occur over various timescales from weeks to decades and are driven by variations in tidal range, currents, storm surges and wave action (Whitehouse et al., 2011). This usually results in sediment eroding from the stoss side and deposited on the lee side of bedforms, resulting in migration in the direction of the prevailing hydrodynamic forcing (Lichtman et al., 2018). Although several studies have alluded to a phenomenon such as reversed migration or counter-current migration, where bedforms migrate in an atypical migration direction (Boggild et al., 2024; Van Landeghem et al., 2012).

It is well established that the impact that bottom or contour currents in shaping the seafloor (Stow et al., 2009; Frey et al., 2022), acting as a key factor in sedimentation processes (Rebesco et al., 2014; Frey et al., 2022). Therefore, understanding near-bed currents is essential to characterise the hydrodynamic regime. Erosional and depositional bedforms can elucidate to strength, variability, continuity and flow direction of bottom currents (Belderson et al., 1982; Kenyon and Belderson, 1973; Stow et al., 2009). Bottom current velocities can be estimated through hydrodynamic modelling (Li et al., 2015; Frey et al., 2022); empirical formulae (Soulsby et al., 1997); and bedform velocity matrices (Belderson et al., 1982; Stow et al., 2009); or through direct measurements such as from acoustic doppler current profiles (ADCP) (Lim et al., 2020) and current meters (Howe et al., 2006; Huvenne et al., 2009). Empirical formulae, such as those proposed by Soulsby et al., (1997), use grain size to estimate current velocity 1 m from the seabed (equation 1). This method to estimate current speeds has been utilised by Lim et al. (2018) to investigate coral mound development and Huvenne et al. (2009) to understand the sediment dynamics of a sandy contourite.

$$\mathcal{U}_{100\,\text{erosion}} = \left(\frac{u_{*cr}}{0.41}\right) \ln\left(\frac{z_{100}}{z_0}\right), \text{ where} \quad (1)$$

z_{100}= level above seabed (1 m)

d = grain diameter = mean grain size

u_{*cr}= critical shear velocity = $\sqrt{\frac{\tau_{cr}}{\rho}}$, where (1.1)

τ_{cr}= threshold bed shear stress (N/m^2)= $g(\rho_s - \rho)\, d\left(\frac{0.30}{1+1.2D_*} + 0.055[1 - \exp(-0.020D_*)]\right)$, where (1.2)

ρ = water density = 1027.4 kg/m^3

ρ_s = grain desnity = 2650 kg/ m^3 (quartz)

D_* = dimensionless grain size = $\left[\frac{g(\rho_s-\rho)}{\rho v^2}\right]^{\frac{1}{3}} d$, where (1.3)

v = kinematic viscosity if water

In addition, threshold bed shear stress can be calculated from the latter equation. For non-cohesive sediments, sediment mobilisation occurs when bed shear stress exceeds threshold bed stress (Coughlan et al., 2021; Hodge et al., 2024). Bed shear stress is defined as the frictional force exerted by the flow per unit of bed, acting as the main hydrodynamic parameter that controls erosion, suspension and deposition (Soulsby and Clarke, 2005). As outlined in Yang et al. (2022), bed shear stress can be calculated by a quadratic equation proposed by Huntley et al. (1994) (equation 2).

$\tau = \rho C_D U_{C100}^2$, where (2)

ρ = water density = 1027.4 kg/m^3

C_D = drag coefficient = 2x10^{-3}

U_{c100} = current speed at 1 m above the seabed (derived from equation 1)

A number of studies have established seabed stability, hydrodynamic and sediment transport pathways in the Irish Sea, specifically with relevance to the development of ORE. Creane et al. (2023) utilised two-dimensional hydrodynamic modelling to investigate the sediment transport regime and identify vulnerabilities on Arklow Bank, in the Irish Sea. Creane et al. (2022) used time-lapse bathymetry and hydrodynamic modelling to assess the development and dynamics of sediment waves in the Southern Irish Sea. Van Landeghem et al. (2012) employed time-lapse bathymetry to evaluate sediment wave migration and map net sediment transport direction in a portion of the Irish Sea. On a regional scale, Coughlan et al. (2021) quantified seabed mobility in the Irish Sea through hydrodynamic and wave modelling coupled with extensive grab sampling. The northern Irish Shelf has also been extensively studied via time-lapse datasets to assess bedform mobility and the hydrodynamic regime (Evans, 2018). In addition, large-scale national studies such as Peters et al. (2020) have produced geological stability models further supporting ORE development.

1.8 Rationale

Firstly, given the extensive coverage of INFOMAR data, encompassing almost 200 million acres of Ireland's marine territory, these datasets remain underutilised. To fully capitalise on their value, novel techniques are required. Offshore geophysical surveys are constrained by high costs, time demands, and well-established environmental impacts. Therefore, national programmes with existing multibeam datasets play a vital role in supporting offshore development (Guinan et al., 2021).

Seabed classification is inherently complex, requiring a range of approaches. Consequently, INFOMAR must employ a range of seabed characterisation approaches, including Quester Tangent Corporation (QTC) Multiview, OBIA, and manual interpretation techniques (Guinan et al., 2021). The latter of which is not feasible for large-scale databases, as it is subjective, labour-intensive, and not repeatable (Ierodiaconou et al., 2018a). To ensure reliability and repeatability, data processing methodologies must be harmonised and standardised across surveys for effective decision-making (Guinan et al., 2021).

At present, seabed characterisation methodologies are fragmented and often different on a site-to-site basis, as methods do not always transfer across different environments (Diesing et al., 2020). Repeatable processing techniques are therefore needed to enable standardised outputs across surveys (Summers et al., 2023). Such methods must be robust across diverse conditions, including varying environments, operating frequencies, legacy and modern sonars, different survey vessels, and a range of water depths, in order to upscale these methods.

Secondly, whilst ARA provides a robust sediment classification, its limited spatial accuracy restricts its widespread application. Numerous studies have attempted to address these limitations. Fonseca et al. (2009) proposing to aggregate sounds by homogeneous substrate types; Che Hasan et al. (2012, 2014) built on this approach through the segmentation of the backscatter mosaic into image-objects, which were used as a framework to group soundings; Parnum (2007) prosed to derive an "angular cube" interpolating discrete incidence angles; Huang et al. (2014) proposing to achieve this through producing multiple backscatter mosaics using different angles for the AVG correction; and Alevizos and Greinert (2018), who compared both approaches.

Despite these efforts, no singular solution has been widely adopted. Many approaches remain time-consuming, bespoke, and difficult to implement; thus, inferring the need for scalable methods that can be applied across the INFOMAR database. Future solutions must be compatible with diverse sensors, water depths, and environments to support large-scale mapping programmes.

Thirdly, OBIA provides an opportunity to extract additional information into image-objects (Ierodiaconou et al., 2018a). While grain size data are typically limited to point locations, recent advancements such as ARA (Fonseca et al., 2009; Fonseca and Mayer, 2007b) provide more spatially comprehensive grain size estimates. Incorporating ARA derived mean grain size enables the calculation of seabed stability and hydrodynamic parameters such as critical current velocity erosional thresholds, threshold bed shear stress, and bed shear stress for each segment across an area, thereby strengthening the value information in the segments.

Lastly, in contrast to studies in the Irish Sea (Van Landeghem et al., 2012; Coughlan et al., 2020a, 2021; Creane et al., 2022, 2023), the Northern Irish Shelf (Evans, 2018), and broader national-scale studies (Peters et al., 2020), the Northern Celtic Sea lacks research integrating time-lapse bathymetry, hydrodynamic modelling and seabed stability analysis, particularly in the context of ORE development. Previous studies in the Celtic Sea have largely focused on subsurface geology, focusing on Quaternary reconstruction linked to the Irish Ice Sheet dynamics (Giglio et al., 2022a; Tóth et al., 2020), subglacial hydrology (Giglio et al., 2022b), past glacial processes (Gallagher, 2002), and deglacial dynamics. Consequently, a clear knowledge gap remains regarding surface geological conditions and marine hydrodynamics in the Irish portion of the Celtic Sea, specifically in relation to ORE development. Moreover, on a national scale, Arosio et al. (2023b) have mapped Ireland's seabed geomorphology utilising semi-automated classification techniques, INFOMAR's vast MBES database, and validation via INFOMAR sediment samples and sub-bottom datasets. While the latter utilised ground truth and sub-bottom datasets to aid the interpretation of geomorphological features, this thesis can complement this work, providing more spatially comprehensive grain size information than that can be derived from INFOMAR sediment samples. Given the importance of sediment composition, playing a major component in seabed morphology, this research can provide valuable insights into Ireland's seabed geomorphology.

1.9 Aims and Objectives

The main aims of this MSc thesis are to enhance traditional ARA methods for sediment distribution mapping, with a specific focus on their scalability to large-scale mapping programmes such as INFOMAR or MAREANO. In addition, this project seeks to demonstrate the effectiveness of these techniques in the context of ORE development, where resulting segments can provide valuable supplementary information. Accordingly, this thesis aims to address the following aims and objectives:

i. Advance existing ARA methodologies by developing an enhanced Angular Range Analysis (eARA) approach, with the aim of improving spatial accuracy and assessing its scalability for large-scale seabed mapping programmes;

ii. Evaluate the influence of sediment sedimentological parameters and sediment sampling strategies on the accuracy of eARA;

iii. Develop a workflow for utilising eARA derived grain size to provide supplementary information in eARA segments to support the development of offshore infrastructure;
iv. Assess the seabed dynamics and geological constraints at the proposed Tonn Nua ORE site to evaluate their implications for ORE development.

Chapter 1 presents the fundamental concepts that this thesis is based on, outlining research to date on this topic. Firstly, it provides an overview of the ORE development in Ireland, an outline of the importance of seabed mapping, and acoustic seabed mapping techniques. It then outlines current automated classification techniques, inherent gaps in literature and research, and how this present research intends to fill these gaps. Finally, presenting the overall aims and objectives for this research.

Chapter 2 "Enhanced Angular Range Analysis: A Novel Object-based Image Analysis Approach for Seafloor Characterisation" develops a novel seabed characterization approach, with upscaling potential to large-scale mapping databases. To achieve this, I integrate ARA and OBIA to develop enhanced angular range analysis (eARA), providing a more spatially accurate seabed characterization technique, applied to four sites offshore Ireland in diverse conditions such as different environments, ranging water-depths, legacy to modern sonars, ranging vessels and operating frequencies. Therefore, this chapter aims to address the following aims and objectives:

i. Determine the segmentation and classification accuracy of eARA; and rank it in comparison to alternative methods;
ii. Determine the method's effectiveness in relation to geophysical parameters (depth and operating frequency);
iii. Evaluate the limitations imposed by sedimentological properties (modality and sorting) and sediment sampling strategies (instrument; and temporal offset between acoustic and sediment sampling survey) on eARA's accuracy; and

iv. Assess the broader implications, required resources, and propose steps for upscaling this workflow across national programmes.

Chapter 3 "Seabed Dynamics and Geological Constraint Mapping for Offshore Renewable Energy Development at Tonn Nua, North Celtic Sea, NE Atlantic" builds on Chapter 2, to apply eARA to Tonn Nua, a proposed offshore wind site in the North Celtic Sea. Here, I utilise time-lapse bathymetry and eARA derived mean grain size to investigate seabed dynamics and geological constraints that may pose a threat to the development of ORE at this site. Therefore, this chapter aims to address the following research aims and objectives:

i. Investigate the geomorphology of the proposed Tonn Nua site;
ii. Assess the spatio-temporal variability of Tonn Nua;
iii. Investigate the hydrodynamics of the site; and
iv. Evaluate the seabed stability of Tonn Nua; and therefore, what are the implications for the development of ORE.

Finally, Chapter 4 provides a conclusion of all the work presented in this thesis, highlighting the impacts of this research, the associated limitations, along with providing recommendations for future research to mitigate limitations on this topic.

Preface to Chapter 2:

This chapter was written in peer-reviewed style. The work was subsequently submitted, reviewed and published by Marine Geophysical Research on 26th May 2025 as an open-access article.

Multibeam backscatter has proven to be a useful tool in deciphering seabed sediments. While traditional image-based backscatter processing methods are commonly used, signal-based approaches such as Angular Range Analysis (ARA) offer a robust sediment-characterisation, albeit with a relatively low spatial-resolution. Thus, this research aims to improve the segmentation accuracy of ARA; and investigate influences on enhanced Angular Range Analysis's accuracy. This research utilises open-source data from the Irish National Seabed Survey and its successor, the Integrated Mapping for the Sustainable Development of Ireland's Marine Resource programme, which spans >20 years. Our framework applies object-based image analysis to backscatter data and incorporates ARA characterisation to create a more spatially robust sediment classification workflow without the need for reprocessing large volumes of MBES data. Here, the developed workflow is applied to four sites offshore Ireland, with ranging water depths (59-2126 m), operating frequencies (12-300 kHz), and multibeam sonars. Statistical analyses focus on: 1) correlation between observed and estimated grain size; 2) thematic accuracy; 3) segmentation accuracy; 4) relationship between residuals (observed - estimated mean grain size) with sediment sedimentological properties (modality and sorting); and 5) sediment-sampling parameters (instrument and temporal offset). Accuracy assessment yielded a Spearman's rank correlation up to 0.75 ($p<0.01$) with overall accuracies up to 96.15% ($k=0.84$) and improved spatial accuracies across almost all standard metrics compared to traditional ARA. Overall, these results showcase the capacity of the workflow as a robust sediment estimator, while improving segmentation accuracy. Therefore, providing a scalable seafloor characterisation approach applicable to large-scale governmental programs.

Author Contributions

Cara Brennan: Conceptualization, Methodology, Formal analysis, Investigation, Software, Validation, Visualisation, Data curation, Resources, Writing-original draft, Project administration. **Gerard Summers:** Methodology, Validation, Resources, Writing- review and editing, Supervision. **Larissa Macedo Cruz de Oliveira:** Methodology, Validation, Resources, Writing- review and editing, Supervision. **Aaron Lim:** Conceptualization, Methodology, Resources, Supervision, Writing- review and editing, Project administration, Funding acquisition.

Chapter 2: Enhanced Angular Range Analysis: A Novel Object-based Image Analysis Approach for Seafloor Characterisation

(Current Status: Published, Marine Geophysical Research,
https://doi.org/10.1007/s11001-025-09574-7)

Cara Brennan[1,2*], Gerard Summers[1,2], Larissa Macedo Cruz de Oliveira[1,2] and Aaron Lim[1,2]

[1] Earth and Ocean Lab, Department of Geography, University College Cork, Cork, Ireland

[2] Sustainability Institute, University College Cork, Lee Road, Cork, Ireland

2.1 Introduction

Advancements in acoustic remote sensing survey techniques such as multibeam echosounders (MBES) have progressed the efficiency of seabed characterisation, enabling the cost-effective characterisation of large areas of the seafloor (Guinan et al., 2021). Hence, MBES is a valuable tool for seabed mapping providing high-resolution bathymetry and backscatter datasets (Gaida et al., 2018). This potential has been widely exploited for a variety of purposes from seafloor characterisation (Thébaudeau et al., 2016; Samsudin and Hasan, 2017), benthic habitat mapping (Hossain and Chen, 2019; McGonigle et al., 2009), and geohazard identification (Kucharczyk et al., 2020). However, only 26.1% of our seafloor has been mapped, as of 2024 (www.seabed2030.org). Accordingly, an international effort is currently underway to map the entirety of the seafloor by 2030, as part of the GEBCO Seabed 2030 project (Mayer et al., 2018b). This global goal has been adopted by national mapping organisations including the Integrated mapping for the Sustainable Development of Irelands Marine resources (INFOMAR) programme. Since 2006, INFOMAR and prior to that, it's predecessor, Irish National Seabed Survey (INSS) have collected and collated MBES data across the Irish shelf, covering approximately 700,000 square kilometers of underwater territory. Such effort has inevitably resulted in vast volumes of data generated. MBES data products such as bathymetry and backscatter represent a considerable output of INFORMAR's mapping efforts. As such, these require repeatable processing techniques to allow for standardised outputs across surveys (Summers et al., 2023).

Backscatter intensity is a measure of the acoustic energy that is returned toward the transmitter by acoustic reflection and scattering, from within the sediment known as volume scattering and at the sediment water interface (Jackson et al., 1986b; Goff et al., 2004; Ferrini and Flood, 2006; De Falco et al., 2010). Backscatter intensity is a well-established means of achieving a high-resolution representation of the acoustic facies of the seafloor. However, inconsistencies in data acquisition between MBES systems produced by different manufacturers, unstandardised approaches to backscatter data mosaicking and interpretation have led to the introduction of ambiguity to these data (Lamarche and Lurton, 2018). For example, angle-varying gain (AVG) corrections are applied to the backscatter intensity data to remove their angular dependence and produce backscatter mosaics (Lurton and Lamarche, 2015; Misiuk and Brown, 2022). However, removing an intrinsic property of the seafloor hinders the robust characterisation of seafloor sediments (Misiuk and Brown, 2022). Moreover, while image-based backscatter processing methods have previously dominated the literature, signal-based approaches are becoming increasingly available due to their consistent and robust sediment classification (Hughes Clarke, 1994b; Rzhanov et al., 2012). Angular Range Analysis (ARA) (Fonseca and Mayer, 2007) allows for high fidelity seabed characterisation, achieved by examining a set of consecutive acoustic pulses across half a swath of a sonar for each individual beam (Fonseca and Mayer, 2007c; Fonseca et al., 2009). ARA should ideally be conducted in homogeneous areas of the seafloor (Alevizos and Greinert, 2018), using operating frequencies of ≤100 kHz (Jackson et al., 1986). However, contemporary studies have successfully applied ARA to datasets acquired using higher operating frequencies (≤300 kHz) (Alevizos and Greinert, 2018; Santos et al., 2018) and in highly hydrodynamic environments (Santos et al., 2018). Although ARA is constrained by its low spatial resolution being limited to half the swath width of the sonar (Fonseca and Mayer, 2007; Santos et al., 2018; Misiuk and Brown, 2022), its capabilities to work on highly dynamic environments and at different frequencies highlight the growing application of ARA for seabed characterisation. Despite its growing popularity, there has been little movement in literature to integrate the high spatial resolution data presented by MBES backscatter with the high-fidelity sediment information presented by ARA. Therefore, a methodology designed to provide a repeatable and scalable sediment classification from MBES backscatter data is crucial in the development of offshore renewable energy (ORE) and marine management in Ireland.

Numerous studies have endeavoured to overcome the spatial resolution limitations associated with angular-response based approaches, many of which were discussed by Misiuk and Brown (2022). Parnum (2007) proposing to derive an “angular cube”, interpolating discrete incidence angles (Misiuk and Brown, 2022). Huang et al. (2014), suggesting this could be achieved through producing multiple backscatter mosaics using different angles for the AVG correction. Alevizos and Greinert (2018), compared both approaches indicating that both produced similar results (Misiuk and Brown, 2022). Furthermore, additional approaches were suggested to improve the spatial resolution of ARA such as: Fonseca et al. (2009) proposing to aggregate soundings by homogeneous patches of seabed. Che Hasan et al. (2012, 2014) developed upon this approach by segmenting the backscatter mosaic into image-objects, which were then used as a framework to group soundings together (Misiuk and Brown, 2022). While, several approaches have been proposed, no singular solution has been widely adopted. Moreover, such solutions are often time-consuming, isolated, bespoke, and difficult to implement. Thus, inferring the need for scalable methods that can be applied across the entire INFOMAR database. Solutions must be established to support a wide range of sensors, depths, and environments that can be scaled across a vast database, further supporting large-scale mapping programmes.

Object-based image analysis (OBIA) offers a scalable and objective framework to effectively integrate the high spatial resolution information presented by the mosaiced backscatter, and the thematic accuracy of the ARA, more efficiently and objectively than manual processing (Diesing et al., 2014). OBIA groups continuous high-resolution pixels with similar properties into meaningful image-objects, which are then treated as the smallest unit of analysis (Hay and Castilla, 2006; Castilla and Hay, 2008; Hossain and Chen, 2019). Thus, maximising both between-object heterogeneity and within-object homogeneity (Blaschke, 2010; Ierodiaconou et al., 2018b). OBIA segmentation offers the potential to accurately discern ‘acoustic facies’ depicted in the high resolution backscatter data, being less susceptible to artefacts such as speckle and nadir noise (Ierodiaconou et al., 2018b). Moreover, with developments in technologies and increasing data resolution, OBIA is becoming increasingly popular for contemporary marine research, providing greater accuracy for higher resolution datasets (Hossain and Chen, 2019).

Given the poor spatial accuracy of traditional ARA and need for scalable robust sediment characterisation approaches, this research proposes a novel workflow, entitled 'enhanced Angular Range Analysis' (eARA). Accordingly, we apply an OBIA framework that integrates the segmentation accuracy of MBES backscatter imagery with the signal accuracy of ARA. We investigate the influence of geophysical parameters, sedimentological properties of sediment samples, and sediment sampling strategies on the accuracy of the method. The results are compared against existing classification results in these same regions. On a broader scale, the method was developed to allow for upscaling across larger governmental programs such as MAREANO and INFOMAR. Therefore, this research aims to achieve the following research objectives: (i) determine the segmentation and classification accuracy of eARA; and rank it in comparison to alternative methods; (ii) determine the methods effectiveness in relation to geophysical parameters (depth and operating frequency); (iii) evaluate the limitations imposed by sediment sedimentological properties (modality and sorting) and sediment sampling strategies (instrument; and temporal offset between acoustic and sediment sampling survey) on eARA's accuracy, and; (iv) assess the broader implications, required resources, and propose steps for upscaling this workflow across national programmes.

2.2 Study Sites

The study area was located within the maritime boundary of Ireland (Fig.2.1a) and comprises of four distinct sub-regions (Fig.2.1b): INSS Zone 3m, now referred to as Site A (Fig.2.1c), which is situated between the southeastern flanks of the Porcupine Bank and northern area of the Porcupine Bight, covering an area of almost 18,000 km^2 with depths ranging from 441 to 2162 m; CE04_03, now referred to as Site B (Fig.2.1e) which is located on the Rockall Bank, northwest of Ireland and separated from the European shelf by the Rockall Trough (Sacchetti et al., 2012), it spans approximately 5,170 km^2 with water depths ranging from 140 to 364 m; CV17_01, now referred to as Site C (Fig.2.1d), positioned in the Celtic Sea, it covers an area of 708 km^2 with a water depth of between 59 to 75 m; and CV18_02 now referred to as Site D (Fig.2.1f), this area is also in the Celtic Sea, with water depths ranging from 84 to 124 m, covering an area of approximately 2,204 km^2.

The collective depth range of these sites extend from approximately 59 to 2000 m, encompassing an area of almost 26,000 km^2. Thus, the variation in depth (and operating frequency), data quality and distinctive characteristics of each site provide ideal conditions to determine the effectiveness of the proposed method; and understand potential influences on its effectiveness. Additionally, particle size analysis (PSA) data is available for each site, providing data for calibration and validation purposes.

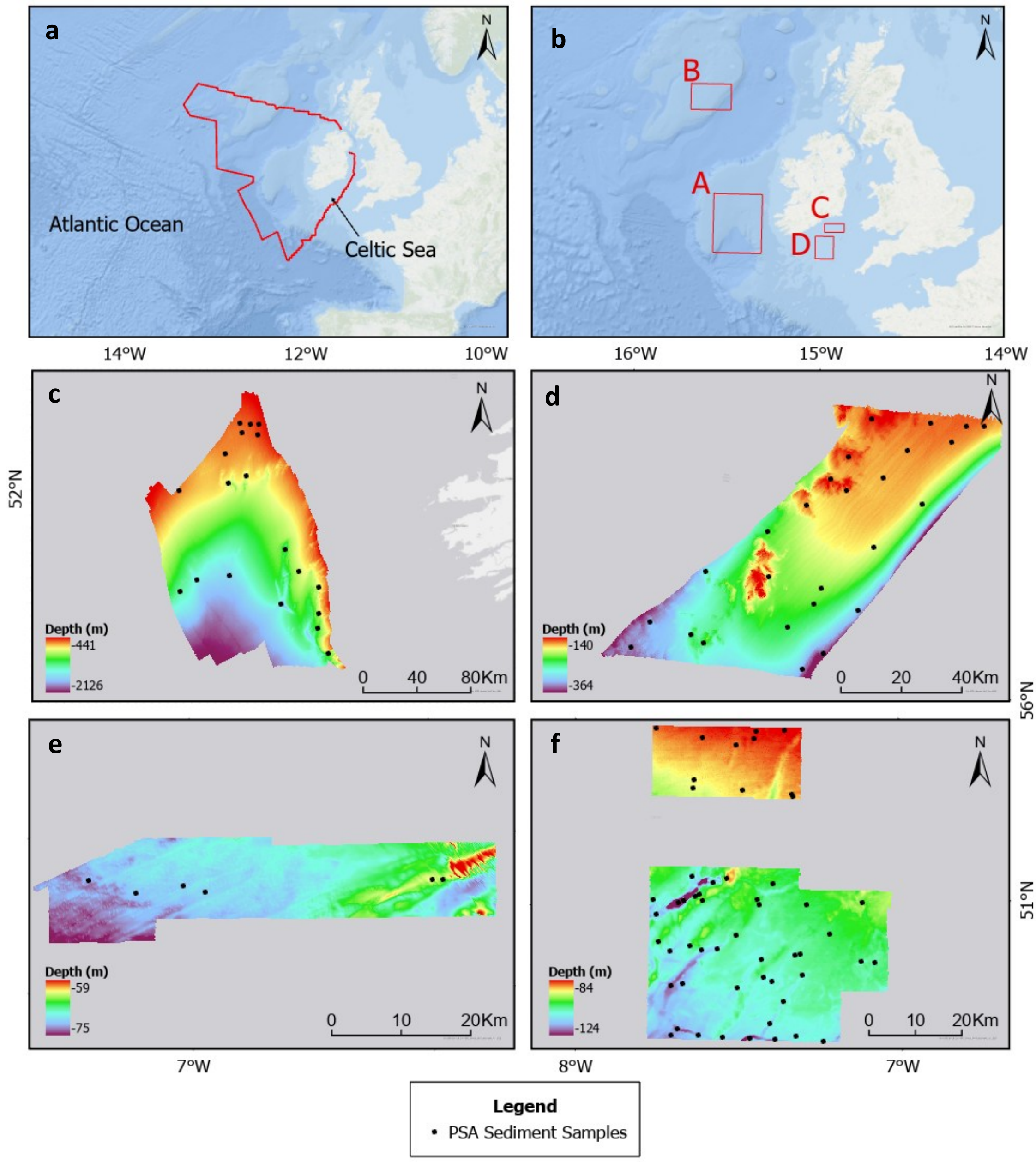

Figure 2.1. (a) Maritime boundary of Ireland; (b) Map of study regions A-D; and (c-f) shaded relief with INFOMAR particle size analysis (PSA) sediment samples represented by black points: (c) Site A (INSS Zone 3), (d) Site C (CV17_01), (e) Site B (CE04_03), and (f) Site D (CV18_02).

2.3 Materials and methods

Our workflow consists of four main stages: data processing, OBIA, eARA prediction accuracy assessment, and residual analysis (Fig.2.2). The data processing stage was completed in QPS FM Geocoder Toolbox (FMGT) v7.11 software. OBIA was completed in ArcGIS Pro v3.2. eARA prediction accuracy assessment and residual analyses were carried out using SPSS v29, Python version 3.11.5, and MATLAB v24.1.0. Results were plotted and visualised in Python's Jupyter Notebook interface.

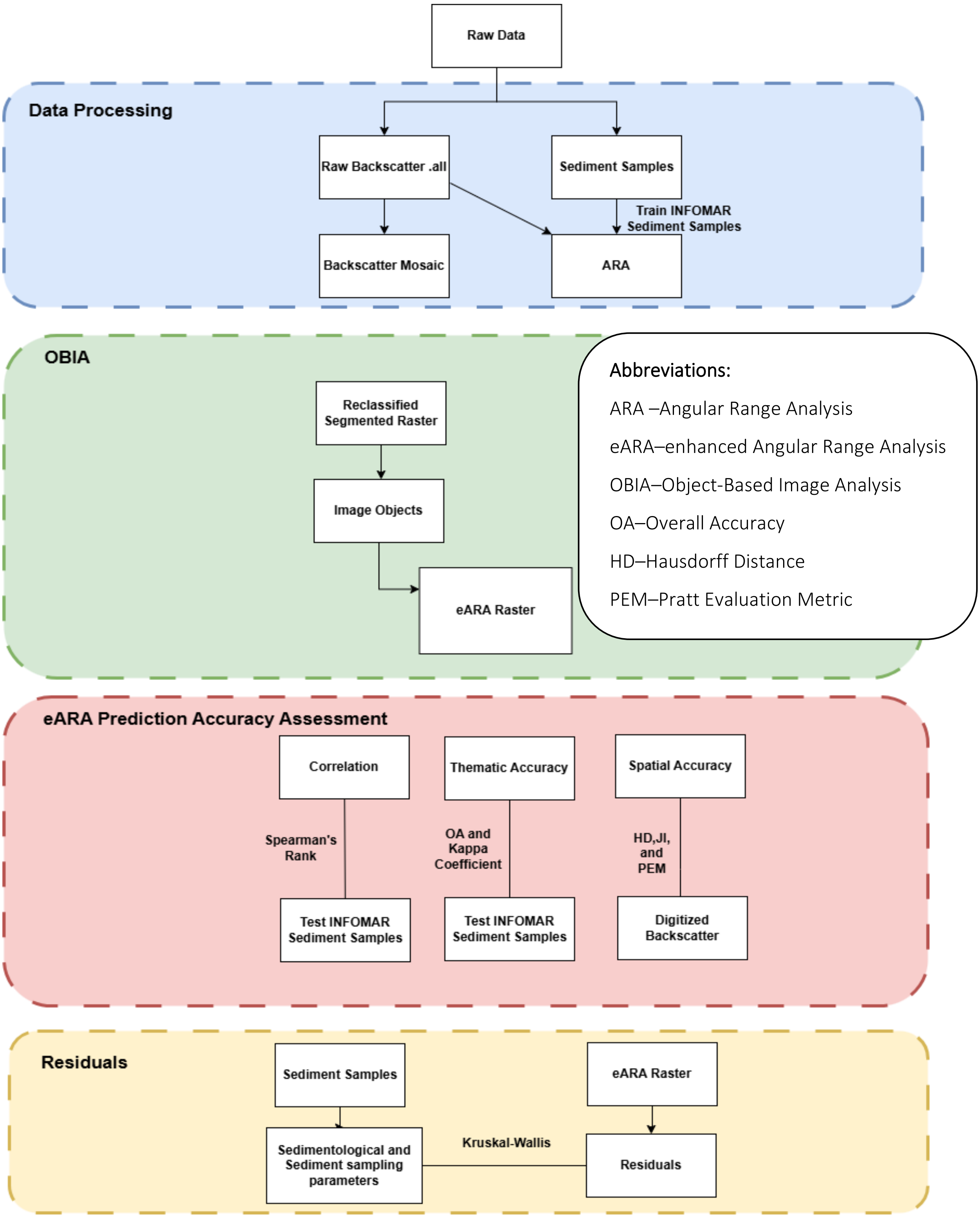

Figure 2.2. Workflow chart; Data processing, Object-based Image Analysis, eARA Prediction Accuracy Assessment, and Residuals.

2.3.1 Sediment samples

Sediment samples were acquired in a period between 2004 and 2022. All PSA data from sediment samples were provided by the INFOMAR in a geodatabase. Samples were acquired using various instruments, including Day Grabs, Remotely Operated Vehicles (ROV), Box Corers, and Shipek Grabs, over several surveys. In total, 106 seabed sediment samples were used as they were located within the four sites. The samples were imported to ArcGIS for further processing and analysis.

The attributes included sediment samples' sedimentological properties and sediment sampling information (see supplementary Table A.1 for full description). Additionally, full grain size analysis data were available via GRADISTAT (Blott and Pye, 2001), from which mean grain size data using the Folk and Ward (Folk, 1954) method was extracted and compiled into the PSA attributes table.

2.3.2 enhanced Angular Range Analysis (eARA)

2.3.2.1 Multibeam echosounder data

This research utilises MBES data collected through the Irish National Seabed Survey (INSS) and its successor programme INFOMAR. The acoustic data were collected between 2001 and 2018 on board the RSV *Siren* for Site A, RV *Celtic Explorer* for Site B and RV *Celtic Voyager* for Sites C and D, respectively (Table 2.1). All data were acquired using Kongsberg multibeam systems (Table 2.1). Raw data were stored in *.all or *.mb56 file formats (subsequently converted to *.all).

Table 2.1. Multibeam echosounder datasets.

Site	Survey Code	Multibeam (Operating Frequency)	Data Acquisition Software	Vessel	Year	Depth Range
A	INSS Zone 3	Kongsberg EM120 (12 kHz)	Kongsberg Merlin	RSV *Siren*	2001	441-2126 m
B	CE04_03	Kongsberg EM1002 (93-95 kHz)	Kongsberg Merlin	RV *Celtic Explorer*	2004	140-364 m
C	CV17_01	Kongsberg EM2040D (300 kHz)	SIS	RV *Celtic Voyager*	2017	59-75 m
D	CV18_02	Kongsberg EM2040 (200kHz)	SIS	RV *Celtic Voyager*	2018	84-124 m

Backscatter data processing was performed in FMGT, following manufacturers recommended processing steps (Quality Positioning Services (QPS), 2022). The raw backscatter data were imported as *.all file formats and all necessary geometric and radiometric corrections were implemented in FMGT software. Angular varying gain (AVG) 'flat' correction was applied to all sites, attempting to smooth out noise in the backscatter signal by reducing minor variations in backscatter level (Schimel et al., 2018; QPS, 2022). Backscatter mosaics were gridded with grid resolution based on water depth: 2 m resolution for shallower sites (Sites C and D; water depths of 59 -125 metres), 8 m resolution for medium water depths (Site B; water depths of 140- 364 metres), and 20 m resolution for the deepest site (Site A; water depths of 441- 2126 metres). The grids were exported as floating point GeoTIFF (.tif) files.

ARA is a technique that calculates the angular response curve (ARC) across either side of the nadir, port and starboard of the sonar. ARA assesses the backscatter, characterising the surface at discrete angles by stacking a series of consecutive acoustic pulses (30, in FMGT) (Santos et al., 2018; Di Stefano et al., 2024), analysing and separating the backscatter angular response (AR) into three zones: near (0°-35°), far (35°-55°) and outer ranges (65°-90°) (Fonseca and Mayer, 2007). ARA was applied within FMGT following manufacturers recommendations (QPS, 2022) to determine the sediment characteristics. One beam pattern correction (BPC) was applied at each site using known mean grain size i.e. INFOMAR sediment sample. Refer to Santos et al. (2018) for a detailed description of the BPC process. For the purpose of this research, the ARA parameter utilised is mean grain size corresponding to the phi scale (Φ) (Krumbein, 1938), as it is one of the most important descriptors of seafloor characteristics (Rzhanov et al., 2012). A spearman's rank correlation was carried out between the observed and estimated mean grain size to determine the accuracy of the estimation with the ground truth data.

2.3.2.2 Object-based image analysis

The resulting backscatter mosaics were segmented using the *Mean Shift Segmentation* algorithm (Comaniciu and Meer, 2002) (Fig.2.3). This algorithm requires adjustment of three parameters: spectral detail (based on attribute values), spatial detail (weighting based on proximity) and minimum segment size (Misiuk and Brown, 2022) to ensure correct delineation of seafloor sediment deposits while reducing the effect of backscatter artefacts. Spectral detail is the level of importance of separating objects based on colour characteristics and spatial details is the based on spatial characteristics, with both parameters having a range of 1 to 20. Values for the three parameters were iteratively selected based on trial and error (Table 2.2).

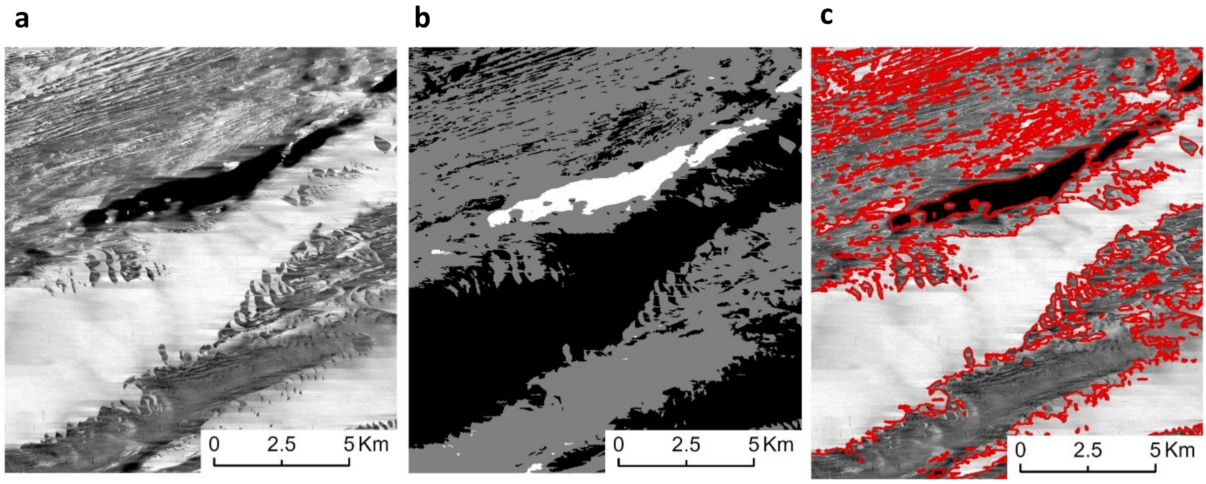

Figure 2.3. Example mean shift segmentation. (a) multibeam backscatter mosaic (2m resolution), (b) segmented output (spectral detail:15.5; spatial detail: 15; and minimum segment size: 800), and (c) segmented output converted to polygons.

Table 2.2. Mean Shift Segmentation spatial detail, spectral detail, and minimum segment size values for sites A-D.

Site	Spatial Detail	Spectral Detail	Minimum Segment Size	Resolution (m)
A	10	14	700	20
B	15	15.5	500	5*
C	15	18	600	2
D	15	15.5	800	2

*INFOMAR backscatter mosaic

A supervised classification was subsequently performed in ArcGIS. Given the homogeneity of backscatter values within each segment, the 'mean' statistic of the *zonal statistics* tool was selected to accurately represent the mean grain sizes derived from the ARA data. The mean grain sizes derived from the ARA output were extracted to the corresponding polygon segments, producing a classified eARA raster in terms of mean grain size (Φ). It is important to note that the classified eARA raster maintains the same spatial resolution of the ARA raster. Sediment classification maps were produced for each study site, illustrating the distribution of estimated sediment types across each site.

2.3.3 eARA Prediction Accuracy Assessment

The accuracy of the prediction produced by eARA was assessed by correlation, thematic, and segmentation accuracy. The accuracy was derived by comparing our estimation against the 102 INFOMAR sediment samples that were not included in the beam pattern correction process.

2.3.3.1 Spearman's rank correlation

Spearman's rank correlation was carried out to quantify the relationship between the estimated and observed grain sizes, as the estimated grain sizes were non-normally distributed. The analyses compared the observed mean, median (d50), and mode grain sizes against estimated mean grain size for each site individually and then for all sites combined. Samples used in the BPC process were excluded from this analysis. As many of the sediment samples were multimodal and poorly sorted, we investigated the correlation between observed grain size (mean, median, and mode) and estimated mean grain size (McGonigle and Collier, 2014; Santos et al. 2018). Subsequent analyses focused on mean grain size, the most important variable identified in the Spearman's rank correlation (Table 2.3).

Table 2.3. Spearman's rank correlation interpretation (Hidayat et al., 2021).

ρ	Interpretation
0.00 – 0.199	Very Weak
0.2 – 0.399	Weak
0.4 – 0.599	Moderate
0.6 – 0.799	Strong
0.8 – 1.00	Very Strong

2.3.3.2 Thematic accuracy

Data were categorised as sand, gravel, or mud based on mean grain size (Φ), derived from sediment samples (true label) and from the eARA output (predicted label). To evaluate the accuracy of the estimated sediment classification output, a confusion matrix was produced for all sites, determining the overall accuracy (%) and Cohen's Kappa Coefficient (Cohen, 1960). Overall accuracy measures the proportion of correctly classified samples out of the total number of samples. Cohen's Kappa Coefficient measures the agreement between the predicted and ground-truth data, accounting for chance agreement between classes (Cohen, 1960).

2.3.3.3 Segmentation accuracy

Comparative spatial analyses between the backscatter mosaic with the eARA and ARA rasters enabled a statistical evaluation of the segmentation accuracy of the prediction. Site A was excluded from this analysis due to poor backscatter data quality. A set of polygons were randomly created over the backscatter mosaic, a polygon was randomly selected at each site. The acoustic facies within the polygon were manually digitised, these digitised backscatter features capture the spatial heterogeneity of the seabed and represent deviations from the dominant sediment facies within the area of interest of each site. These manually digitised polygons were employed to appraise the representativeness of the sediment facies outlined by the eARA workflow. The framework developed to complete this comparison incorporated a series of statistical analyses that were adapted from Arosio et al. (2024). Several methods were employed to quantitatively evaluate the degree of similarity between the manually derived polygons (ground-truth) and the polygons produced during the segmentation phase of the eARA workflow (Fig.2.3): Pratt Evaluation Metric (PEM) Figure of Merit (Pratt, 2001), Hausdorff Distance (HD), and Jaccard Index (JI). PEM uses the edge detection method as a measure of performance (Pratt, 2001), ranging from 0 to 100 (%), with higher values indicating greater correlation. HD evaluates the degree to which the boundary between the ground truth and predicted match (Survarachakan et al., 2022), with lower values indicating better agreement. HD is calculated by measuring the maximum distance between a point on the predicted perimeter to the nearest point on the ground truth perimeter (Arosio et al., 2024). The JI compares the similarity between datasets, calculating the ratio of intersection versus their union, running from 0 to 1, with lower values indicating poorer similarity (Mulrooney et al., 2024). All spatial analyses metrics were calculated for each site using Python with associated libraries (Rasterio, Fiona, GeoPandas, and NumPy) and MATLAB (PEM algorithm) (Bhadouria, 2024).

2.3.4 Residual statistical analyses

The residuals (Φ) (i.e. the difference between observed and estimated mean grain size) were analysed to investigate the influence of sediment sedimentological properties (modality and sorting) and sediment sampling strategies (instrument; and temporal offset between acoustic and sediment sampling survey) on the performance of eARA (Table 2.4). The univariate statistical analysis combined visual data interpretation and non-parametric tests to assess the influence of predictor variables. Residuals were calculated as:

$$x_i = M_z(observed) - M_z(eARA) \quad (1)$$

where Mz represents mean grain size (Φ).

Residuals were plotted against categorical variables (instrument, sorting, and modality) as violin plots for all sites combined, which included bar charts showing the distribution of samples for each type. Boxplots were utilised to evaluate the impact of the temporal offset between the acoustic survey and sediment sample acquisition on eARA's prediction errors. All sediment samples were categorized into time intervals based on the number of years between the MBES survey and sample acquisition: 0, 1-5, 6-10, 11-15, and 16-20. The intervals were chosen to ensure there was a sufficient amount of samples available per group.

To assess the impact of categorical variables on prediction errors (residuals), a univariate analysis was carried out by compiling and analysing each variable across all sites combined. The Kruskal-Wallis test was carried out on variables as variables did not exhibit a normal distribution across groups. When significant results were identified (p-value of <0.05), post hoc tests were performed, pair-wise comparisons were conducted using the Dunn method (Dunn, 1964). Where a statistically significant difference was found, a Bonferroni correction was applied for multiple comparisons to reduce type-I errors.

Table 2.4. List of variables used to determine the relationship with residuals (Φ) along with the variable type, methods and post-hoc tests.

Term	Variable	Variable Type	Method	Post-Hoc Test
Sedimentological Properties	Modality	Categorical	Kruskal-Wallis	Dunn's test
	Sorting	Categorical	Kruskal-Wallis	Dunn's test
Sediment Sampling Strategies	Instrument	Categorical	Kruskal-Wallis	Dunn's test
	Temporal offset between acoustic and sediment sampling survey	Categorical	Kruskal-Wallis	Dunn's test

2.4 Results

2.4.1 Multibeam echosounder data

Backscatter mosaics and sediment sample compositions illustrate the distribution of sediments in Sites A-D (Fig.2.4). At Site A (Fig.2.4a), backscatter features are difficult to define due to poor backscatter data quality and resulting artefacts such as bubble wash. Sediment samples are mainly comprised of finer grained sediments throughout the site. Sites D (Fig.2.4b) and C (Fig.2.4c) are heterogeneous with high spatial variation, dominated by sediment waves and sand ribbons. Site B (Fig.2.4d) is also dominated by finer grained sediments with coarser grained backscatter features to the west and north-west of the site.

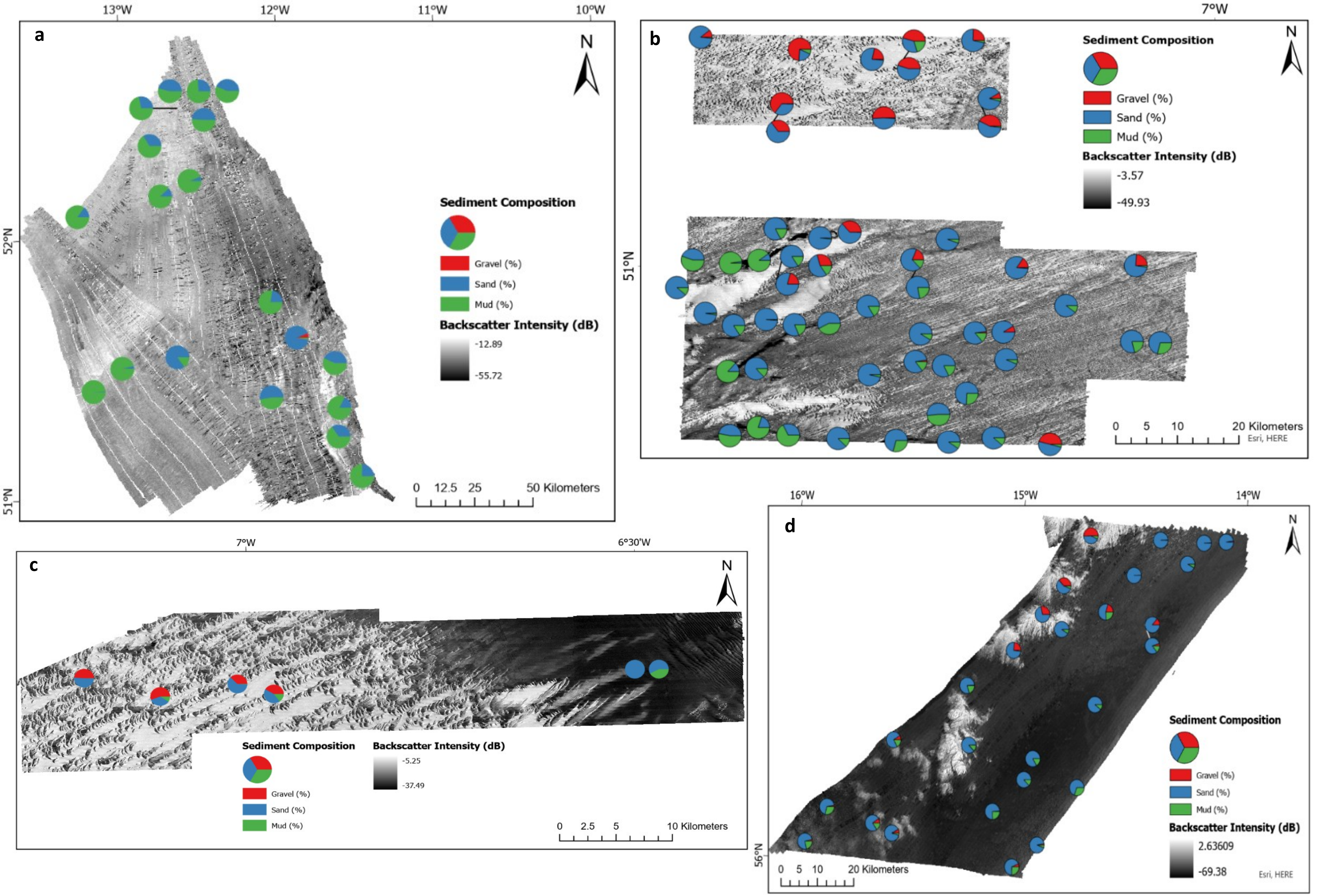

Figure 2.4. Backscatter mosaics displaying sediment composition (%) data of all sediment samples for (a) Site A, (b) Site D, (c) Site C, and (d) Site B.

The analysis of mean grain size across observed and estimated data derived from the ARA output at Sites B and D, revealed a robust positive correlation, (r(24)=.71, p<.001) and (r(51)=.72, p<.001), respectively. Sites A and C did not show a statistically significantly significant correlation between observed and estimated mean grain size, derived from the ARA output, (r(16)=.04, p=.890) and (r(3)=.45, p=.450), respectively.

2.4.2 eARA prediction accuracy

2.4.2.1 Spearman's rank correlation

Overall, the observed and estimated mean grain size displayed the highest overall correlation compared to the observed mode and median grain sizes (Fig.2.5a-d). The analyses across the observed and estimated mean grain sizes, derived from the eARA output at Sites B and D, revealed a robust positive correlation, (r(24)=.67, p<.001) and (r(51)=.75, p<.001), respectively. Sites A and C did not show a statistically significant correlation between observed mean grain size and estimated mean grain size (p = .506 and p=.450, respectively). The analysis of across the observed median and estimated mean grain size, derived from the eARA output at Sites B and D, revealed a significant and robust positive correlation, (r(24)=.60, p<.001) and (r(51)=.72, p<.001), respectively. Sites A and C did not show a statistically significant correlation between observed median grain size and estimated mean grain size (with p-values of .470 and .718, respectively). The analysis of across the observed mode and estimated mean grain size, derived from the eARA output at Sites B and D, revealed a robust positive correlation (r(24)=.44, p=.025) and (r(51)=.66, p<.001), respectively. Sites A and C did not show a statistically significant correlation between observed mode grain size and estimated mean grain size (with p-values of .228 and .685, respectively). Moreover, the analysis of the observed and estimated mean grain size, encompassing all study sites and a total of 102 sediment samples, revealed a significant and robust positive correlation (r(100)=.80, p <0.01). The results suggest a high level of consistency between the estimated and observed grain size data.

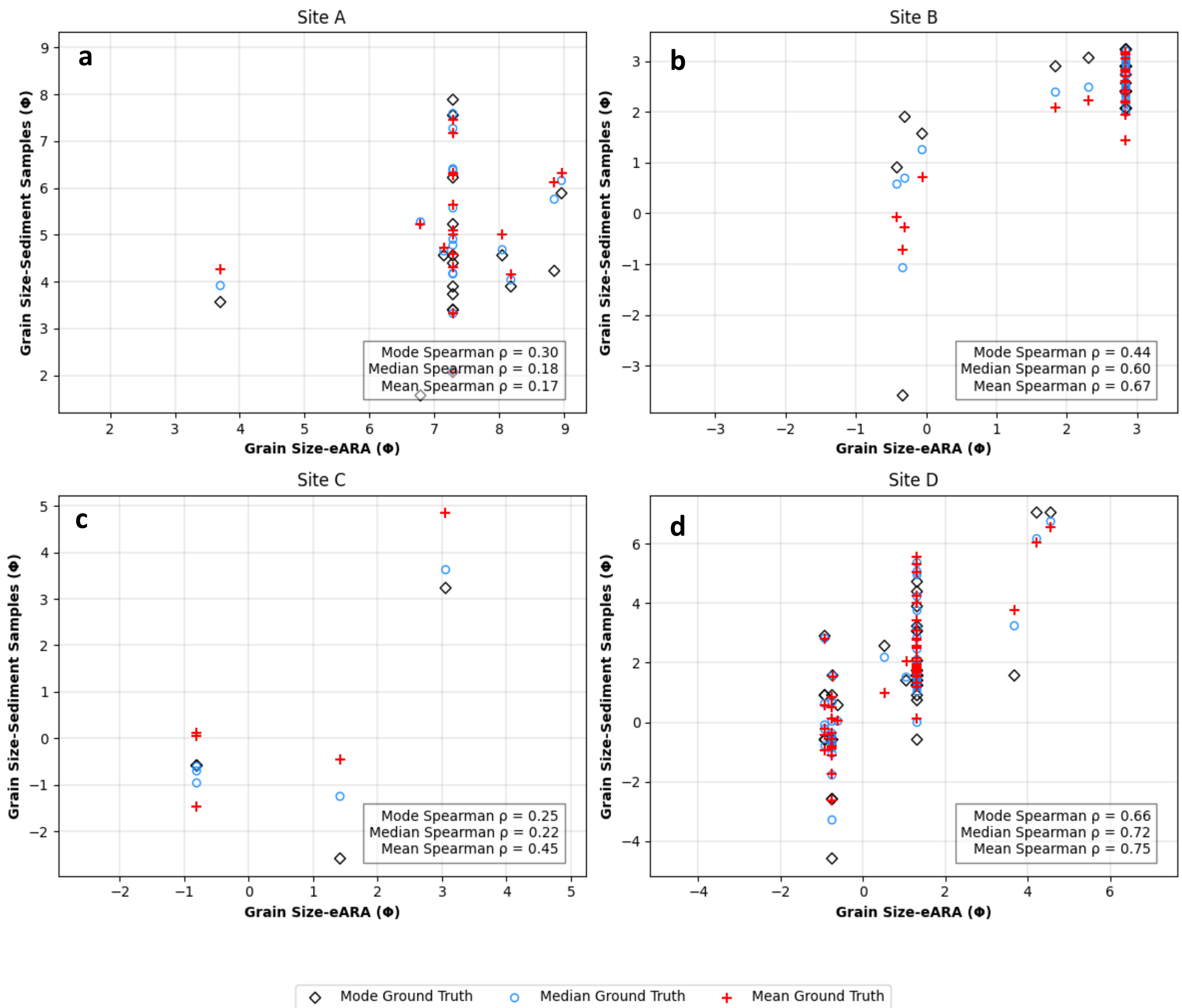

Figure 2.5. Spearman's rank correlation between mean grain size eARA (Φ) and observed mean, median, and mode grain size (Φ) for (a) Site A, (b) Site B, (c) Site C, and (d) Site D.

2.4.2.2 Thematic accuracy

Site B demonstrated the highest overall accuracy (96.15%), followed by Site A (83.3%), Site D (75.47%), and Site C (20%) (Fig.2.6a-d). The sediment prediction at Site B achieved a Cohens Kappa coefficient of 0.84, indicating an almost perfect agreement. Site D demonstrated a Kappa coefficient of 0.53, signifying a moderate agreement. Sites A and C, performed poorly, with Kappa coefficients of-0.08 and-0.33 respectively, indicating no agreement.

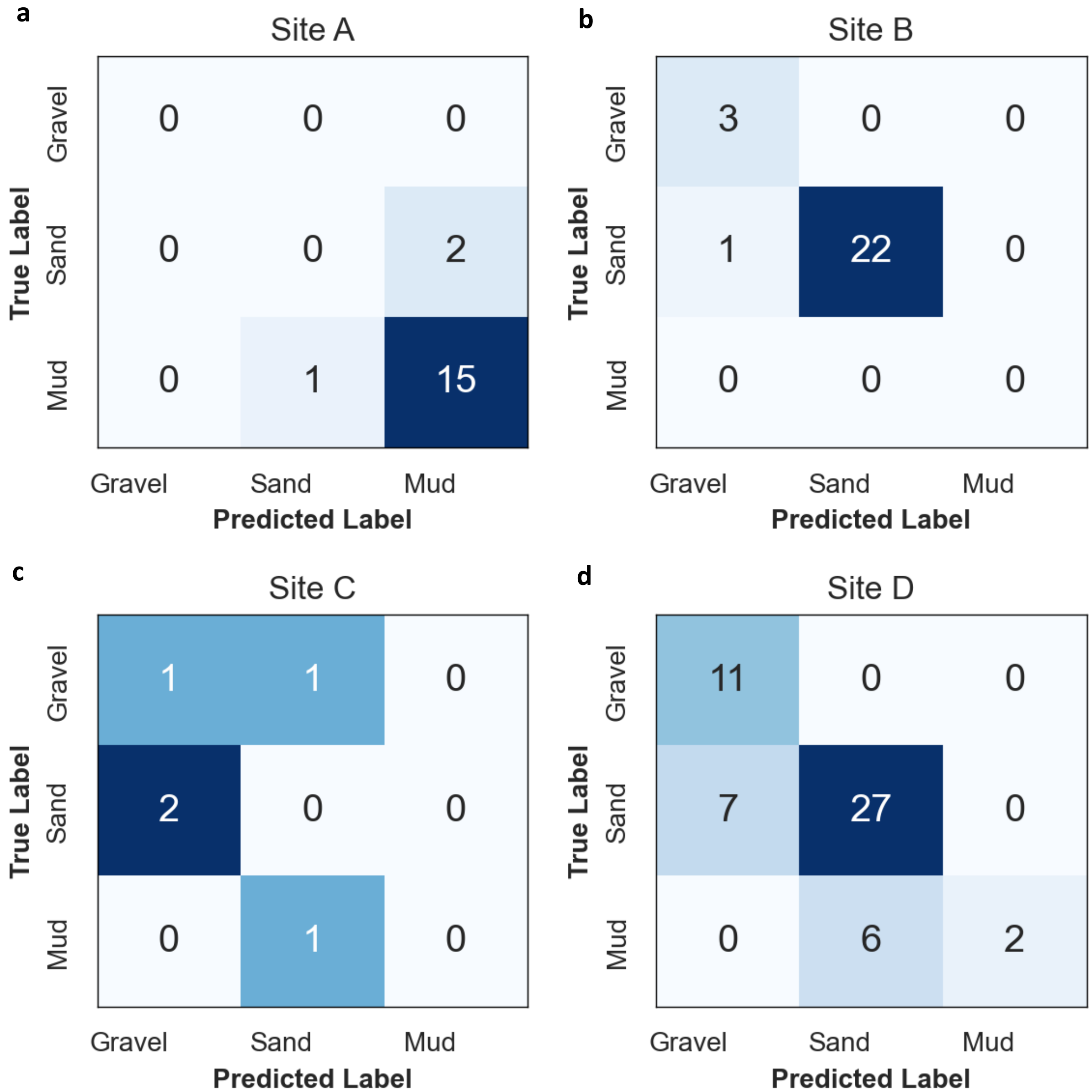

Figure 2.6. Confusion matrix for: (a) Site A, (b) Site B, (c) Site C, and (d) Site D.

2.4.2.3 Segmentation accuracy

Segmentation accuracy could not be calculated for the ARA at Site B due to the poor segmentation accuracy of the ARA prediction (Table 2.5). While at the same site, the eARA displayed a poor segmentation accuracy, performing poorly in delineating sediment boundaries observed in the backscatter mosaic, achieving a PEM of 43.32, a HD of 73.50, and a JI of .69. At Site C, eARA achieved a higher score in two of three metrics compared to ARA, achieving a PEM of 96.57% compared to 90.24%, a JI of .81 compared to .69. While, displaying a poorer HD of 62.43, compared to ARA's 61.40, in which the lower values are preferred. At Site D, eARA achieved a higher score in two of three metrics compared to ARA, achieving a PEM of 84.03% compared to 74.1%, a JI of .72 compared to .54, while, displaying a poorer HD of 68.12, compared to ARA's 64.20.

Table 2.5. ARA and eARA segmentation accuracy assessment results; PEM, HD, and JI for Sites B-D.

	B		C		D	
	ARA	eARA	ARA	eARA	ARA	eARA
PEM (%)	-	**43.32**	90.24	**96.57**	74.1	**84.03**
HD	-	**73.50**	**61.40**	62.43	**64.20**	68.12
JI	-	**0.29**	0.69	**0.81**	0.54	**0.72**

The resultant map output for site D is presented in Fig.2.7, depicting the distribution of sediments in terms of mean grain size (Φ). Sections of the classified map outputs for Sites A-D are presented in Fig.8. The eARA classified outputs (Fig.2.8c, 2.8f, 2.8i, and 2.8l) demonstrate improved segmentation accuracy compared to the corresponding ARA outputs in Fig.2.8c, 2.8e, 2.8h, and 2.8k.

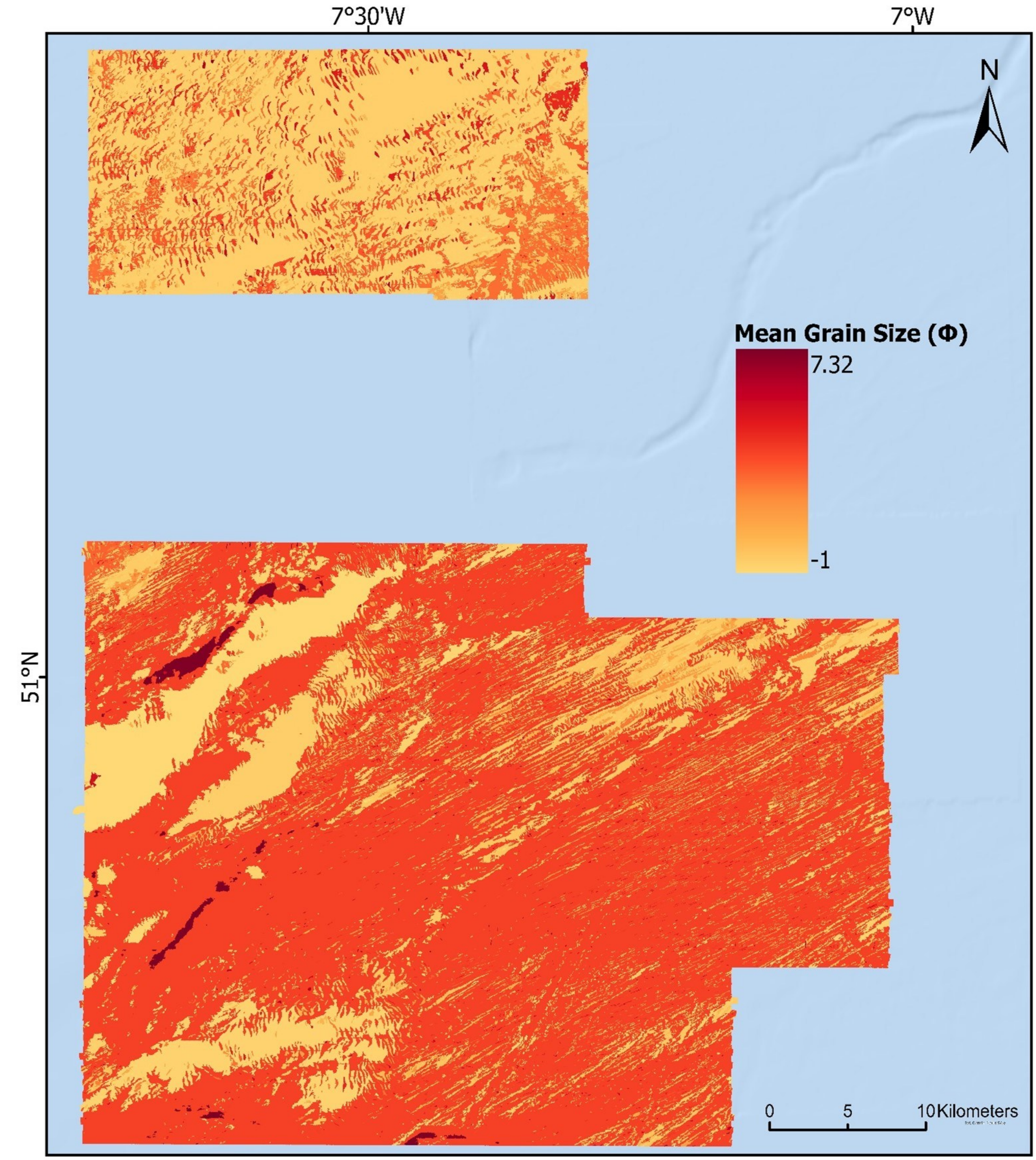

Figure 2.7. eARA classified map in terms of mean grain size (Φ) for site D.

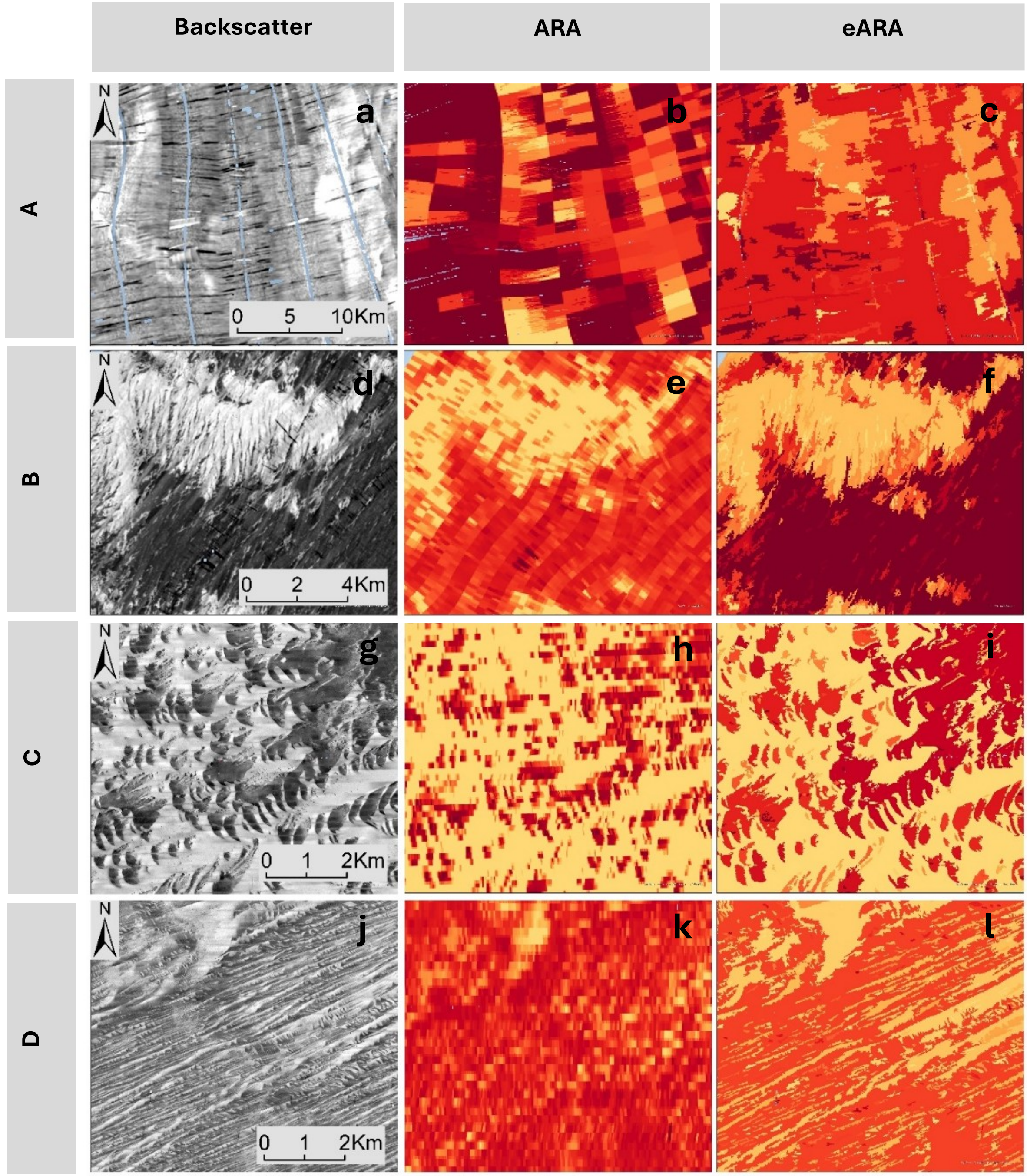

Figure 2.8. Close-up examples from Site A: backscatter mosaic, ARA, and eARA (a-c), respectively; Site B: backscatter mosaic, ARA, and eARA, (d-f) respectively; Site C: backscatter mosaic, ARA, and eARA, (g-i) respectively; and Site D: backscatter mosaic, ARA, and eARA (j-l), respectively. Backscatter mosaics presented as grayscale images, with darker hues indicating lower backscatter intensities (dB). ARA and eARA are displayed by a scale representing mean grain size (Φ), with finer sediments represented by darker red hues and coarser sediments represented by lighter cream hues.

2.4.3 Residual statistical analyses

2.4.3.1 Sediment sedimentological properties

A Kruskal-Wallis H test was conducted to compare residual (Φ) values across modality of observed sediment samples for all sites combined (Supplementary Fig.A.1). The result were not statistically significant, $p=.249$. A Kruskal-Wallis H test was conducted to compare residual (Φ) values across sorting of observed samples for all sites combined (Supplementary Fig.A.2). The analysis did not demonstrate statistically significant differences among the groups for all sites combined, $p=.231$.

2.4.3.2 Sediment sampling strategies

A Kruskal-Wallis H test was conducted to compare residual (Φ) values across instruments for all sites combined (Supplementary Fig.A.3). The analysis demonstrated statistically significant differences among the groups, $H(3)=27.157$, $p<.001$. Post-hoc comparisons using Dunn's test with Bonferroni correction for all sites combined indicated that the residual (Φ) values were significantly different across the following pairs: ROV-Day Grab; ROV-Shipek Grab; Box Corer- Day Grab; and Box Corer-Shipek Grab (Table 2.6).

Table 2.6. Kruskal-Wallis post-hoc pairwise comparison between groups for all Sites combined.

Sample 1-Sample 2	Test Statistic	Std.Error	Std. Test Statistic	Sig.	Adj.Sig.[a]
ROV-Box Corer	-17.244	10.601	-1.627	.104	.623
ROV-Day Grab	36.226	9.636	3.760	<.001	.001
ROV-Shipek Grab	-61.935	14.166	-4.372	<.001	.000
Box Corer-Day Grab	18.982	7.010	2.708	.007	.041
Box Corer- Shipek Grab	-44.691	12.529	-3.567	<.001	.002
Day Grab- Shipek Grab	-25.709	11.724	-2.193	.028	.170

Each row tests the null hypothesis that the Sample 1 and Sample 2 distributions are the same.

Asymptotic significance (2-sided tests) are displayed. The significance level is .050.

a. Significance values have been adjusted by the Bonferroni correction for multiple tests.

Sediment samples that were obtained the same year as the acoustic survey, median residual values remain close to 0 Φ with larger deviations from this median value for samples collected 6-20 years after the acoustic survey (Fig.2.9a). While there were no sediment samples acquired in the same year as the acoustic survey for Site A (Fig.2.9b) nor Site C (Fig. 2.9d). Conversely, at Site B, all samples were acquired the same year as the acoustic survey (Fig.2.9c). A Kruskal-Wallis H test was conducted to compare residual (Φ) values across time intervals (based on the years lapsed between the acoustic and sediment sampling survey) for all sites combined. The analysis demonstrated statistically significant differences among the groups, $H(3)=33.348$, $p<.001$. Post-hoc comparisons (Dunn's test) with an applied Bonferroni correction indicated that the residual (Φ) values were significantly different across the following pairs: 0 years and 6-10 years; 0 years and 16-20 years; and 1-5 years and 6-10 years; and 1-5 years and 16-20 years (Table 2.7). These results suggest that there is no statistically significant change in residuals within the first 5 years following the original acoustic survey across Sites A-D. However, beyond this timeframe, residuals tend to increase following a 5-year period from the original MBES survey.

Table 2.7. Pairwise comparison following the Kruskal-Wallis test displaying the relationship between different time intervals on residuals (Φ).

Sample 1-Sample 2	Test Statistic	Std. Error	Std. Test Statistic	Sig.	Adj. Sig.[a]
6-10-16-20	-12.929	16.775	-.771	.441	1.000
6-10-0	51.542	15.200	3.391	<.001	.004
6-10-1-5	62.417	17.083	3.654	<.001	.002
16-20-0	38.613	8.643	4.468	<.001	.000
16-20-1-5	49.488	11.640	4.251	<.001	.000
0-1-5	-10.875	9.226	-1.179	.239	1.000

Each row tests the null hypothesis that the Sample 1 and Sample 2 distributions are the same.

Asymptotic significances (2-sided tests) are displayed. The significance level is .050.

a. Significance values have been adjusted by the Bonferroni correction for multiple tests.

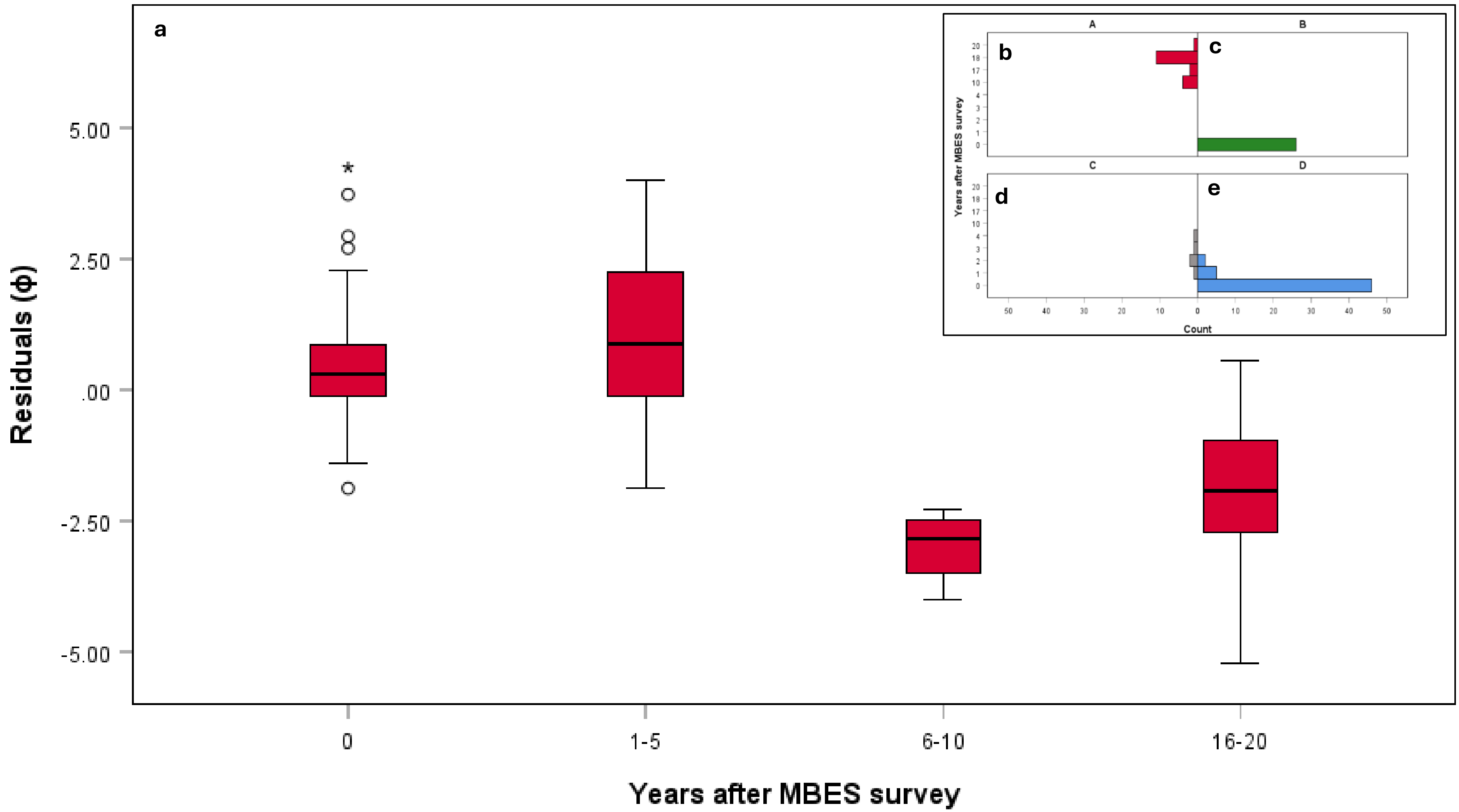

Figure 2.9. (a) Boxplot displaying residuals (Φ) based on the years after the MBES survey the sediment samples were acquired for all sites combined; and subplots (b-e) displaying the distribution of samples across years after the MBES survey: (b) Site A, (c) Site B, (d) Site C, and (e) Site D.

2.5 Discussion

The primary aim of this study was to improve the spatial accuracy of ARA, while maintaining or improving it's classification accuracy. The suitability of the outlined workflow is assessed for its applicability to seabed substrate classifications by large-scale national programmes.

2.5.1 eARA's segmentation and classification accuracy

Spearman's correlation between observed and estimated mean grain size demonstrate eARA's potential to improve traditional ARA's classification accuracy, with three out of four sites either maintaining or improving ARA's accuracy (see section 2.4.1, and Fig.2.5). ARA yielded a higher correlation at only one site (ρ=.71), compared to eARA's (ρ=.67). Moreover, eARA yielded higher overall accuracies for Sites B (96.15%) and D (75.47%), when compared to the overall accuracies derived from the sediment classification scheme employed by INFOMAR at these sites (37% and 46.3%, respectively; Fig.2.10). While Site A was not classified by INFOMAR, this research achieved an overall accuracy of 83.3%. However, eARA's overall classification accuracy for Site C performed poorly with an overall classification accuracy of 20% compared to INFOMAR's accuracy of 50%. It is important to note that eARA's thematic classification was based on three groups (sand, gravel, and mud) compared to INFOMAR's Folk 5 classification (Coarse Sediment; Mixed Sediment; Mud to muddy Sand; Sand; and Rock and Boulders), the latter of which was not seen at all four sites. Lower classification accuracies observed in this study may be attributed to lack of sediment samples, the positioning error of samples (Santos et al., 2018), and other confounding variables (section 2.4.3). Moreover, differences between correlation and overall accuracies are likely attributed to the broad classes assigned, i.e. sand, gravel, and mud. Our findings demonstrate that eARA improves the spatial accuracy of ARA while maintaining its classification accuracy, consistent with classification accuracy results reported in other studies. For example, Santos et al. (2018) achieved a maximum Pearson's correlation of 0.83 (mean) and 0.92 (mode) between ARA derived mean grain size and observed mean grain size; and McGonigle and Collier (2014), achieving an R^2 of 0.23 (Hamon Grab) and 0.69 (Clamshell Grab) between observed and ARA derived mean grain size, however both constrained by poor spatial accuracy associated with traditional ARA. Misiuk and Brown (2022) utilised a multiple imputation approach for multiple AR data achieving an overall accuracy of 95% (k=0.82), although requiring multiple frequencies. Che Hasan et al. (2012) produced a substratum classification though combining angular response classification and backscatter imagery segmentation achieving a maximum overall accuracy of 80.2% (k=0.67), based on three classes. Alevizos and Greinert (2018) applied the interpolated hyper-angular cube (iHAC) and synthetic HAC (sHAC) methods achieving a maximum kappa coefficient of 0.73 and 0.61, respectively. The former of which relies on >100% survey overlap (Alevizos and Greinert, 2018), which is unfeasible for national seabed mapping programmes given the time and cost associated with mapping marine territories.

The segmentation accuracy of eARA is higher in comparison to ARA (Table 2.6). Furthermore, eARA outperformed ARA in two of three segmentation accuracy metrics at Sites C and D. Poor segmentation accuracy was observed at Site B, which can be attributed to the relatively smaller image-objects, with a mean area of 0.015 km^2 and mean length of 0.77 km, within an overall survey area of 5,170 km^2. Consequently, these features were not identified within the eARA classification and exerted a disproportionate influence on the segmentation accuracy assessment. Additionally, while large tracts of seafloor were accurately classified, their impact on the overall analysis was diminished due to their lower frequency within the segmentation accuracy assessment area. The ARA output at Site B was composed entirely of polygons, thus when converting the segments into gridded NumPy-type arrays, the algorithm could not differentiate between the inside and the outside of these polygons, thereby preventing the calculation of the segmentation accuracy metrics. Notably, only small regions within the study sites were assessed in terms of segmentation accuracy as it was not viable to manually digitise the entire survey area of almost 26,000 km^2. Thus, potential uncertainty may have been added to the results as a consequence of this design. According to Che Hasan et al. (2012), the poor spatial resolution of backscatter angular response-based classifications can be solved with segmentation approaches which allows repeatability in contrast to the manual digitising techniques demonstrated in Fonseca et al. (2009). Furthermore, OB segments provide a framework to extract ancillary data (Ierodiaconou et al., 2018b) such as bathymetry, bathymetric derivatives (e.g. slope, rugosity, and bathymetric position index (BPI)), and backscatter derivatives. However, MBES backscatter presents difficulties in segmentation due to inconsistencies in data quality, the heterogeneity of seabed sediments, and the presence of artefacts, particularly nadir artefacts. Moreover, the different resolutions of data present within this study further compounded these issues. Therefore, segmentation parameters were iteratively selected on a site-to-site-basis.

Although this current study focused solely on the segmentation of MBES backscatter, the integration of additional layers such as bathymetry, bathymetric derivatives, and other ARA layers may provide meaningful information to aid the optimal segmentation prior to classification. Additionally, previous research aiming to improve the segmentation accuracy of AR based approaches are often isolated and bespoke. Therefore, eARA provides a robust and efficient approach for MBES applications, comparable to other studies, attaining similar classification accuracies, whilst only requiring single frequency systems, standard survey overlap, and limited ground truth samples. Hence, eARA provides a more robust seabed classification framework than that offered by both traditional ARA, INFOMAR's current classification scheme, and previous research.

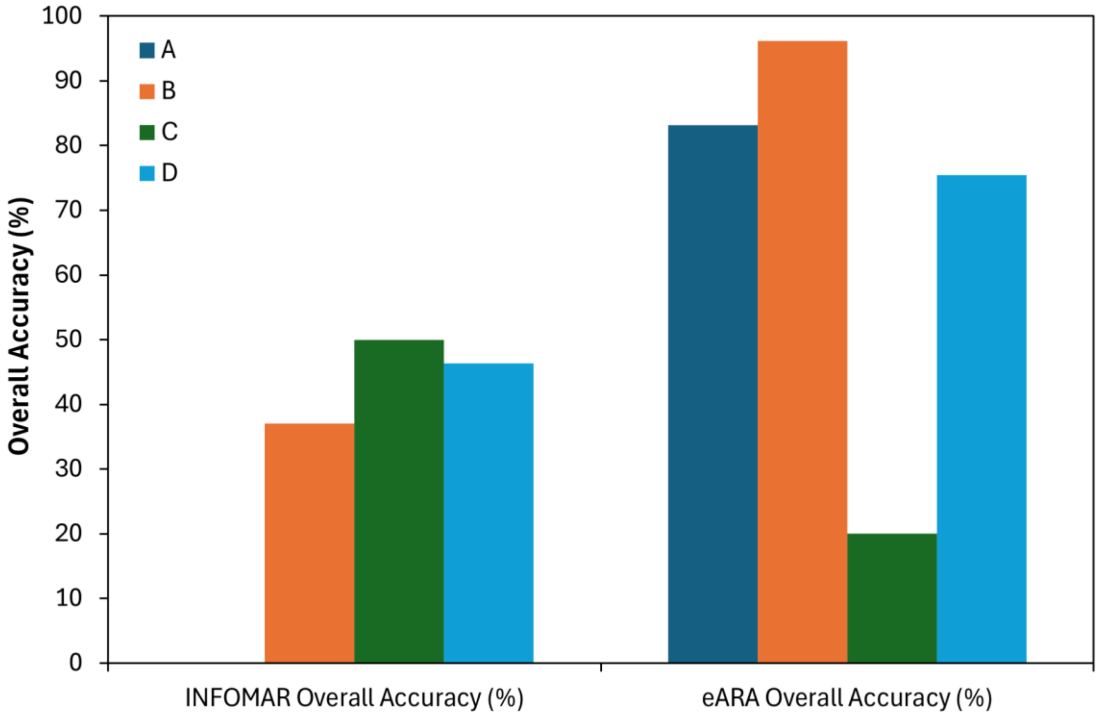

Figure 2.10. Bar graphs comparing the overall accuracy (%): INFOMAR overall accuracy (%) using Folk Classification scheme for Sites A-D (Site A remains unclassified for INFOMAR); and eARA Overall Accuracy (%) for Sites A-D. INFOMAR accuracy was validated against the same sediment samples used for eARA's accuracy assessment.

2.5.2 eARA's effectiveness in relation to geophysical parameters

Results demonstrate variations in both correlation strength and thematic accuracy at different depths; and thus, operating frequencies. Site D achieved the highest correlation between observed and estimated mean grain size, where the data were acquired at an operating frequency of 200 kHz and at depths of 84 - 124 metres, followed by Site B (93-95 kHz; 140 - 364 metres), and Site C (300 kHz; 59 - 75 metres). Site A displayed the poorest correlation, acquired at 12 kHz in deeper waters of 441 -2126 metres. While in terms of overall thematic accuracy, deeper sites and lower operating frequencies displayed a higher overall accuracy (Fig.2.11). Site A obtained poor accuracy results despite being acquired using lower operating frequencies, which is unusual given that ARA is typically assumed to be effective at operating frequencies of <100 kHz, as based on model produced in Jackson et al. (1986). Lower frequencies penetrate the seabed to greater depths (Anderson et al., 2008), particularly in finer sediments such as at Site A. The increased penetration can cause backscatter signals to vary, due to the presence of subsurface layers (Gaida et al., 2019a), which may contribute to poorer classification accuracies at this site. Although, only one site is available at each frequency, several confounding factors such as the temporal offset between the acquisition of datasets, poor data quality, and weather conditions may influence the results. Thus, while this research provides insights into the influence of depth and operating frequencies on eARA, other confounding factors should be considered.

Overall, this research demonstrates that operating frequencies of <200 kHz tend to attain higher accuracies. Although the research topics regarding the influence of depth/operating frequency on the accuracy of ARA have been less explored, previous work has countered the assumption that ARA is limited to operating frequencies of ≤100 kHz, being successfully employed to higher operating frequencies (McGonigle and Collier, 2014; Santos et al., 2018). It is noteworthy that these studies were acquired in relatively shallow waters (<70m) and approximately 300 kHz operating frequencies, with results generally consistent with our study. Therefore, the results herein show that ARA and eARA can be applied to higher operating frequencies than previously assumed and shallower depths. Whilst depth is not a direct assumption of ARA - unlike operating frequency, for example, there are no explicit assumptions regarding how depth affects ARA classifications, aside from its influence on resolution. That said, sedimentary classifications based on physical models, such as the Jackson Model, are typically limited to relatively deep waters and moderately sloping beds (<10°) (Jakeman and Tough, 1988). While the mean slope across all four sites is less that 10°, the maximum slope at each site exceeds this threshold, which may influence classification accuracy. Additionally, a study conducted by Runya et al. (2021), using multi-frequency MBES backscatter showed that lower operating frequencies (30 kHz and 95 kHz) displayed the highest correlation between backscatter strength and observed mean grain size. Given the similar trend between the correlation of estimated and observed mean grain size; and backscatter strength and mean grain size (Supplementary Fig. A. 4), it is likely that higher correlations between mean grain size and backscatter strength will produce more accurate ARA and eARA results. Until now, no research has been completed to determine the influence of operating frequency and depth on ARA. However, it is important to note that that while this study was not conclusive in discerning the influence of depth and operating frequency on ARA and eARA, it provides some clearer indication that operating frequency is likely to have an influence on eARA's and ARA's accuracy. Thus, this knowledge could be further exploited in future research involving multifrequency backscatter ARA and eARA to eliminate the influence of additional variables, providing clearer insight regarding the influence of depth and operating frequency.

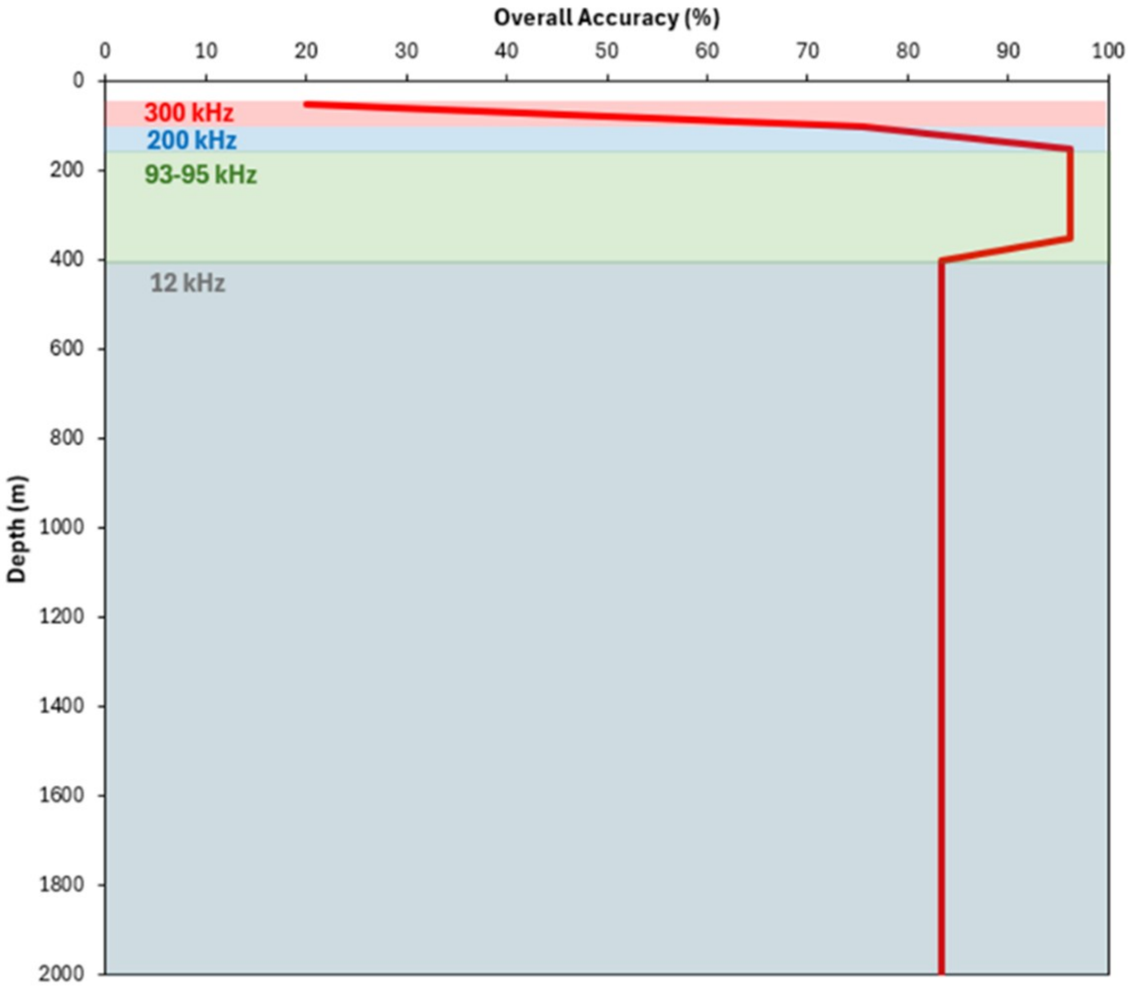

Figure 2.11. Thematic accuracy (corresponding to the red line) based on depth and operating frequency. The grey polygon represents depths of 441 – 2126 metres (12kHz), the green polygon represents depths of 140 – 364 metres (93 – 95 kHz), the blue polygon represents depths of 84 – 124 metres (200 KHz), and the red polygon represents depths of 57-75 metres (300 kHz).

2.5.3 The limitations imposed by sediment sedimentological properties and sediment sampling strategies

Although our results indicate a high-accuracy, differences between the measured mean grain size and estimated mean grain size (i.e. residuals) may be explained by various factors such as the time between acoustic and sampling surveys as well as sampling instrument. The difference between measured and estimated grain size was not significantly different based on modality of sediment samples (i.e. unimodal, bimodal, and trimodal) and sorting. Thus, there is not significant differences in the error of the estimation based on the modal distribution or sorting. This is generally consistent with previous research (Santos et al., 2018), where ARA performed well despite several multimodal compositions and poorly sorted samples. However, Santos et al. (2018) reported higher residuals were located in poorly sorted areas, therefore may be indicative of significant differences in residuals based on the sorting of the sediment samples and thus, potentially the modality of sediment samples. Which is generally consistent with contemporaneous research as sorting plays an important role in backscatter sediment relationships (Goff et al., 2004; Ferrini and Flood, 2006; Huang et al., 2018).

We analysed residuals to determine the influence of the instrument of sediment sampling (Section 2.4.3). Table 2.6 shows that this difference varies from instrument to instrument i.e. ROV and Day Grab; ROV and Shipek Grab; Box Corer and Day Grab; and Box Corer and Shipek Grab. This is to be expected given the volume of retrieved sample, the penetration depth, surface area of instrument, and ability of the instrument to retrieve sample undisturbed to the vessel. This is generally consistent with McGonigle and Collier (2014) as different instruments obtained different classification accuracies: R^2 of 0.23 (Hamon Grab) and 0.69 (Clamshell Grab) between observed and ARA derived mean grain size, which may be indicative of the footprints of the instruments 0.1m^2 and 1m^2, respectively. Furthermore, as Box Corers (>3L) can penetrate up to 1m with a surface area of 0.25m^2 (INFOMAR, 2007), samples may be disturbed, therefore this may account for the significant difference between Box Corers and Shipek Grabs (p=.002); and Day Grabs (p=.041). Whilst, day grabs and shipek grabs (<3L) can only penetrate <15cm and <10cm, with a surface area of 0.01m^2 and 0.04m^{2,} respectively (INFOMAR, 2007). Additionally, the penetrative depth of the MBES system, dependent on the sediment composition and the operating frequency which may lead to discrepancies between the observed and estimated mean grain size. Backscatter datasets acquired using higher operating frequencies (300 – 450 kHz) are generally representative of surficial sediments, while backscatter acquired at lower operating frequencies (90 – 100 kHz) may vary, due to the presence of subsurface layers (Gaida et al., 2019a). Lower frequencies penetrate the seabed to greater depths (Anderson et al., 2008), especially in finer sediments. Various depths of penetration have been reported dependent on operating frequency and sediment composition, <12 m in fine sediments (12 kHz) (Schneider Von Deimling et al., 2013), 0.1 m to 1 m depending on sediment composition and grazing angle at 95 kHz (Fonseca et al. 2002), and between 2 and 10 mm in fine sediments using higher frequencies (300 kHz) (Zimmer et al., 2010). Positional error of sediment samples that were acquired on the border of acoustic facies may have led to discrepancies between estimated and observed grain sizes (Santos et al., 2018), assuming a positioning error of 5-6 metres in approximately a water depth of 100 metres (Blaschke, 2010). This case may be prevalent for Sites C and D due to the spatial heterogeneity of the seafloor sediments. Additionally, unbalanced data may contribute to this, in particular at Site D; Day Grab (n=46) and Shipek Grab (n=7) (Supplementary Fig.A.3). Albeit, as mentioned by McGonigle and Collier (2014), irrespective of the unequal sample sizes, the different sampling strategies may be of relevance in terms of the success.

The temporal offset between the acquisition of the MBES data and the sediment sampling was also used to explain the difference between measured and estimated mean grain sizes (Section 2.4.3), while residuals typically remain lower for samples acquired within the same year or a few years after the acoustic survey (Fig. 2.8). Post-hoc analyses indicated significant differences between estimated mean grain sizes and ground truth grain size data for sediment samples acquired >5 years after the acoustic survey (Table 2.7). Surprisingly, no significant difference was observed between the 6-10 and 16-20 time intervals, this is possibly due to limited samples within the 6-10 year period. These findings are relevant to the training of ARA data through BPCs, these samples should ideally be acquired within the same year as the acoustic survey. This is particularly relevant in highly hydrodynamic environments where significant changes may be observed due to the movement of surficial sediments particularly in areas dominated by finer sediments. Moreover, in regards to Site A, previous literature within or in close proximity to this site suggest current velocities of approximately 34-40 cm s^{-1} (Dorschel et al. 2007; Lim et al., 2018), while scour features around coral mounds indicate low-frequency high magnitude events (Lim et al., 2018). Furthermore, previous research suggests that the Belgica Mounds in the Porcupine Seabight are influenced by strong bottom currents in a very dynamic environment between currents, sedimentation and active transport (Foubert et al., 2011). Further stating that geomorphological features (e.g. sand waves, furrows and barchan dunes) are indicative of active sediment transport and even erosion (Foubert et al., 2011, 2005; Huvenne et al., 2005; Wheeler et al., 2005). Foubert et al. (2011) suggest more instantaneous, low-frequency high amplitude velocities, with peak velocities of 60 cm s^{-1} (Roberts et al., 2005). Therefore, given the relatively long temporal offset (>20 years) between the acoustic and sediment sampling survey at Site A, this may attribute to the larger residuals found at this site. Previous research completed in the Irish Sea may be indicative of similar conditions for study sites in the Celtic Sea. For example, Coughlan et al. (2021) postulated that up to 35% of sediment coverage is mobilised more than 50% of the time, while only 2% of the area experiencing 0% sediment mobility within a one-year period, on average, in the Irish Sea. This could contribute to larger residual errors, especially in areas dominated by finer sediments (Fig.2.3a), which are susceptible to sediment mobilization. Although. there was no significant difference in residuals in Sites C and D, all sediment samples located in the Celic Sea region were acquired in a relatively short time frame after the acoustic survey (0 – 5 years). Given, the relatively short time frame and relatively deep water, the main short-term stressors on the seabed in this region may be due to anthropogenic activities such as fishing, which is extensive in this region (Thompson et al., 2017). Albeit, we did not see a statistically significant difference in residuals within this time frame. Of course, there are other factors contributing to larger residuals e.g. lower resolution datasets for deeper waters. McGonigle and Collier (2014) suggests a significant capacity for changes in distribution of surficial sediments over a period of 201-261 days between the acquisition of ground truth and acoustic datasets in a site with water depths of <70 m. These findings align with Santos et al. (2018), who observed moderate to large differences in correlations between observed and estimated grain sizes for samples acquired up to 5 years after acoustic surveys. Albeit, their shorter temporal offset (<5 years) likely reflect higher hydrodynamics experienced in the River Tagus estuary compared to the ≤20-year period observed in this study.

2.5.4 The broader implications, required resources, and propose steps for upscaling this workflow across national programmes

As nations endeavour to expand ORE capacity, characterisation of seafloor sediments is pertinent (Coughlan et al., 2020b). Given the time, cost and environmental impacts associated with offshore geophysical surveying, national programmes with existing multibeam data will play a vital role in supporting offshore development (Guinan et al., 2021).

Given the timely nature of this research, driven by the vast volumes of data generated from large-scale mapping programmes and the increasing global demand for ORE, a standardised, objective, and efficient approach is required to more accurately characterise the seafloor. Given that as MBES data has a 'shelf life', the requirement of higher resolution multibeam data and backscatter data at the same resolution, is crucial to aid the development of ORE (GDG, 2021), in-turn resulting in greater volumes of data. Thus providing the ability to create higher resolution seabed substrate maps at both regional and national levels. Accordingly, data processing methodologies must be harmonised and standardised across surveys, as reliable data regarding the marine environment and how we make use of data is essential (Guinan et al., 2021). Currently, seabed characterisation methodologies are fragmented, differing on a site-to-site basis, as methods may not transfer to all environments (Diesing et al., 2020). Subsequently, due to the complexities of marine sediment classification, INFOMAR must employ a range of approaches including Quester Tangent Corporation (QTC) Multiview, OBIA, and manual interpretation techniques (Guinan et al., 2021). The latter of which is not feasible across the large-scale databases, as it is subjective, time consuming, and not repeatable (Guinan et al., 2021). Among these techniques, OBIA offers a scalable approach for different resolution datasets (Summers et al., 2021), which is essential for large-scale mapping programmes such as INFOMAR and MAREANO. Accordingly, eARA has proven successful in a variety of environments, acquired using a range of operating frequencies, sonars from older legacy sonars to modern sonars, vessels, and in ranging water depths. Findings presented here and previous literature supports the applicability of ARA to different environments such as environments with strong hydrodynamic influences (Santos et al., 2018), using a range of operating frequencies (McGonigle and Collier, 2014; Santos et al., 2018), and at different depths. However, it is important to note that this workflow may be subject to limitations. Sites B-D were dominated by features with sharp demarcations between sediment types, which are more conducive to an OBIA approach (Guinan et al., 2021). Therefore, the effectiveness of eARA may be limited in regions with gradational sedimentary boundaries. Moreover, poor results for Site A, may be attributed to poor backscatter data quality that can be seen across several INSS backscatter data areas. Thus, this approach may not be applicable to those INSS areas with poorer backscatter data quality. Nonetheless, eARA provides the potential to upscale this method across the INFOMAR database, showcasing its repeatability and consistently as a robust and standardised approach to seabed classification, additionally providing grain-size distribution information unlike INFOMARs current Folk Classification scheme, which is invaluable to a variety of sectors.

The research presented here provided classified seabed maps at a the same spatial resolution of the ARA, while improving spatial accuracy and providing more meaningful classifications of seabed facies. While, in terms of training-datasets, only one sample was required per site, additional PSA data are required for the validation of classifications especially in those areas suitable for ORE infrastructure (GDG, 2021). Moreover, this research has also given insights into the struggles classifying deeper water Sites (>400m) of INSS data due to the quality of datasets, spatial resolution, and the temporal offset between acoustic and sediment sampling surveys. This has indicated that additional datasets within these locations are required to effectively manage these areas.

2.6 Conclusion

This research aimed to develop a robust sediment classification framework, which could subsequently be applied across large-scale databases such as INFOMAR. Results presented herein demonstrate an overall improved classification accuracy compared to existing classification results in these same regions. Through the integration of image-based backscatter processing with OBIA and ARA enhances current ARA workflows providing a robust and scalable approach for seabed characterisation. While many studies have alluded to the integration of OBIA and ARA, few studies have applied this coupled methodology for seafloor substrate classification. Moreover, though several studies have endeavored to improve the spatial accuracy of ARA, many of which are isolated, resource-intensive, and have yet to be widely implemented. Thus, eARA is a promising approach for achieving a relatively high classification and segmentation accuracy in a repeatable and scalable approach, requiring limited training data, establishing a framework that can be applied to large-scale mapping programs such as MAREANO and INFOMAR. Although this research was constrained by lack of sediment samples, poor data quality, and temporal offset between hydrographic and sampling surveys, presenting difficulties to conclusively discern the influence of depth and operating frequency on the classification. Nevertheless, this research offers insights into the influence of depth; operating frequencies; sediment sedimentological parameters; and sediment sampling strategies on eARA. Future research will focus on extracting additional information into eARA segments such as bathymetry, bathymetric derivatives, and magnetometry data to eARA segments, enhancing the value of the information that can be derived from existing datasets. Recommendations coincide with Seabed 2030 and the growing global demand for ORE, emphasising the need to better utilise open-access datasets and provide scalable approaches for seabed characterisation to aid marine management and spatial planning.

Preface to Chapter 3

This chapter was written in peer-reviewed style. The work was subsequently submitted to Applied Ocean Research on 3rd September 2025.

The Irish government has faced persistent challenges in meeting EU renewable energy targets, leading to an urgent demand for offshore renewable energy (ORE) in Ireland. In turn, Ireland has transitioned from a developer-led, decentralised approach to a centralised, plan-led approach in relation to the development of ORE and at the forefront of this is the South Coast Designated Maritime Area Plan (SC-DMAP), which is zoned for fixed-foundation ORE structures. A comprehensive understanding of seabed dynamics and geological constraints is crucial for the de-risking and timely development of ORE within SC-DMAP. In this research, high-resolution, time-lapse bathymetry datasets, grain size information via enhanced angular range analysis and various theoretical formulae are employed to understand the spatio-temporal seabed change and investigate the hydrodynamics within Tonn Nua, in the North Celtic Sea. Analyses show that sandwaves are relatively stable, migrating at an average of 0.25 and 0.26 m yr^{-1} between 2007 - 2024 and 2013 - 2024, respectively. A mean residual current of 41 cm s^{-1} is estimated in northeast – southwest prevailing flow, coincident with legacy current velocity measurements and landform derived current velocity estimations. These findings elucidate the presence of mobile sediment, seabed scour, sandwaves and potential bedrock outcrops that may influence the development of ORE at the site. The identified constraints allow for more effective cable route planning and foundation design to ensure the safe development and longevity of offshore subsea structures.

Author contributions

CB: Conceptualization, Methodology, Formal analysis, Investigation, Software, Validation, Visualisation, Data curation, Resources, Writing-original draft, Project administration. **GS:** Methodology, Resources, Writing- review and editing, Supervision. **LO:** Methodology, Resources, Writing- review and editing, Supervision. **AL:** Conceptualization, Methodology, Resources, Supervision, Writing- review and editing, Project administration, Funding acquisition.

Chapter 3: Seabed Dynamics and Geological Constraint Mapping for Offshore Renewable Energy: Insights from Tonn Nua, North Celtic Sea, NE Atlantic

(Current Status: Under Review Applied Ocean Research)

Cara Brennan[1,2*], Gerard Summers[1,2], Larissa Macedo Cruz de Oliveira[1,2] and Aaron Lim[1,2]

[1] Earth and Ocean Lab, Department of Geography, University College Cork, Cork, Ireland

[2] Sustainability Institute, University College Cork, Lee Road, Cork, Ireland

3.1 Introduction

Ireland's location along the NE Atlantic Ocean offers one of the highest resources of wind and wave energy in the world (Cummins and McKeogh, 2020; Gaughan, 2020). Despite this vast resource of offshore renewable energy (ORE) (Dinh et al., 2021), Ireland is falling behind its European counterparts in terms of capitalising on its ORE resources (Cummins and McKeogh, 2020). Harnessing these resources is fundamental to Ireland's decarbonization efforts to meet European Union (EU) targets, providing a sustainable energy source and enhancing energy security. The European Green Deal has pledged to address the emissions of greenhouse gases to achieve net-zero emissions by 2050 (Martinez and Iglesias, 2022). In line with these goals, renewable energy targets set by the EU have been the main driver behind the development of both onshore and offshore wind (OW) energy (Cummins and McKeogh, 2020). However, the further development of onshore wind is constrained by factors such as visual impacts, noise pollution, and a lack of suitable locations (Martinez and Iglesias, 2022).

To address these issues, the Irish government has set ambitious targets to deliver 5 gigawatts (GW) of OW capacity by 2030 and 37 GW by 2050 (Cummins and McKeogh, 2020; DECC, 2024; Esmaeili et al., 2024). Fixed-bottom and floating OW technologies are vital to meet this capacity and address these targets (O'Hanlon and Cummins, 2020). This drive has led to a plan-led approach for marine spatial planning, exemplified by the South

Coast Designated Maritime Area Plan (SC-DMAP), which identifies four key potential ORE maritime areas offshore Ireland: Tonn Nua; Lí Ban; Manannán and; Danu (DECC, 2024). Therefore, reliable, high-resolution marine data is an essential prerequisite to provide essential knowledge on the marine environment for marine spatial planning (Guinan et al., 2021) and marine management (Cogan et al., 2009).

The mapping of geohazards, both natural and anthropogenic, is crucial to the development of ORE infrastructure. Natural constraints may pose risks to the development and lifetime of offshore structures, such as sandwaves (Whitehouse et al., 2000), seabed scour (Whitehouse et al., 2011), mobile sediment (Coughlan et al., 2020a), shallow gas (Li et al., 2025) and slope instability (Song et al., 2023). Sandwaves, commonly referred to as dunes, are typically indicative of an abundant sediment supply and a mobile seabed (Whitehouse et al., 2000), exhibit wavelengths of 5–500 m, heights of 0.5–5 m, with average flow velocities of 0.3–0.75 m s^{-1} (Stow et al., 2009). These features act as a sediment transport mechanism and are commonly found on continental shelves and submarine canyons (Yang et al., 2022), such as in the Irish Sea (Creane et al., 2022), northern South China Sea (Yang et al., 2022), western Barents Sea (Bellec et al., 2019), and North Sea (Leenders et al., 2021). Research has highlighted the potential risk of sandwaves to ORE developments, such as exposure of pipelines and cables, influencing the design bed level of a structure, and indicating sediment mobility (Whitehouse et al., 2000). Additionally, scour around marine structures is a well-recognised issue associated with the development of ORE, resulting from natural features such as rock outcrops or anthropogenic features such as pilings, shipwrecks and foundations (Quinn and Smyth, 2018; Whitehouse et al., 2011), threatening the stability and longevity of the structure (Wei et al., 2024).

Seabed erosion and sediment transport, including the movement of bedforms, occur over various timescales from weeks to decades and are driven by variations in tidal range, currents, storm surges and wave action (Whitehouse et al., 2011). Bedload transport via bedform migration can occur under mean, wave current, or combined wave current conditions (Coughlan et al., 2021; Lichtman et al., 2018). This usually results in sediment eroding from the stoss side and deposited on the lee side of bedforms, resulting in migration in the direction of the prevailing hydrodynamic forcing (Lichtman et al., 2018). However, in some cases, phenomena such as reversed or counter-current migration may occur where bedforms are shifting in an atypical direction (Boggild et al., 2024; Van Landeghem et al., 2012). Understanding near-bed currents is essential to characterise the hydrodynamic regime. Bottom current velocities can be estimated through hydrodynamic modelling (e.g., MIKE Software), empirical formulae (Soulsby et al., 1997) and bedform velocity matrices (Stow et al., 2009). Empirical formulae, such as Soulsby et al., (1997), use mean grain size to estimate current velocity 1 m from the seabed. Although grain size data are often limited to point locations, recent developments such as Angular Range Analysis (ARA) (Fonseca et al., 2009; Fonseca and Mayer, 2007b) provide a more spatially comprehensive and robust grain size estimation to incorporate into such formulae or models. While ARA is constrained by its poor spatial resolution, enhanced Angular Range Analysis (eARA) provides a more spatially robust characterisation of mean grain size through integrating object-based image analysis (OBIA) and multibeam backscatter data (Brennan et al., 2025).

Large-scale national studies, such as Peters et al. (2020), have produced geological stability models supporting ORE. Furthermore, Arosio et al. (2023b) mapped Ireland's marine geomorphology at a national scale. At a regional scale, the northern Irish Shelf has also been extensively studied via time-lapse datasets (Evans, 2018) and hydrodynamic modelling (Evans, 2018), relevant to ORE developments. Similarly, research within the Irish Sea has concentrated on ORE through seabed mobility modelling (Coughlan et al., 2021), geological and geotechnical constraint mapping (Coughlan et al., 2020a), and time-lapse bathymetry to track sediment wave migration (Creane et al., 2022; Van Landeghem et al., 2012). Conversely, within the Celtic Sea, near to the Tonn Nua site, studies primarily focused on subsurface geology to reconstruct Quaternary events linked to the Irish Ice Sheet dynamics (Giglio et al., 2022a; Tóth et al., 2020), subglacial hydrology (Giglio et al., 2022b), past glacial processes (Gallagher, 2002), and deglacial dynamics (Lockhart, 2019). Despite this research, there is a distinct gap relatingto surface geological conditions and marine hydrodynamics with a specific focus on ORE within the Irish portion of the Celtic Sea.

In this study, we integrate well-established theoretical formulae and estimated grain size via eARA with time-lapse bathymetry data to investigate the seabed conditions and hydrodynamic regime of the Tonn Nua site. Thus, this research aims to address the following research aims and objectives: i) Investigate the geomorphology of the proposed Tonn Nua site; ii) Assess the spatio-temporal variability of Tonn Nua; iii) Investigate the hydrodynamics of the site; and iv) Evaluate the seabed stability of Tonn Nua and therefore what are the implications for the development of ORE.

3.2 Study Site

The Celtic Sea is a semi-enclosed shelf sea to the northwest of Europe, connected to the tidally energetic Irish Sea through St. George's Channel (Carrillo et al., 2005). Currents during spring tide near Nymphe Bank are ~0.3 m s^{-1} compared to St. George's Channel, where current speeds exceed 1 m s^{-1} (Carrillo et al., 2005). Tides play an important role in the Celtic Sea, with the M_2 and S_2 constituents accounting for 90% of the total tidal Kinetic energy (Pingree, 1980). Previously glaciated by the British Irish Ice Sheet (Tóth et al., 2020), the Celtic Sea Shelf is comprised of surficial glaciogenic Quaternary deposits, mud, sand, boulders and bedrock outcrops (Hamilton et al., 1980; Lockhart et al., 2018; Pantin and Evans, 1984; Scourse et al., 1990).

Previous studies within the study site or surrounding area include restricted or high-resolution multibeam bathymetric data and various sources of seismic data (Gallagher, 2002; Gallagher et al., 2004; Tóth et al., 2020) and onshore digital terrain data (Tóth et al., 2020). These studies reveal a series of submerged glaciogenic erosive and depositional features. Gallagher et al. (2004) identified a series of NNW-SSE trending bathymetric ridges south-west of Hook Head, interpreted as glacial moraines divided into "Inner Arcs" and "Outer Arcs" associated with the retreat of the Irish Sea Ice Stream eastward. Re-interpreted as an esker, the "Outer Arcs", north-south oriented seabed ridge represents southward-flowing subglacial meltwater during a limited advance of the Irish Ice Sheet onto the Celtic Sea shelf (Tóth et al., 2020). Offshore between Dungarvan and Kilmore Quay, the Quaternary stratigraphic record documents a sequence of deposition and erosion consistent with regional glacial models (Tóth et al., 2020).

Situated in the north Celtic Sea off the coast of County Waterford, our study site extends between Dungarvan and Dunmore East to the eastern portion of the site. The Tonn Nua site is one of four proposed offshore renewable energy sites within Ireland's SC-DMAP (Fig.3.1), being the closest in proximity to shore (approximately 12 km). Tonn Nua covers an area of approximately 306 km^2 (DECC, 2024), with a minimum water depth of 47 m and a maximum water depth of 69 m. The proposed site has been identified as a proposed location for fixed foundation ORE development (DECC, 2024).

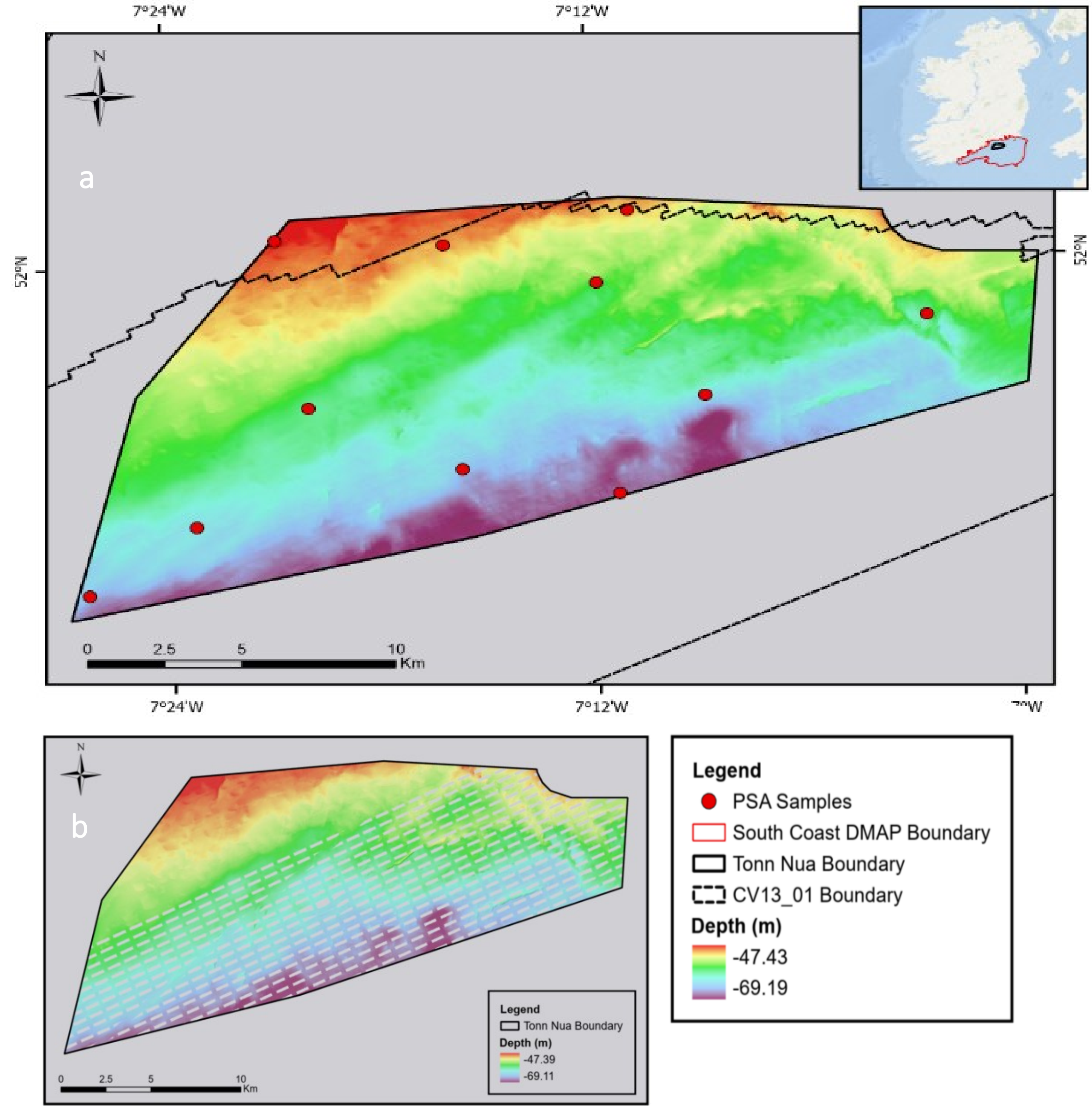

Figure 3.1. (a) Bathymetry of Tonn Nua study site within the South Coast DMAP acquired between 2007 and 2013, displaying particle size analysis (PSA) INFOMAR sediment samples. The dashed line represents the CV13_01 survey extent within the site, while the northern part of the site is derived from CV07_02 survey. (b) New bathymetry for the Tonn Nua site acquired in 2024 (TC24_016).

3.3 Materials and Methods

3.3.1 Sediment Sampling

Grain size data were obtained through particle size analysis from laser granulometry with a Malvern Mastersizer (INFOMAR, 2007). Particle Size Analysis (PSA) sediment samples utilised in this research were acquired over various surveys in Irish waters and were provided by the Marine Institute (MI). A total of 11 sediment samples from this database were acquired within our study site between 2013 and 2021. These data were extracted and converted to UTM 29N co-ordinates and imported into ArcGIS Pro v3.2. Ten of these samples were obtained using day grabs with only one sample acquired using a shipek grab. In this research, mean grain size using Folk and Ward (Folk, 1954) was the only parameter used from these samples.

3.3.2 Multibeam Echosounder

Multibeam data utilised in this research were acquired over three separate surveys in a period between 2007 and 2024 aboard the RV *Celtic Voyager* and RV *Tom Crean* (Table 3.1). The older datasets (CV07_02 and CV13_01) were acquired as part of the INFOMAR programme, while the newest dataset (TC24_016) was acquired by the Department of Climate, Energy and the Environment (DECC). All data were acquired using Kongsberg multibeam systems. Data acquired during survey CV07_02 were acquired using a hull mounted Kongsberg Simrad EM1002 at an operating frequency of 93–95 kHz, with an angular coverage of approximately 66–68˚, 111 soundings per ping, and at a survey speed of 7.5 knots (Sheehan and Borovik, 2007). Data acquired during survey CV13_01 were acquired at a survey speed of 7 – 8 knots with a hull mounted Kongsberg Simrad EM3002 at an operating frequency of 300 kHz, with 508 soundings per ping and a maximum angular coverage of 70˚ per head (Sheehan, 2013). Data acquired during survey TC24_016 were acquired using a Kongsberg Simrad EM2040 MKII dual head multibeam at 300 kHz fitted on a retractable pole, with ≥800 beams per ping and a maximum beam width of 200˚(Marine Institute, 2024). Raw data were stored in *.all or *.kmall file formats.

Table 3.1. Survey information for all three multibeam echosounder datasets acquired between 2007 and 2024.

Survey ID	Year	Month	Vessel	IHO Standard	Source
CV07_02	2007	Sept - Oct	RV Celtic Voyager	IHO Order 1	INFOMAR
CV13_01	2013	April - May	RV Celtic Voyager	IHO Order 1a	INFOMAR
TC24_016	2024	July	RV Tom Crean	IHO Order 1b	DECC

Processed bathymetric grids and backscatter mosaics were obtained via the INFOMAR Marine Data Download Portal (see Table 3.1), while the 2024 dataset was obtained from DECC. The TC24_016 survey data were divided into crosslines and mainlines within the Tonn Nua site. All bathymetric grids and backscatter mosaics were resampled to a 5 m resolution and projected to WGS 1984 UTM Zone 29. The bathymetric grids were merged and smoothed using the ArcGIS focal statistics tool with a mean filter and a circular radius of 5 to reduce the impact of acquisition artefacts in the datasets, while preserving small scale features. The focal statistics tool applies a neighbourhood-based operation that generates an output raster, where the value of each cell is determined by the values of surrounding cells with a defined neighbourhood (Gafeira et al., 2018). This process was repeated for the CV07_02 and CV13_01 surveys. The smoothed bathymetric grids were then used for subsequent analysis. The backscatter mosaics for the CV07_02 and CV13_01 surveys were harmonised and merged into one backscatter mosaic using the Bulk-Shift method implemented in R Studio v2024.12.0+467 as outlined by Misiuk et al. (2020). This method was then applied to the mainlines and crosslines for the TC24_016 dataset, merging the crosslines and mainlines into one backscatter mosaic. The two merged backscatter mosaics were then used for subsequent analysis.

Angular Range Analysis (ARA) was applied within QPS FM Geocoder Toolbox (FMGT) v7.11 software on raw backscatter data following manufacturers' recommendations (Quality Positioning Services (QPS), 2022) as detailed in Brennan et al. (2025) to determine mean grain size (Φ). ARA could not be produced for survey CV07_02 due to sound velocity errors and variable heights between lines, which could not be resolved in post-processing. One beam pattern correction (BPC) was applied to CV13_01 using the known mean grain size derived from MI sediment samples. While no BPC was applied to the TC24_016 dataset, due to the limited sediment samples.

3.3.3 Seabed Geomorphology

To investigate the seabed geomorphology of the study site, a set of terrain variables and bathymetric derivatives were derived from the processed bathymetric grids (Table 3.2). Geomorphons is an algorithm that isolates ten landform elements from a bathymetric DEM based on the principle of pattern recognition, where every scan of the DEM assigns an appropriate geomorphon class to each raster cell and self-adapts to find the most appropriate spatial scale (Jasiewicz and Stepinski, 2013). Geomorphons produces an integer raster that assigns a number to each raster cell between 1 and 10 (Arosio et al., 2023b). A set of bathymetric derivatives were calculated using Benthic Terrain Modeller (BTM) (Walbridge et al., 2018) (Table 3.2). Slope measures changes in elevation along the steepest incline on the seafloor (Strachan, 2021; Wilson et al., 2007). Based on Topographic Position Index (TPI) (Weiss, 2000), BPI classifies seabed structure based on changes in slope position over two scales (broad and fine scale BPIs) (Walbridge et al., 2018), representing the positional difference of a pixel compared to the mean elevation of all cells in an annulus (Arosio et al., 2023a; Walbridge et al., 2018). Vector Terrain Ruggedness (VRM) is a measure of the difference in elevation between adjacent cells in a DEM (De Oliveira et al., 2020), running on a scale of 0 to 1, the latter of which indicates complete variation (Evans et al., 2015). Aspect is a measure of surface orientation (Walbridge et al., 2018), with Cos Aspect relating to northness and Sin Aspect relating to eastness (Walbridge et al., 2018). Aspect identifies the downslope direction of the maximum rate of change of each cell value to the neighbouring cells (Arosio et al., 2023a). Profiling tools in ArcGIS were used to determine sandwave morphology (Height (m), Wavelength (m), Stoss Length (m), Lee Length (m), Depth (m), and Lee Slope (˚)) within an area of interest (AOI).

Table 3.2. List of terrain variables used in this study along with information regarding the methodology used to obtain variables.

Terrain Variable	Notes	Method
Bathymetry	Water depth	Section 3.3.2
Backscatter	Seafloor hardness	Section 3.3.2
eARA	Mean grain size	Section 3.3.4 (Brennan et al., 2025)
Geomorphons	Identifies seabed landforms	*Geomorphon Landforms* tool ArcGIS (Jasiewicz and Stepinski, 2013)
Slope		3 x 3 window Benthic Terrain Modeller (BTM) (Walbridge et al., 2018)
Vector Ruggedness Measure (VRM)		Neighbourhood size 19 BTM (Walbridge et al., 2018)
Multiple Scale BPI	Fine scale and broad scale BPI. Annulus neighbourhood defined by inner and outer radius	Inner radius 5, 25 Outer radius 25, 250 Scale factor 125, 1250 BTM (Evans et al., 2015; Walbridge et al., 2018)
Aspect		BTM (Walbridge et al., 2018)

3.3.4 enhanced Angular Range Analysis (eARA)

To investigate the mean grain size (Φ) and spatial distribution of seabed sediments across our study site, the merged backscatter mosaic for the TC24_016 dataset was first segmented in ArcGIS using the mean-shift segmentation algorithm (Comaniciu and Meer, 2002). The same method was then applied to the merged backscatter mosaic derived from the CV07_02 and CV13_01 surveys. Mean grain size estimates, derived from the corresponding ARA data, were extracted into the underlying segments using the ArcGIS *Zonal Statistics* tool (see Brennan et al. (2025) for a detailed description). As the ARA could not be produced for the CV07_02 dataset, the eARA derived from the combined CV07_02-CV13_01 mosaic is restricted to the CV13_01 survey area. Accordingly, mapping the spatial distribution of sediments throughout the site for both datasets.

3.3.5 Seabed Change

Time-lapse surveys were available over three periods within the study site (see Table 3.1). Bathymetric datasets for surveys CV07_02, CV13_01 and TC24_016 were utilised to quantitatively evaluate the vertical and horizontal change over time, therefore providing an understanding of the morphodynamics within the region.

Monitoring seabed change is commonly assessed through the comparison of Digital Elevation Models (DEMs), derived from time-lapse hydrographic surveys (Schimel et al., 2015). To quantify changes in elevation and highlight areas of erosion and accretion, a DEM of Difference (DoD) is produced (Schimel et al., 2015). However, as detailed in Schimel et al. (2015), uncertainty in bathymetric datasets can hinder accurate assessment of seabed change. In this study, processed INFOMAR bathymetry grids were used, limiting our ability to quantify such uncertainty. To account for the horizontal and vertical uncertainty, a minimum quality of data accepted for this study was IHO S-44 Order 1, as we were restricted by the availability of datasets in the region. The CV07_02 MBES dataset was vertically levelled to Lowest Astronomical Tide (LAT) using tide gauge data and datum shifts, whilst the CV13_01 and TC24_016 MBES datasets were vertically levelled to LAT via the Vertical Offshore Reference Frame (VORF) model. Despite this, acquisition artefacts present in the INFOMAR datasets complicated the interpretation of DoD outputs, making vertical elevation changes difficult to discern. Neither the application of filters nor a static vertical offset between datasets significantly improves this issue. Albeit distinct changes in elevation were observed around bedforms. Subsequently, the ArcGIS *change detection* tool was applied to compare the geomorphons layers to detect changes around geomorphic features. Values from the DoD (derived via subtraction of the bathymetric datasets) were then extracted within these regions to determine vertical elevation specifically around geomorphic features.

Line profiles were drawn across selected geomorphic features, and the resulting profiles were extracted and plotted in R Studio to visualise areas of deposition and erosion. Additionally, the elevation change along the profiles were measured to ensure that no static offset errors were present.

An AOI was selected in the study site (as shown in Fig.3.4) as it encompassed sandwaves from all three surveys without the presence of gaps seen in the newest dataset. Moreover, this research adapted the methodology used in Creane et al. (2022) to estimate the migration rates and direction of sandwaves in an AOI within the study site (as shown in Fig.3.4). Geomorphon landforms were reclassified as shoulder, peak and ridge landforms within the AOI and thinned to reduce the azimuth bias when manually delineating features. Crestline features between successive surveys were manually digitised with the aid of slope and rugosity rasters. Points were generated spaced at 10 metres apart along the digitised line for the older crestline. Perpendicular transects were generated along the old crestline at 10 metres spacing and the *Intersect* tool was used to determine the intersection point with the newer crestline. The x and y coordinates were calculated for each point on the oldest crestline and the intersection point with the newest crestline. The *Spatial Join* tool was used to merge the point files into a single shapefile, with the x and y coordinates of the old and new points. The distance and bearing between the lines were then calculated using the *Field Calculator*. This process was applied to the datasets for period 1 (2007 and 2024) and period 2 (2013 and 2024) for sandwave features within the AOI.

3.3.6 Current velocity estimation and hydrodynamics

As detailed by Lim et al. (2018), to understand the benthic hydrodynamic conditions within our study site, we estimated current velocity from the mean grain size. The mean grain size derived from the eARA raster was used to estimate the current velocity for each eARA segment. Grain sizes less than 10 µm (approximately > 6.64 Φ) can be disregarded as they are subject to flocculation (McCave et al., 1995). Critical current velocity erosional threshold from particle size distribution, as proposed by Soulsby (1997), can be calculated from equation 1. Therefore, this approach assumes that particle size reflects the benthic current regime and estimates the critical current velocity 1 m above the seabed that is required to transport sediment grains (Lim et al., 2018).

$$\mathcal{U}_{100\,\text{erosion}} = \left(\frac{u_{*cr}}{0.41}\right) \ln\left(\frac{z_{100}}{z_0}\right), \text{ where} \quad (1)$$

z_{100}= level above seabed (1 m)

d = grain diameter = mean grain size

u_{*cr}= critical shear velocity $= \sqrt{\frac{\tau_{cr}}{\rho}}$, where (1.1)

τ_{cr}=threshold bed shear stress (N/m^2) = $g(\rho_s - \rho)\, d\left(\frac{0.30}{1+1.2D_*} + 0.055[1 - \exp(-0.020D_*)]\right)$, where (1.2)

ρ = water density = 1027.4 kg/m^3

ρ_s = grain desnity = 2650 kg/ m^3 (quartz)

D_* = dimensionless grain size = $\left[\frac{g(\rho_s-\rho)}{\rho v^2}\right]^{\frac{1}{3}} d$, where (1.3)

v = kinematic viscosity if water

Bed shear-stress (τ), defined as the frictional force exerted by the flow per unit area of the seabed, is the primary hydrodynamic parameter controlling erosion, suspension and deposition of mud and sands (Soulsby and Clarke, 2005). As outlined by Yang et al. (2022), this parameter can be estimated using the following quadratic equation (Huntley et al., 1994) for each eARA segment.

$$\tau = \rho C_D U_{C100}^2 \text{ , where} \quad (2)$$

ρ = water density = 1027.4 kg/m^3

C_D = drag coefficient = $2x10^{-3}$

U_{c100} = current speed at 1 m above the seabed (derived from equation 1)

3.4 Results

3.4.1 Seabed Sediments

Spatial variations in mean grain size (for the newest time-lapse dataset) can be seen throughout the site, ranging from -1 Φ, predominantly to the west of the site, to 9 Φ, with an average grain size of 1.53 Φ and a standard deviation of 1.26 Φ (Fig.3.2a). Classified as sand, gravel and mud, the site is mainly comprised of sandy sediments, particularly towards the centre of the site, along with sandy patches towards the NW of the site (Fig.3.2b). Towards the western portion of the site, gravel is dominant, along with some patches towards the north and NE. A few very small, sparsely distributed patches of mud are seen throughout the site, the majority of which are located towards the southern flanks of the site. Potential bedrock outcrops have been mapped by (Arosio et al., 2023b), predominantly located towards the eastern portion of the site. The spatial variation of sediments for the CV13_01 dataset can be seen in the supplementary material (Supplementary Fig A.5).

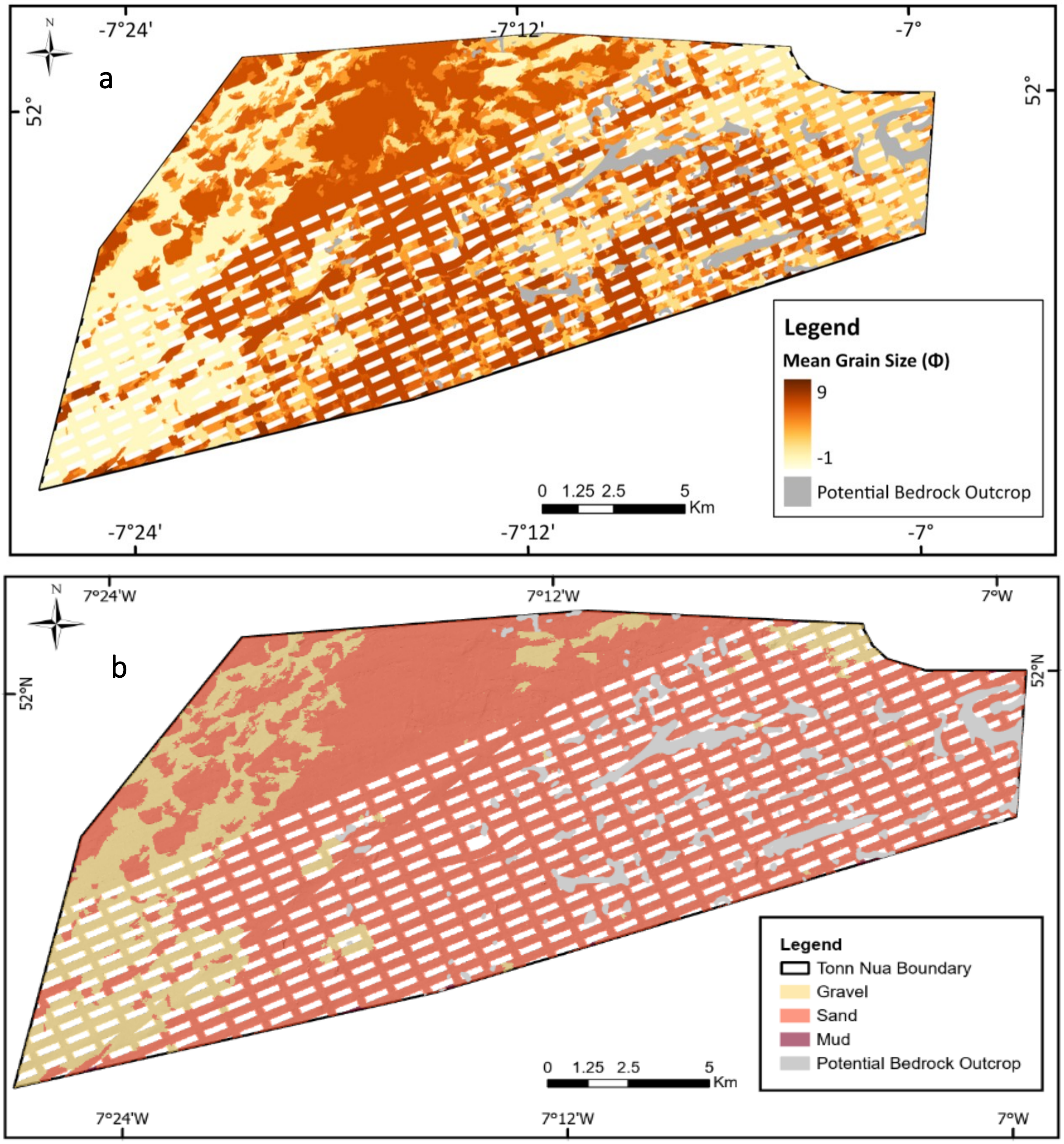

Figure 3.2. Spatial distribution of seabed sediments, based on theTC24_016 dataset: (a) Mean grain size (Φ) and (b) Seabed classification based on mean grain size.

3.4.2 Geomorphological Characterisation

The bathymetric coverage and derivatives reveal a gently sloping seabed to the south, with an average slope of 0.22˚, with various glacial landforms, transverse bedforms perpendicular to prevailing current direction and linear bedforms parallel to flow direction.

3.4.2.1 Glacial Features

3.4.2.1.1 Eskers

Several eskers have been identified throughout the site in previous literature (Tóth et al., 2020; O'Toole et al., 2022; Arosio et al., 2023), previously interpreted as moraines (Gallagher et al., 2004). Eskers can be seen oriented NNW SSE to the east of the site, while predominantly oriented NNE SSW to the centre and north of the site. A higher density of eskers are seen towards the east and south of the site with in a variety of sizes. The largest esker is fragmented (seen in Fig.3.3a), located to the east of the site and spans a length of ~10,000 m within the site. As shown in cross-profiles (Fig.3.3b), the more northerly part of the esker displays a sharper peak than seen in the southerly part of the esker (Fig.3.3c). The northern part is also more asymmetrical, wider and lower in height (<4 m). Whilst, as you go south, the esker tends to slightly increase in height (~5 m), displays a more rounded peak, and narrows.

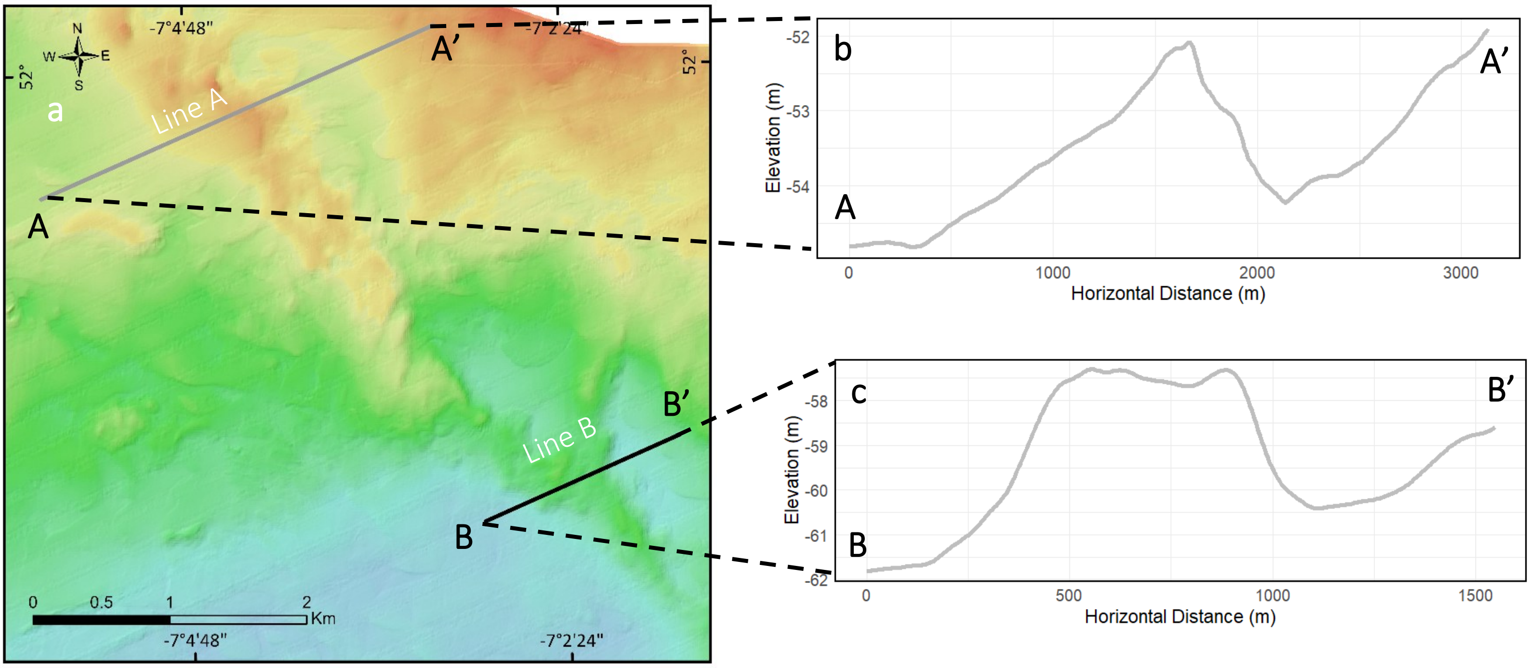

Figure 3.3. (a) Map showing the extent of Line A (represented by the gray line) and Line B (represented by the black line) which display a ridge, interpreted as an esker (Tóth et al., 2020; O'Toole et al., 2022; Arosio et al., 2023), previously interpreted as a moraine (Gallagher et al., 2004), (b) Cross-profile of Line A, and (c) Cross-profile of Line B.

3.4.2.2 Transverse Bedforms

3.4.2.2.1 Sandwaves

Sandwaves are seen throughout the site in fields (defined as multiple sandwaves) or, in some cases, isolated. Sandwaves are particularly prominent towards the northwest of the site within the AOI (Fig. 3.4a) and towards the centre of the site. In a planar view, sandwaves crestlines are sinuous, low-sinuosity or straight. Crestlines of sandwaves within the AOI (Fig.3.4a) are generally east-west oriented, with the stoss side facing northeast (30 – 40˚) and the lee side facing southwest (Fig.3.4b and 3.4c). Sandwaves within the AOI are better defined and more sparsely spaced, while towards the centre of the site are more densely spaced. Sandwaves in the central portion of the site are less well defined, and in general, the stoss side is oriented northeast, at a higher bearing angle (>50 ˚) than those found in the AOI. In some cases, those sandwaves within the centre of the site are superimposed on ridge features.

Morphological characteristics of the sandwaves within the AOI (Fig. 3.4a) are shown Table 3.3, derived from the cross-profiles of the newest time-lapse bathymetry dataset. The sandwaves exhibit asymmetry and are relatively low in height (<1m), with relatively short lee lengths (mean: 27.23 m) and longer stoss lengths (mean: 344.33 m). Wavelengths vary considerably, ranging from 144 m to 825 m, with a mean of 372.53 m. The stoss sides are gently sloping, with an average slope of 344.33˚ (Fig.3.4c). However, the lee slopes are relatively gently sloping, with an average slope of 1.89˚. The cross-section profiles show crestlines appearing as both rounded and sharp (Fig.3.4e).

Table 3.3. Sandwave morphology characteristics within the area of interest based on the newest time-lapse survey (TC24_016).

	Height (m)	Wavelength (m)	Stoss Length (m)	Lee Length (m)	Depth (m)	Lee Slope (˚)
Mean	0.48	372.53	344.33	27.23	52.81	1.89
Max	0.85	825.00	1013.00	40.00	55.42	6.68
Min	0.25	144.00	56.00	10.00	48.27	0.09

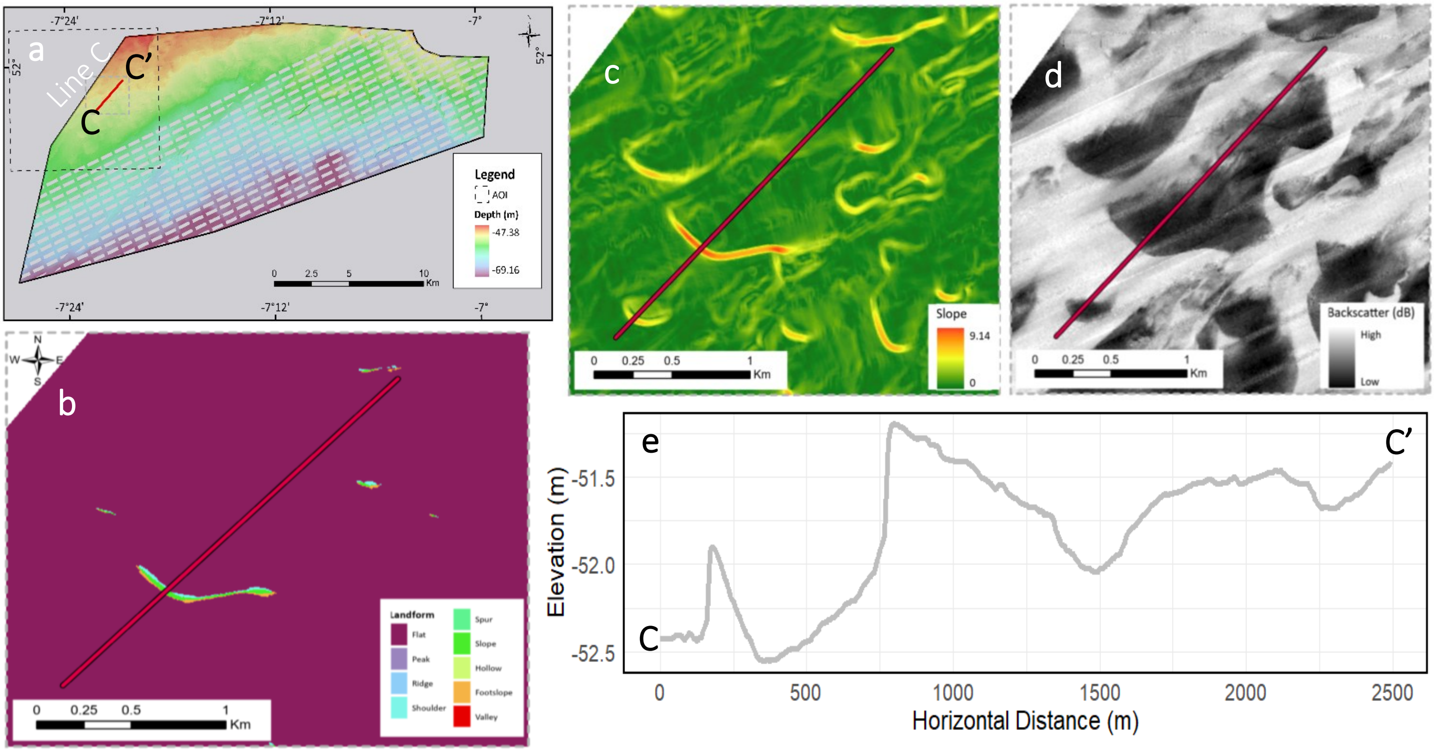

Figure 3.4. (a) TC24_016 bathymetry highlighting the area of interest (AOI) for sandwave assessment and the extent of B-D (dashed grey polygon. (b) Geomorphon landforms. (c) Slope. (d) Backscatter. (e) Cross-profile of Line C.

3.4.2.3 Linear Bedforms

3.4.2.3.1 Sediment Ribbons

Several elongated parallel ridges with positive topography are present towards the southeast (see Fig. 3.5a and b) of the site, trending southwest–northeast (~45˚), previously interpreted as sediment ribbons (Arosio et al., 2023b). Some of the features are comprised of gravelly sediments, while others are characterised as sand. The features exhibit various morphologies, while being low in height <1 m, shown in Fig.3.4c.

3.4.2.3.2 Elongated Ridges

Towards the centre of the site, two adjacent elongated parallel ridges are seen with a similar orientation as the sediment ribbons, displaying a slightly higher bearing angle (~50˚), shown in Fig.5B. These features were previously interpreted as sediment ribbons

(Arosio et al., 2023b). They exhibit a wide morphology of over 1000 m and a height of over 1 m (Fig.3.5d). These features are superimposed by sediment waves.

3.4.2.3.3 Sediment Streaks

Straight to sinuous parallel Sediment Streaks, comprised of sandy or gravelly sediment, can be seen in the backscatter around the SS Miami Engineer and SS Feltria, elongated in a northeast – southwest orientation, see section 3.4.8.

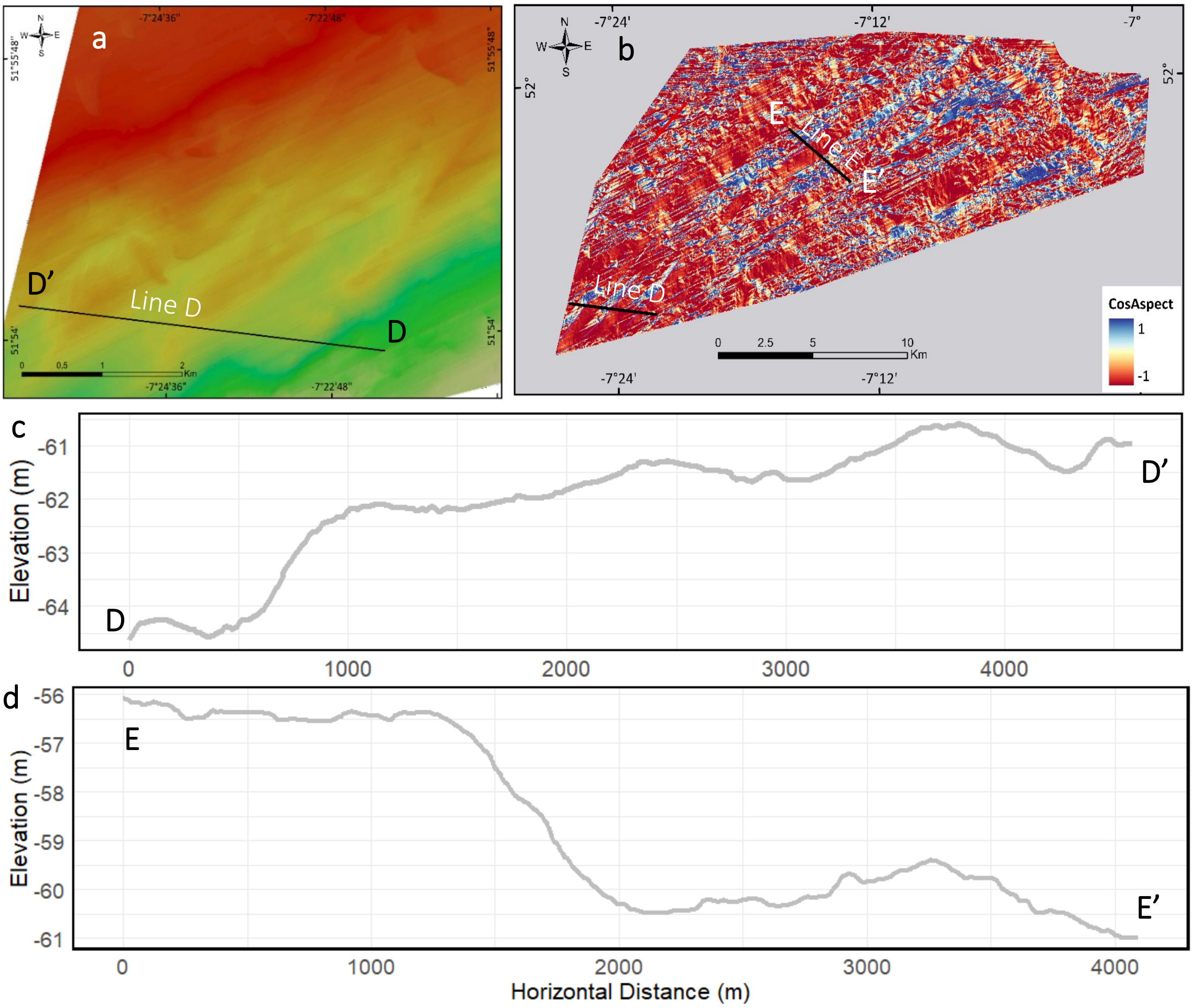

Figure 3.5. (a) Shaded relief showing Line D. (b) CosAspect (northness) with blue values indicating northness (1) and red values indicating southness (-1). (c) Cross-profile of Line D. (d) Cross-profile for Line E

3.4.3 Seabed Change

3.4.3.1 Erosion and Accretion around Landforms

Spatial variations in erosion and accretion around geomorphic features are shown in Fig.3.6a. Erosion is prominent around sandwaves, especially along their footslopes towards the lee side, with sediment being eroded from the southwest (Fig.3.6b and 3.6c), which is also shown in the cross-profile in Fig.3.6e. Erosion is also observed on the stoss sides of the sandwaves and near the outermost part of the crestlines (Fig.3.6b). Small amounts of accretion can be seen around the sandwaves, predominantly on the north facing side (Fig.3.6b and 4.6c), albeit in a relatively low abundance. Accretion is occurring towards the northern part of the site, specifically around the base of the north-south oriented esker (Fig.3.6d), which can also be observed along the cross-profile (Fig.3.6f). The fragmented esker to the east of the site, orientated NNW-SSE, also shows signs of accretion, especially to the north and the northeast. In some instances, erosion can be seen around the base of potential bedrock outcrops. Both erosion and deposition are observed around three out of four of the wrecks, except for the wreck located towards the southwest of the site (IE_GSI_shipwk_ID_346), which shows no signs of erosion or deposition. Overall, accretion tends to be more active in the shallower parts of the site, whereas erosion is more prominent towards the deeper parts of the site.

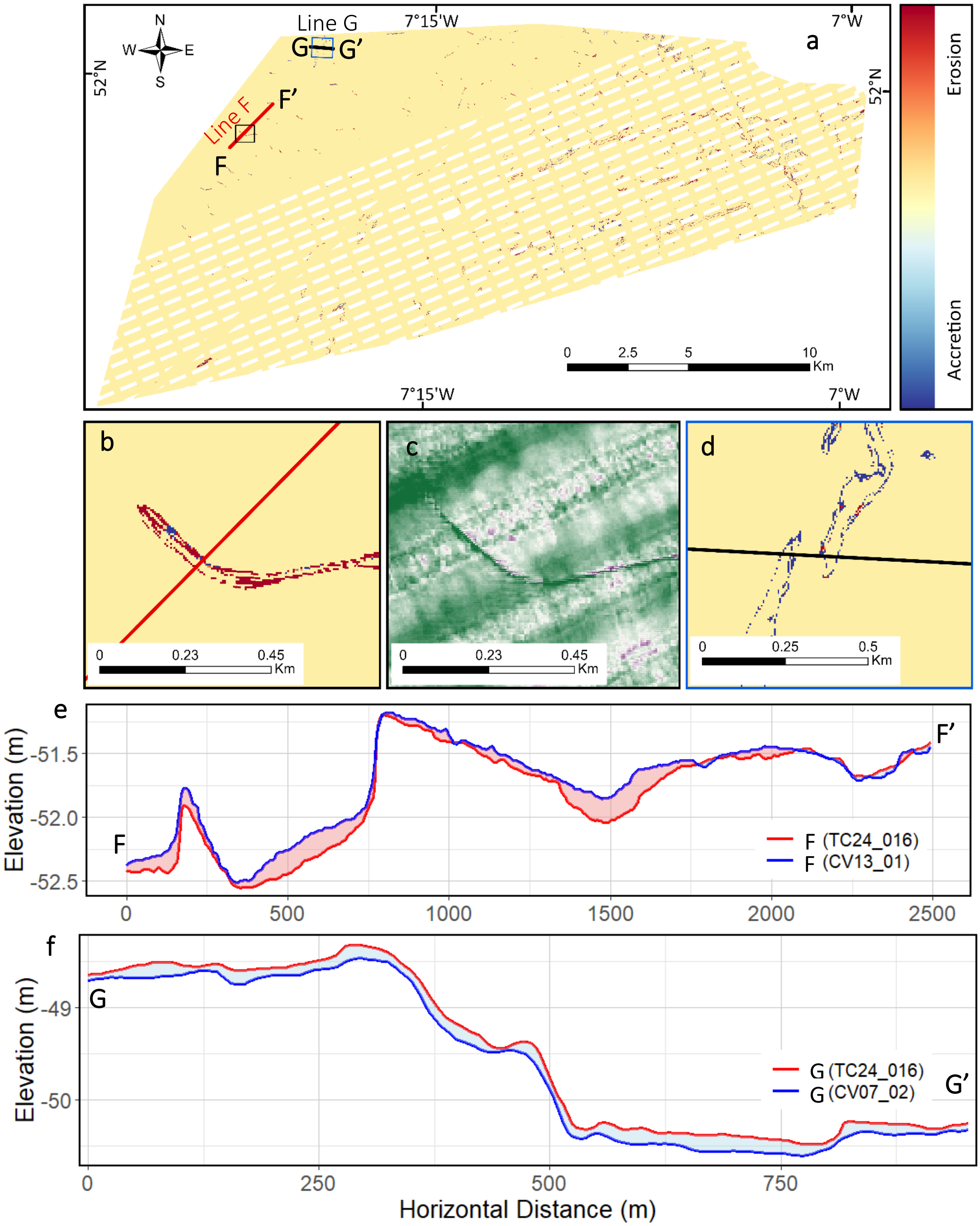

Figure 3.6. (a) Map showing areas of erosion (red) and accretion (blue) around landforms. (b) Close-up example of erosion around a sandwave (extent shown by the black polygon in a). (c) Close-up example showing change-detection of the same feature in B, green represents erosion and purple indicated accretion. (d) Close-up example of deposition around an esker (extent shown by the blue polygon in a). (e) Line-profile for line F showing areas of erosion (pink shading) and accretion (blue shading) around sandwaves. f) Line-profile for line G showing areas of erosion (pink shading) and

3.4.3.2 Sandwave Migration

Sandwave migration rates and direction were assessed within an AOI (Fig.3.4a) to the NW of the study sites over two periods; 2007–2024 (herein referred to as period 1) and 2013–2024 (herein referred to as period 2) (Table 3.4). Measurement of crest-to-crest migration yields a range of distances from 0–22.28 m in period 1 and from 0–9.98 m in period 2, yielding a mean distance of 4.26 m in period 1 and 2.90 m in period 2. This equates to average yearly rates of 0.25 and 0.26 m yr^{-1} for period 1 and period 2, respectively.

Table 3.4. Distance and rate of change of migration of sandwaves within the area of interest for period 1 (2007–2024) and period 2 (2013–2024).

	Distance (m)					Rate of Change (m yr^{-1})				
Time Period	*Min*	*Max*	*Mean*	*Median*	*Std. Dev.*	*Min*	*Max*	*Mean*	*Median*	*Std. Dev.*
2007 – 2024	0.00	22.28	4.26	3.84	3.39	0.00	1.31	0.25	0.23	0.20
2013 – 2024	0.00	9.98	2.90	2.45	2.20	0.00	0.91	0.26	0.22	0.20

As shown in Fig.3.7a, the endpoints of the crestlines tend to display higher migration rates than other points along the crest during both period 1 and 2. No clear spatial trends in migration rates is observed for either period, instead points along the crest are migrating at varying rates, indicating an non-uniform movement across the crestline. Additionally, many points along the crestline migrate in different directions, rather than in a consistent direction. Suggesting that the crestlines are fragmenting or changing shape, rather than undergoing coherent migration.

Despite this variability, both periods display an overall northward trend in migration direction. Period 1 (Fig.3.7b), migration is predominantly towards the northwest, though some points are migrating in a northeast, east and southerly direction. Period 2 (Fig.3.7c), migration is predominantly oriented in a strong north-northeast, north-northwest, and north direction, with some migration to the south.

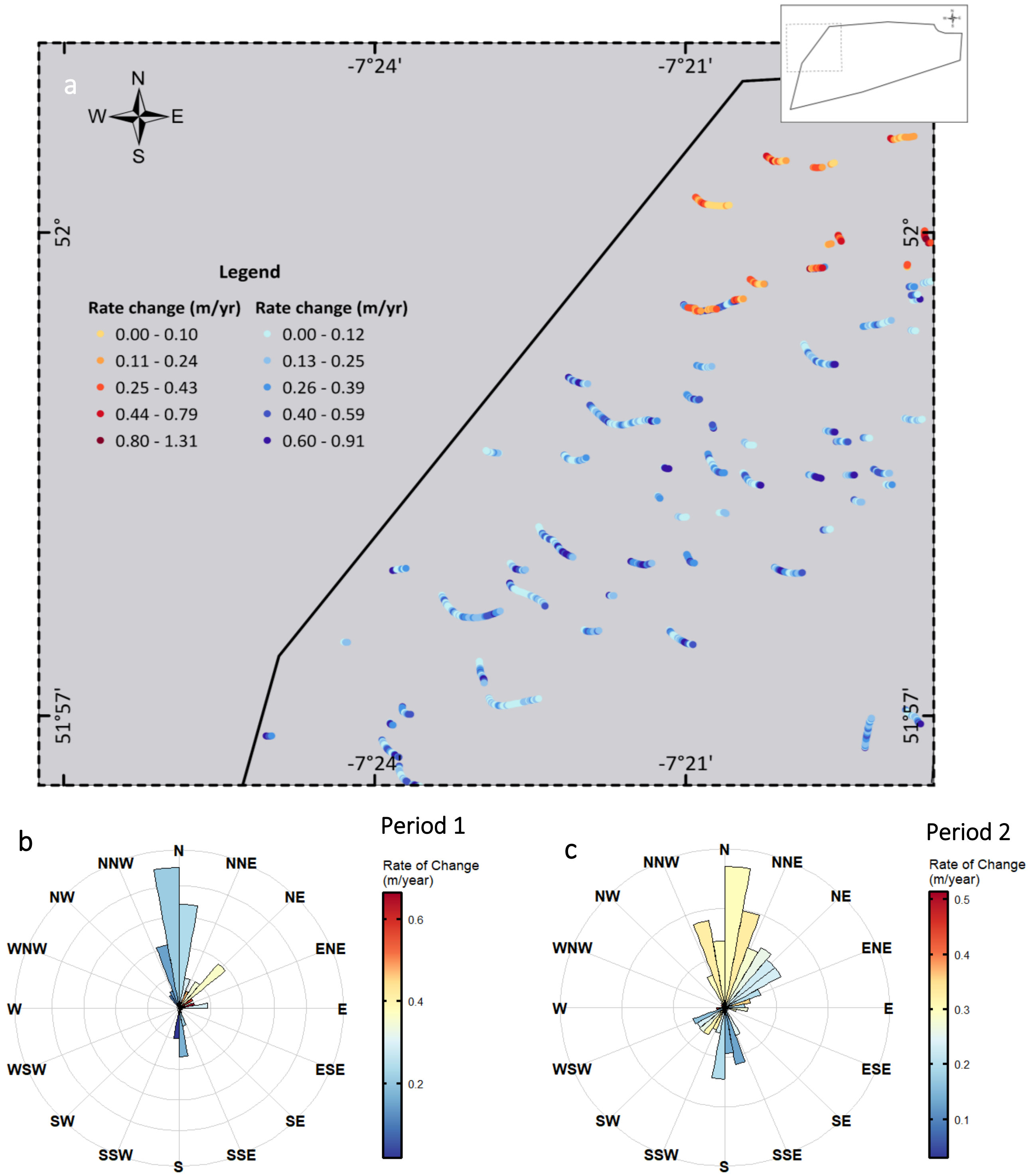

Figure 3.7. (a) Sandwave migration rates of change (m yr^{-1}) within the area of interest: period 1 (CV07_02 and TC24_016) represented by the oranges points and period 2 (CV13_01 and TC24_016) represented by the blue points. Each point represented the rate of change at points spaced 10 m apart on each digitised crestline. (b) Rose diagram displaying the direction of sandwave migration for period 1, coloured by the rate of change. (c) Rose diagram displaying the direction of sandwave migration for period 2, coloured by the rate of change.

3.4.4 Erosional Current Velocity Threshold

The spatial variation of the erosional current velocity threshold required for transporting sediment across the Tonn Nua site can be seen in Fig.3.8. The erosional current velocity threshold for transporting sediment within the study area ranges from 11.22–71.84 cm s^{-1}, yielding an average of 40.58 cm s^{-1}. Higher erosional current velocity thresholds for eroding sediments can be seen to the west of the site where coarser gravelly sediments are located, and towards the north-east of the site. Whilst most of the site typically displays relatively low critical current velocity threshold values.

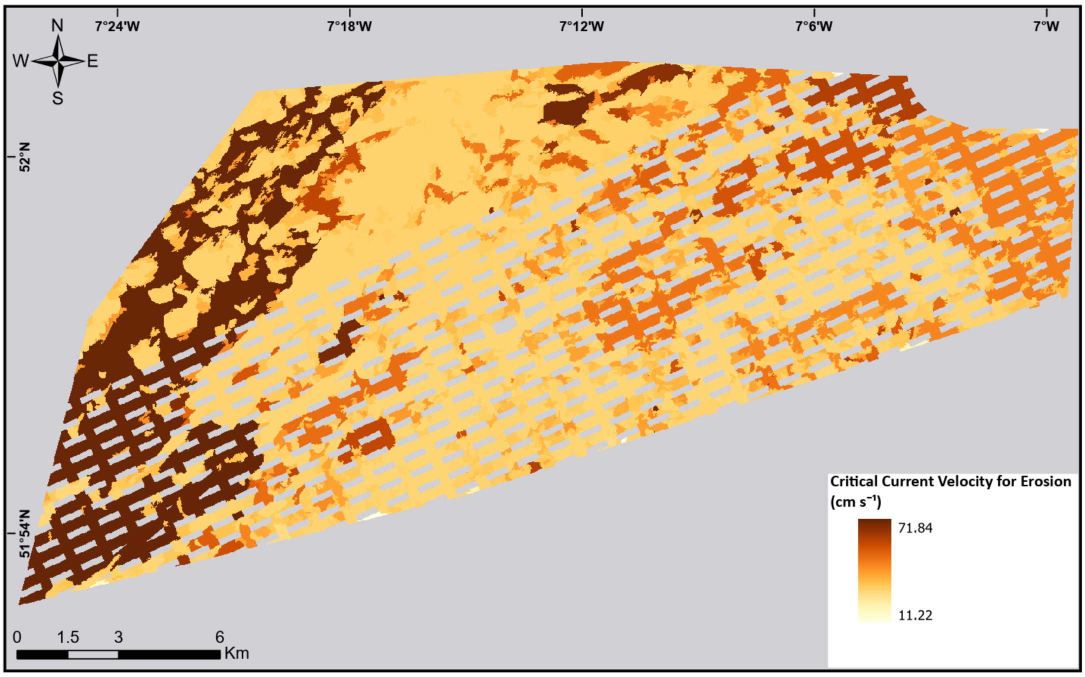

Figure 3.8. Critical current velocity for erosion (cm s^{-1}) for TC24_016 (Soulsby, 1997), based on mean grain size (Φ) derived from eARA.

3.4.5 Seabed Stability

The spatial variation of the threshold bed shear stress (τcr), derived from equation 1.2, using the most recent time-lapse dataset (TC24_016), can be seen in Fig.3.9a. The threshold bed shear stress ranges from 0.01–1.18 N m^{-2}, with an average threshold bed shear stress of 0.30 N m^{-2}. The highest values can be seen to the west of the site, with the centre of the site displaying the lowest values.

The spatial distribution of the bed shear stress (τ), derived from equation 2 using the most recent time-lapse dataset, is shown in Fig.3.9c. Estimated values range from 0.03–1.06 N m^{-2}, yielding an average value of 0.35 N m^{-2} and a standard deviation of 0.16 N m^{-2}. The highest bed shear stress values are observed in areas for gravelly sediments, particularly in the western part of the site, with high bed stress patches towards the north of the site. The central portion of the site typically exhibits lower shear bed stress values.

Four shipwrecks previously identified by INFOMAR are located within the site, located to the south and southwest of the site. Near-field seabed scour is visible at two of the wrecks, SS Manchester Engineer and IE_GSI_SHIPWK_ID_339, seen in Fig.3.9c and 9F, respectively. Seabed scour is visible to the southeast and east of the IE_GSI_SHIPWK_ID_339 shipwreck. Both seabed scour patches cover an area of ~160 m^2 each, within a radius of <10 m from the wreck. Scour can be seen around the SS Manchester Engineer to the southeast (105 m^2) with some deposition to the northwest of the wreck. Potential near-field scour can be seen to the northeast Southwest of the SS Feltria, albeit it is difficult to discern. Elongated parallel sediment streaks (straight to sinuous) are visible in the backscatter mosaic around SS Manchester Engineer (Fig.3.9d) and SS Feltria (Fig.3.9e) in a NE-SW crest orientation, not displaying any obvious bifurcations. Sediment streaks around the SS Feltria are less closely spaced >20 m apart, whilst, around the SS Manchester Engineer wreck they are more closely spaced (>10 m apart). IE_GSI_SHIPWK_ID_346 is the only shipwreck to not show any visible signs of scour or streaks.

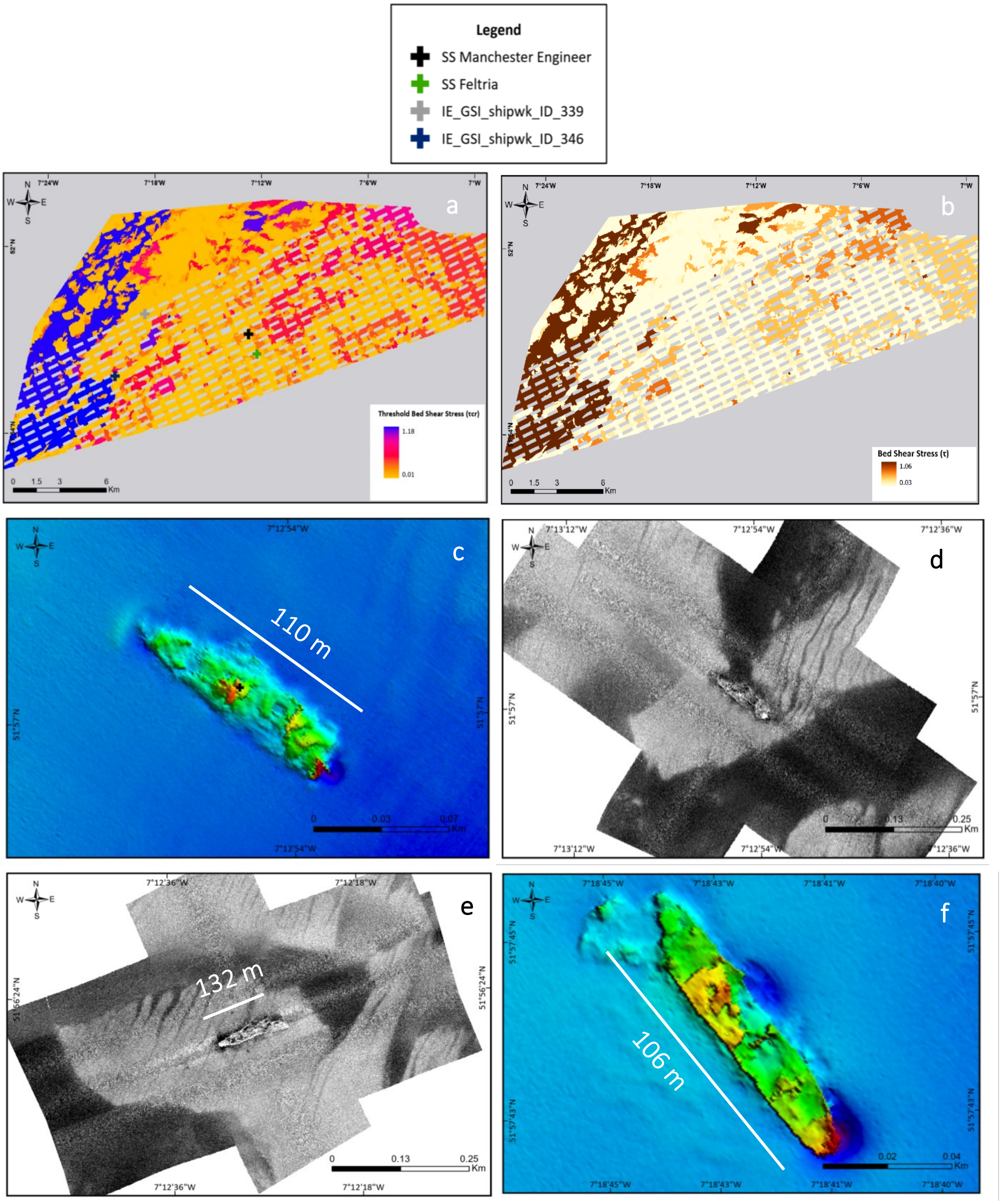

Figure 3.9. (a) Threshold bed shear stress (τcr) in N/m^2 derived from equation 1.2, based of TC24_016 data; (b) Spatial variation of bed shear stress (τ) for each eARA segment, ranging from 0.03 N/m^2 to 1.06 N/m^2, derived from equation 2. (c) SS Manchester Engineer shaded relief; (d) SS Manchester Engineer backscatter mosaic at 56 m water depth (lighter colours represent lower backscatter intensity while darker colours correspond to higher backscatter intensities); (e) SS Feltria backscatter mosaic at 65 m water depth (lighter colours represent lower backscatter intensity while darker colours correspond to higher backscatter intensities); and (f) IE_GSI_SHIPWK_ID_339 shaded relief at 49.9 m water depth.

3.5 Discussion

3.5.1 What is the Geomorphology of the proposed Tonn Nua site?

Mapping of the Tonn Nua site reveals a gently sloping seabed with current-induced linear and transverse bedforms, glacial landforms and potential bedrock outcrops (Section 3.4.1;Table 3.5). Several eskers are seen throughout the site predominantly oriented north to south (Fig.3.10). Eskers were identified in previous literature (Toth et al., 2020; O'Toole et al., 2022; Arosio et al., 2023b), while previously interpreted as a moraine (Gallagher et al., 2004). Arosio et al. (2023) have mapped potential outcropping bedrock throughout the site, particularly towards the southeastern part of the study area.

Sandwave fields dominate the northwestern part and towards the centre of the study area, while some individual sandwaves can be seen. In planar view, sandwave crestlines are mainly sinuous, with a general crestline orientation of west to east, with the steeper lee side facing southwest, indicating a net sediment transport from northeast to southwest (Figure 4). The lateral horns of the crests appear to be backwards i.e., in the direction of the stoss rather than the lee side, similar to parabolic dunes (May, 2015), which was also observed in the Gulf of Valencia (Albarracín et al., 2014). The sandwaves are relatively low in height (<1 m), with relatively long stoss lengths (mean: 344.33 m). Sandwaves are typically sediment abundant features (Boggild et al., 2024). However, the prominent erosion of sandwaves coupled with a lack of accretion and low migration rates, suggests sandwaves found here are sediment starved. This is consistent with Arosio et al. (2023b), who suggest the northern and central parts of the Celtic Sea are sediment starved. Given the subdued morphology of sandwaves in the region, rounded crests in some cases, the lack of sandwave migration and the prominent erosion of these features suggests they are moribund or relict. This is further supported by Albarracín et al. (2014), who suggest that sandwaves at water depths such as this are likely to be moribund or relic features of a shallower hydrodynamic regime. These bedforms take relatively longer to form compared to smaller features, therefore reflecting persistent high velocity currents over a period of several hours to weeks (Stow et al., 2009).

Analysis of bathymetry and derivatives along,, with previous literature (Arosio et al., 2023b), reveal sediment ribbons in the southeast of the study area trending southwest – northeast, comprised of gravelly or sandy sediment. These features exhibit various morphologies, while being low in height, < 1 m. Towards the centre of the site, two adjacent elongated parallel ridges are seen with a similar orientation as the sediment ribbons, displaying a wide morphology of over 1000 m in width and a height of over 1 m, potentially superimposed by sediment waves (Table 3.3). The sediment ribbons located in the south western part of the study area generally exhibit coarser sediment in the troughs with finer sediments along the topographic high, which is characteristic of sand ribbons (Goff et al., 1999; Kenyon, 1970). Both the sediment ribbons and elongated parallel ridges are roughly oriented parallel to the prevailing NE-SW prevailing flow direction. Some potential elongated sand ribbons are also observed near the sediment ribbons to the west of the site, where topographic highs display lower backscatter intensities (indicating finer sediments) and are surrounded by coarser sediments in the troughs, albeit displaying a lower relief. Sediment ribbons are typically sediment-starved features (Boggild et al., 2024), which coincide with our interpretation of the sandwaves in the region. Sediment ribbons are formed under generally high velocities (0.7–1.5 m s^{-1}), requiring longer periods for formation, although the time period is not yet known (Flood, 1983; Stow et al., 2009). The required velocity to form sediment ribbons is at the higher end of the sediment-derived estimated current velocity (Fig.3.8), which is predominantly seen towards the west of the site. However, given this high velocity and long period required for the formation of these features, it is possible that they were formed under past stronger oceanographic conditions, when currents were strong enough to form these features. It is also possible that these features were misinterpreted as sediment ribbons.

The higher-resolution multibeam backscatter around the wreck sites revealed sand and gravel streaks “stringers” elongated in an NE-SW crest orientation (Fig.3.9). Stringers can also be seen in various other locations around the site, however given the lower resolution of the backscatter datasets (5 m), compared to the wreck (<1 m), these features have not been mapped apart from those observed at the wreck sites as they are difficult to discern given the resolution. These bedforms flow sub- to parallel to flow direction, and may merge laterally/longitudinally, although some have been referred to as sediment ribbons (Nanson et al., 2023; Stow et al., 2009), forming under velocities of 0.1 to 0.5 m s^{-1} (Stow et al., 2009).

While this study has provided a comprehensive analysis of the geomorphology at the Tonn Nua site focused on seabed features, the inclusion of shallow, high resolution seismic data will provide more information on sub-surface features that are not visible on the surface and provide additional information on the internal structure of these features e.g., the presence of cross-bedding in sandwaves. Moreover, higher resolution datasets will provide more detail on features that are not visible in the resolution of the datasets used in this study. Albeit, this research provides a detailed overview of surface geomorphological features that can inform preliminary stages of the development of offshore structures.

Table 3.5. Summary of geomorphological features, ISS (Irish Ice Sheet).

	Feature	Bottom current orientation	Current velocity	Interpretation
Glacial Landforms	Eskers			Southward flowing subglacial drainage associated with the IIS (Toth et al., 2020)
Transverse Bedforms	Sandwaves	Crest perpendicular to flow direction	0.3 to 0.75 m s^{-1} (Stow et al., 2009)	Formed under conditions of higher sediment availability, now moribund or relict
Linear Bedforms	Sediment Ribbons	Parallel to flow direction	0.7 to 1.5 m s^{-1} (Stow et al., 2009)	Limited availability of mobile sediment, formed under stronger currents
	Ridges	Parallel to flow direction		Limited availability of mobile sediment
	Sediment Streaks	sub- to parallel to flow direction	0.1 to 0.5 m s^{-1} (Stow et al., 2009)	Limited availability of mobile sediment

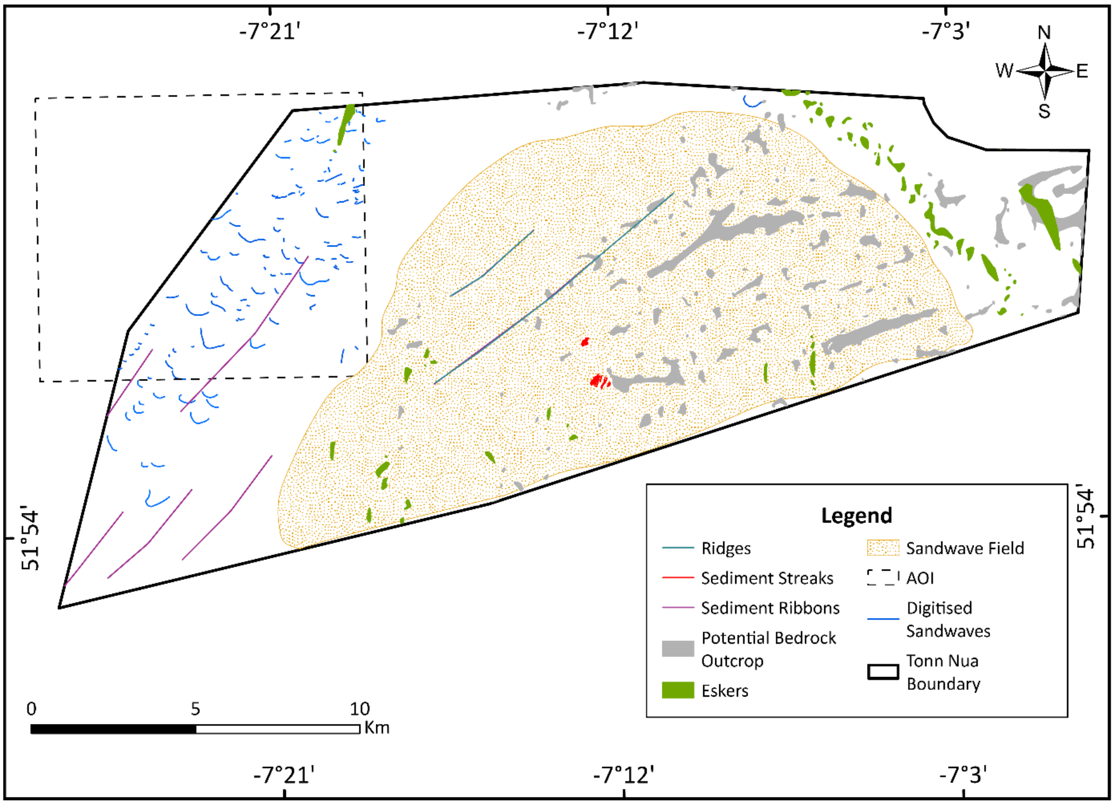

Figure 3.10. Geomorphological map of Tonn Nua displaying ridges, sediment streaks, sediment ribbons (Arosio et al., 2023b), potential bedrock outcrops (Arosio et al., 2023b), eskers (Toth et al., 2020; O'Toole et al., 2022; Arosio et al., 2023b), sandwave fields, AOI (area of interest) for sandwave analysis, digitised sandwave crests (including individual sandwaves and a sandwave field), and the Tonn Nua Boundary.

3.5.2 What is the spatio-temporal variability of Tonn Nua?

Overall, accretion tends to be more active in the shallower (approximately 47 – 51 m) parts of the site, whereas erosion is more prominent towards the deeper (approximately 54 – 69 m) parts of the site (Fig.3.6). Erosion is more prominent around sandwaves, especially along their footslopes towards the lee side, with sediment being eroded from the southwest. Erosion is also observed on the stoss sides of the sandwaves and near the outermost part of the crestlines. Small amounts of accretion can be seen around the sandwaves, predominantly on the north facing side. Sandwaves are relatively stable with an average rate of change of 0.25 m yr^{-1} over a seventeen year period (2007 to 2024) and 0.26 m yr^{-1} over an eleven year period (2013 to 2024) (Table 3.4). Both periods show similar migration rates and directions, both primarily migrating north (Fig.3.7). Therefore, the sandwaves are relatively stable and rather than migrating in one uniform direction, they are changing shape and eroding rather than migrating based on the results of the migration analysis. The lee slope of sandwaves within the AOI (Fig.3.10) are becoming less steep with a maximum slope of 6.68˚, compared to 2007 and 2013. Accretion is occurring towards the northern part of the site, specifically around the base of the north-south oriented esker. In some instances, erosion can be seen around the base of potential bedrock outcrops, which may be indicative of seabed scour. Both erosion and deposition are observed around three out of four of the wrecks, except for the wreck located towards the southwest of the site (IE_GSI_shipwk_ID_346), which shows no signs of erosion or deposition.

Whilst previous research has discussed the reverse migration of sediment waves in the Irish Sea (Van Landeghem et al.,2012), due to the interaction of quarter-diurnal (M4) and semi-diurnal (M2) tidal constituents with an appropriate phase shift (Besio et al., 2004). Van Landeghem et al. (2012) discussed a variety of reasons which may result in the reversed migration or counter current migration of sediment waves, such as the possibility that the features are antidunes. This is unlikely as they must have a Froude value of greater than 0.84 based on Ashley (1990), which is far above measured in our site. Van Landeghem et al. (2012) in addition discussed that this may be due to the upper part of the crest flexing from a shift in residual sediment transport. However, given the low rate of change in comparison to sandwave migration analysis in the Irish sea with an average rate of change of 6 m yr^{-1} (Van Landeghem et al., 2012) and 1.1 to 79 m yr^{-1} (Creane et al., 2022); 32 m yr^{-1} in the Danish Wadden Sea (Bartholdy et al., 2002); and -3.6 to 10 m yr^{-1} in the North Sea (Van Dijk and Kleinhans, 2005), it is possible that the sandwaves are stable and due to erosion processes are changing shape rather than wholly migrating. Moreover, given the morphology of the sediment waves in this study i.e., low in height and displaying relatively low steepness, indicates a loss in bedform mobility and therefore slower migration rates (Kubicki, 2008; Van Landeghem et al., 2012). These results are generally consistent with the modelled current velocity published in Coughlan et al. (2021), that estimated relatively low seabed disturbance, along with reduced tidal induced current velocities. This may attribute to the relatively stable seabed conditions seen at the Tonn Nua Site.. Given the relatively low rates of change between the crestlines, it is also feasible that this could also be due to the inaccuracy of the delineated crest lines. In addition, as mentioned by Knaapen (2005), the migration rates are within the same order of magnitude as the errors of the horizontal uncertainty.

It is important to note that in terms of assessing the change in sandwaves, we were limited to a relatively small area within our study site due to the gaps within the newest time-lapse dataset. In addition, limited to three time periods, with a very small area of overlap between the three, therefore limited to two analysis periods. Albeit this is the first study within the region that utilises time-lapse bathymetry data to quantify the spatio-temporal seabed change. Moreover, given the timely nature of this research, it provides a preliminary assessment of the variability of seabed features and the mobility of bedforms, which is critical to preliminary foundation design and cable route planning for ORE development.

3.5.3 What are the hydrodynamics?

The estimated sediment derived current velocity to erode sediments of 11.22 cm s^{-1} to 71.84 cm s^{-1}, yielded an average of 40.58 cm s^{-1} (Fig.3.8), coincident with bedform flow velocities indicated by Stow et al. (2009) as well as legacy current velocity measurements (maximum current velocity of 31.5 cm s^{-1}) within close proximity to our study site and modelled near bed current speeds (see supplementary materials Table A.2, for a detailed description). Venterra (2025) modelled maximum near bed current velocity for ebb and flood tide using a hindcast dataset for a 40-year period (1980 to 2020), estimating current velocities between 0.16 to 0.35 m s^{-1}. The bedforms observed here (sandwaves, sediment ribbons, and sediment streaks) require velocities of 0.3 and 0.75 m s^{-1}, 0.7–1.5 m s^{-1}, and <0.5 m s^{-1}, respectively (Stow et al., 2009). The orientation of bedforms, sandwaves orientated with their steepened lee slope facing southwest; elongated ridges, sediment streaks and sediment ribbons orientated northeast to southwest, indicates a prevailing current direction of northeast to southwest. This is coincident with legacy current meter measurements close to our study site, with a prevailing northeast and southwest flow, with a stronger southwest flow velocity, corresponding to the sandwaves asymmetrical shape, indicative of tidal asymmetry (Stride, 1963), indicating a stronger ebb tide.

Model-derived current velocities, as presented by Coughlan et al.(2021) can further strengthen and elaborate on the results that are presented in this current study. Results of modelled depth-averaged tidal current velocity in Coughlan et al.(2021) indicate relatively low mean and maximum current velocities, typically less than 0.5 m $^{-1}$, in comparison to the stronger current velocities seen in the Irish Sea of up to 1.5 m s $^{-1}$. .

Wrecks can also be used as indicators of local hydrodynamics and be beneficial for ocean engineering (Majcher et al., 2022), as marks serve as indicators of local dominant current direction (Garlan et al., 2015). The wrecks are orientated 90˚, 45 ˚, and 225 ˚ to prevailing south westerly flow for the SS Manchester Engineer, IE_GSI_SHIPWK_ID_339, and SS Feltria, respectively (Fig.3.9c-f). Given that scour was primarily observed towards the northern sides of the wrecks, and deposition towards the northern side of the wrecks, this may be further indicative of the stronger south-westerly flow. These scouring processes may be localised short-term events (minutes to hours) or long-term scouring around the complete structure (days to decades) (Quinn, 2006). Therefore, more regular time-lapse datasets are required to effectively understand the scouring processes occurring in the study site.

Whilst this present study did not focus on the main drivers of hydrodynamics in the region, previous research overlapping our study site suggests that wave action is the dominant process resulting in sediment mobilisation within our study area (Coughlan et al., 2020a). Metocean characterisation of the SC-DMAP by Venterra (2025) reveals a south westerly prevailing wave direction, coinciding with the results presented in this study. It is therefore possible that wave action is the primary hydrodynamic forcing within our study area. Further research should focus on quantifying yearly sediment mobilisation and assessing the main drivers of hydrodynamics in the regions on a local scale, similar to this study.

3.5.4 What is the seabed stability of Tonn Nua and therefore what are the implications for the development of ORE?

The threshold bed shear stress ranges from 0.01 to 1.18 N m^{-2}, with an average threshold bed shear stress of 0.30 N m^{-2} (Fig.3.9a). The highest threshold bed shear stress values can be seen to the west of the site, with the centre of the site displaying the lowest values. Bed shear stress values range from 0.03 N m^{-2} to 1.06 N m^{-2}, yielding an average value of 0.35 N m^{-2} with the highest bed shear stress values observed in areas of gravelly sediments, particularly in the western part of the site, with high bed shear stress patches towards the north of the site (Fig.3.9b). The central portion of the site typically exhibits lower shear bed stress values. In the central and eastern part of the site, the bed shear stress exceeds the threshold bed shear stress (Fig.3.11), therefore indicating the mobilisation of sediments (Coughlan et al., 2021). Whilst towards the western part of the bed shear stress does not exceed the threshold bed shear stress, therefore being relatively stable. However, this does not consider seabed mobilisation frequency or the drivers of seabed disturbance i.e., waves, currents or combined as modelled in Coughlan et al. (2021). Albeit bed shear stress values coincide with reported bed shear stress values for combined current and wave (Coughlan et al., 2021), displaying lower bed shear stress values than those seen in the Arklow Bank, Ireland's only operating windfarm. Additionally, Peters et al. (2020) reported relatively high seabed stability based on slope, bathymetry and coded sediment properties; and Coughlan et al. (2021) further support this through seabed disturbance and sediment mobility indices, indicating relatively stable seabed conditions, particularly in comparison to seabed conditions within the Irish Sea. As threshold bed shear stress and bed shear stress was calculated based on mean grain size derived from eARA, multi-modal sediments may comprise of fine components that may be prone to mobilisation by a bed shear stress value lower than the grain size value predicts (Coughlan et al., 2021; Griffin et al., 2008). Moreover, the use of estimated mean grain size rather than ground-truthed grain size may lead to further uncertainty. Albeit, eARA has proven to provide an accurate representation of mean grain size across acoustic facies (Brennan et al., 2025), providing a spatially comprehensive estimate of mean grain size that can be integrated into theoretical formulae such as the ones utilised in this research.

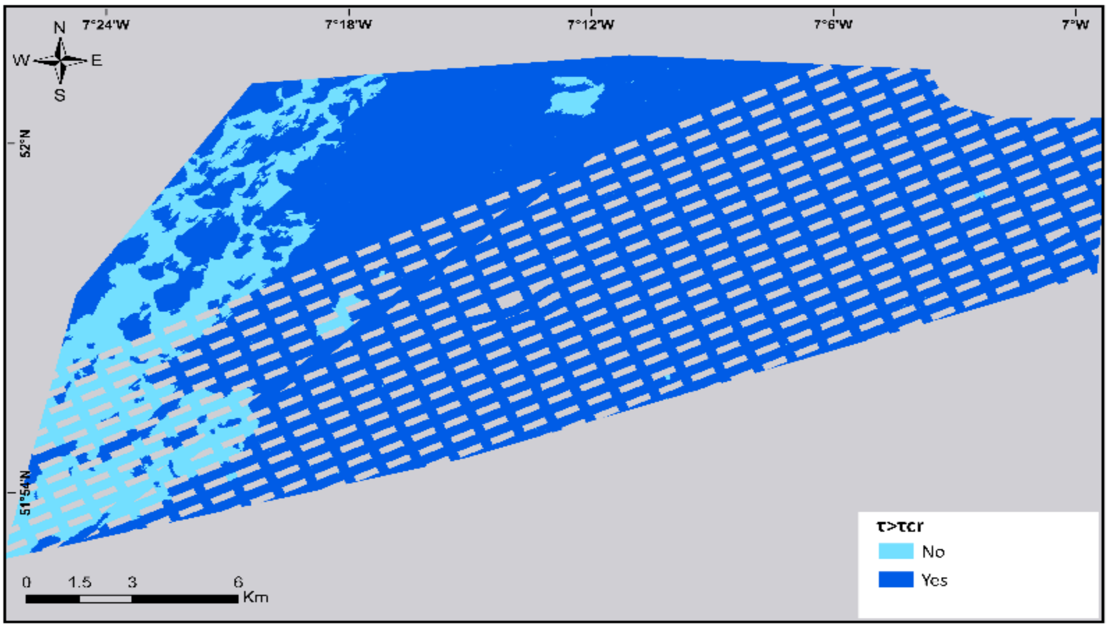

Figure 3.11. Spatial distribution of where the bed shear stress (t) exceeds critical bed shear stress (tcr), indicated by yes (dark blue) or no (light blue).

Updated knowledge on the seabed stability and mobility of sandwaves in the Tonn Nua site provides preliminary results to inform the development of offshore infrastructure in this region. Submarine cables in offshore windfarms cost between 11-14% of overall capital expenditure (CAPEX), with 70 – 80 % of insurance claims costs related to cable failure (Walsh et al., 2024). Cables must be buried beneath the seabed to protect them, typically between 1 to 4 m below the seabed (BVG Associates, 2019). However, he growth and migration of sandwaves can expose pipelines and cables, thus increasing the risk of damage; influence the design bed level for a structure (Whitehouse et al., 2000); interact with wind turbine foundations and destabilise bed protections (Nemeth et al., 2003). Conversely, the overburial of cables also presents a challenge as lifting a cable for repair results in further cable damage (Langhorne, 1978), hence deposition of sediments must be considered. Therefore, in order to de-risk offshore wind (OW) sites and lower the levelised cost of energy from OW, a complete understanding of sandwave dynamics is critical to ensure safe design of submarine cables and scour protections (Roetert et al., 2017). Whilst the sandwaves located in our study site are relatively stable, changes in sandwave asymmetry can also lead to the free spanning of cables and pipelines irrespective of sandwave migration (Nemeth et al., 2003). Seabed scour is considered as a primary uncertainty in the design of fixed-foundation OW turbines (Negro et al., 2014), with scour acting as one of the main causes of failures in fixed-foundation OWT structures (Wei et al., 2024). An increase in sediment transport and erosion will occur when an OWT foundation is installed, increasing the hydrodynamic field locally (Whitehouse et al., 2011). Given the vast distribution of sand throughout the site, sand is highly mobile and erodible, being highly susceptible to scour and liquefaction, requiring less time for scouring processes to occur and the ability for increased scour depths (Whitehouse et al., 2011), particularly compared to gravelly sediments located towards the west of the site. Whilst scouring around wrecks is present, in comparison to wrecks or similar sizes and in slightly deeper waters, such as discussed by Garlan et al. (2015), the scour marks affect a smaller portion of the seafloor. Whitehouse et al. (2011) compared scour at several offshore windfarms with various characteristics and found that OWFs with lower current speeds are still capable of mobilising sand, but not clay or gravel. Consequently, whilst scour is not likely as prevalent an issue as seen in sites such as Arklow bank with stronger current speeds, faster bedform migration rates and the presence of sandbanks, the scour detected in this site could influence the longevity of OW structures. Therefore, scour protections may be required in areas where scour is anticipated around foundations and submarine cables to ensure the safety and longevity of structures.

Hence, given the results presented in this research and previous literature, the seabed conditions at the Tonn Nua site appear to be relatively stable. The integration of additional geophysical datasets (seismic, higher resolution and more frequent MBES and side scan sonar), geotechnical and ground truthed datasets, coupled with modelled metocean data, will enable a holistic assessment of sub-surface and surface seabed conditions along with the main drivers of hydrodynamic forces.

3.6 Conclusion

To address the need for a comprehensive understanding of the spatio-temporal seabed change, seabed dynamics and geomorphological constraints at the Tonn Nua site for the development of fixed-foundation OW, we utilised high-resolution time-lapse bathymetry datasets and theoretical formulae. Furthermore, we have demonstrated the potential to apply eARA to estimate the spatial distribution of mean grain size and incorporate these estimations into theoretical formulae to assess the critical current velocity required for erosion, threshold bed shear stress and bed shear stress. This presented research has yielded a number of key insights:

1. The geomorphology of the Tonn Nua site consists of glacial features: eskers, linear bedforms: sediment ribbons and sediment streaks; and flow transverse bedforms: sandwaves.
2. Analysis reveals sandwaves are relatively stable, migrating at an average rate of 0.25 and 0.26 m yr^{-1}, based on two time periods in a primarily north migration direction. Whilst the sandwaves are migrating against the typical migration direction, we conclude that they are stable, eroding and changing shape rather than wholly migrating in one direction.
3. We estimate a mean current of 41 cm s^{-1} in a northeast – southwest prevailing flow, coincident with legacy current velocity measurements nearby and landform derived current velocity estimations.
4. The results demonstrate that the seabed is relatively stable, but key considerations must be made for the burial of cables, cable route planning, foundation design, scour protections, and turbine layout.

Given the timely nature of this research, the results presented herein provide preliminary insights into seabed stability and hydrodynamics to better inform future research and decision-making for the efficient development of OW at the Tonn Nua site. Future work should focus on utilising higher-resolution, more frequent time-lapse bathymetry datasets, combined with hydrodynamic modelling, and direct current velocity measurements, and in-turn identify the dominant hydrodynamic forces. This research represents the first study to address seabed dynamics in the context of ORE development at the Tonn Nua site and within the Irish portion of the Celtic Sea.

Chapter 4: Conclusion

This thesis presents a novel approach for sediment distribution mapping, compared to traditional ARA, thus improving the segmentation and classification accuracy. As such, this research also presents a scalable approach that can be used across large-scale mapping programmes such as MAREANO and INFOMAR and on local scales to support the development of ORE. Therefore, this research has addressed all of the aims, objectives and research questions set out (see Chapter 1).

In order to improve the spatial accuracy and classification accuracy of traditional ARA, this research leveraged the high spatial accuracy of backscatter mosaics with the high-fidelity sediment information provided by ARA through OBIA (Chapter 2). Subsequently, I assess the segmentation accuracy through the manual digitisation of the backscatter mosaic and assessed the spatial accuracy in terms of standard spatial accuracy metrics. The classification accuracy was measured in terms of correlation between observed and estimated grain size; and thematic accuracy via error matrices to answer the following research question: **What is the segmentation and classification accuracy of eARA; and rank it in comparison to alternative methods?** eARA maintained or improved the classification accuracy of traditional ARA in terms of correlation in three out of four sites; and in terms of thematic accuracy, eARA yielded overall accuracies of 20% to 96.15%, demonstrating higher overall accuracies compared to INFOMAR's classification scheme at two out of four sites, with one site remaining unclassified within INFOMAR's current classification scheme. Moreover, in comparison to previous research that utilised traditional ARA, our results are generally consistent with those results (McGonigle and Collier, 2014a; Santos et al., 2018), while the latter studies are constrained by poor spatial accuracy. In addition, our results are generally consistent with previous research that endeavored to overcome the spatial resolution limitations of traditional ARA (Alevizos and Greinert, 2018; Che Hasan et al., 2012; Misiuk and Brown, 2022). However, these studies are subject to notable drawbacks, limited to three sediment classes, requiring multiple frequencies and the synthetic HAC (sHAC) method relying on >100% survey overlap, respectively. Therefore, given the drawbacks of many of these methods, they are unsuitable for large-scale mapping programs. Therefore, eARA provides an estimation of mean grain size without the requirement of >100% overlap or the use of multiple frequencies.

In terms of segmentation accuracy, eARA presented higher segmentation accuracies compared to traditional ARA, with only one site displaying poorer segmentation accuracies, which can be attributed to the relatively smaller image-objects that were not identified within the eARA classification and exerted a disproportionate influence on the segmentation accuracy assessment. Given the novelty of this method, there are no studies that are comparable in terms of spatial accuracy, apart from the ARA segmentation accuracy in this research.

This method was applied to four sites offshore Ireland with ranging depths (approximately 59 – 2000 m) and operating frequencies (12 – 300 kHz) to address the following question: **What is the methods effectiveness in relation to geophysical parameters (depth and operating frequency)?** The results demonstrate variations in both correlation strength and thematic accuracy at different depths; and thus, operating frequencies. Site D achieved the highest correlation between observed and estimated mean grain size, where the data were acquired at an operating frequency of 200 kHz and at depths of 84 - 124 metres, followed by Site B (93-95 kHz; 140 - 364 metres), Site C (300 kHz; 59 - 75 metres), and Site A (12 kHz; 441 -2126 metres). While in terms of overall thematic accuracy, deeper sites and lower operating frequencies displayed higher overall accuracies (Fig.2.11). Although the deepest site, and thus lowest operating frequency, yielded poor accuracy, which may be a result of lower operating frequencies penetrating the seabed to greater depths (Anderson et al., 2008). Particularly, in finer sediments such as at this site, especially due to the presence of subsurface layers (Gaida et al., 2019a). Moreover, this site was constrained by poor data quality and a high temporal offset between the sediment sampling survey and the acoustic data acquisition. Overall, this research demonstrates that operating frequencies of <200 kHz tend to attain higher accuracies.

To address the following question, residuals (difference between the observed and estimated grain size) were calculated to investigate the influence of several parameters on the error of the estimation. A Kruskal-Wallis test and post-hoc analyses via Dunn's test were carried out to address the following question: **What are the limitations imposed by sediment sedimentological properties (modality and sorting) and sediment sampling strategies (instrument; and temporal offset between acoustic and sediment sampling survey) on eARA's accuracy?** Sediment sampling properties (modality and sorting) did not lead to statistically significant differences in the error of the grain size estimation. Whereas, sediment sampling strategies (sampling instruments; and the temporal offset with the acoustic and sediment sampling survey) did lead to statistically significant differences between the estimated and observed grain size. In terms of the sampling instruments, this may be attributed to the volume of retrieved sample, the penetration depth, the surface area of the instrument, and the ability of the instrument to retrieve a sample undisturbed to the vessel. This is generally consistent with McGonigle and Collier (2014), as different instruments obtained different classification accuracies between observed and ARA derived mean grain size, based on the instrument used. This may be further attributed to the penetrative depth of the MBES system (Anderson et al., 2008; Gaida et al., 2019a). In terms of the time-lag between the acquisition of the acoustic data and sediment samples, it was found that samples acquired >5 years after the acoustic data led to statistically significant differences between the observed and estimated grain size.

The combined results from Chapter 2 have allowed us to address this question: **What are the broader implications, required resources, and proposed steps for upscaling this workflow across national programmes?** Previous literature, as well as this current study, showcase the scalability of OBIA for different resolution datasets (Summers et al., 2021), which is essential for large-scale mapping programmes such as INFOMAR and MAREANO. Accordingly, eARA has proven successful in a variety of environments, acquired using a range of operating frequencies, sonars from older legacy sonars to modern sonars, vessels, and in ranging water depths, demonstrating its pertinence across a wide range of conditions. In-turn, offering the potential to upscale this method across the INFOMAR database, showcasing its repeatability and consistency as a robust, standardised approach to seabed classification. In terms of training-datasets, only one sample was required per site, however, additional particle size analysis data are required for the validation of classifications, especially in those areas suitable for ORE infrastructure (GDG, 2021).

Moreover, this research has also given insights into the struggles of classifying deeper water Sites (>400m) of INSS data due to the quality of datasets, spatial resolution, and the temporal offset between acoustic and sediment sampling surveys. This has indicated that additional datasets within these locations are required to effectively manage these areas.

In Chapter 3:, to assess the geomorphology at the Tonn Nua site, I utilised bathymetry, bathymetric derivatives, backscatter, and eARA derived grain size data, along with previous literature, to qualitatively address the following question: **What is the geomorphology of the proposed Tonn Nua site?** Mapping of the Tonn Nua site reveals a gently sloping seabed to the south with current-induced linear (sediment ribbons and sediment streaks) and transverse bedforms (sandwaves), glacial landforms (eskers) and potential bedrock outcrops. Several eskers exist throughout the site, predominantly oriented north to south which were also identified in previous literature (Toth et al., 2020; O'Toole et al., 2022; Arosio et al., 2023b). Arosio et al. (2023) have mapped potential outcropping bedrock throughout the site, particularly towards the southeastern part of the study area. Sandwave fields dominate the northwestern part and towards the centre of the study area, with a general crestline orientation of west to east, with the steeper lee side facing southwest, indicating a net sediment transport from northeast to southwest. Some sandwave features are likely moribund or relict. Sediment ribbons are observed in the southeast of the study area, trending southwest – northeast, comprised of gravelly or sandy sediment, while being low in height <1 m. Towards the centre of the site, two adjacent elongated parallel ridges are seen with a similar orientation as the sediment ribbons, displaying a wide morphology of over 1000 m in width and a height of over 1 m, potentially superimposed by sediment waves (Table 3.3). Sediment ribbons are typically sediment-starved features (Boggild et al., 2024), which coincide with our interpretation of the sandwaves in the region. As sediment ribbons are formed as a result of generally high velocities (0.7–1.5 m s^{-1}), requiring longer periods for formation (Flood, 1983; Stow et al., 2009), given this high velocity and long period required for the formation of these features, it is possible that they were formed as a result of stronger past oceanographic conditions or incorrectly identified as sediment ribbons. The higher-resolution multibeam backscatter around the wreck sites revealed sand and gravel streaks “stringers” elongated in an NE-SW crest orientation, forming under velocities of 0.1 to 0.5 m s^{-1} (Stow et al., 2009).

Iutilised time-lapse bathymetry to: 1) assess the seabed change around landforms; 2) assess seabed change in a 2-dimensional space via cross-profiles, and; 3) assess the migration direction and rates of sandwaves within an AOI to address the question: **What is the spatio-temporal variability of Tonn Nua?** Overall, accretion tends to be more active in the shallower parts of the site, whereas erosion is more prominent towards the deeper parts of the site. Erosion is more prominent around sandwaves, especially along their footslopes towards the lee side, with sediment being eroded from the southwest. Sandwaves are relatively stable with an average yearly migration rate of 0.25 m yr^{-1} in the northern portion of the AOI and 0.26 m yr^{-1} in the southern portion of the AOI, in a primarily northern migration direction. Therefore, the sandwaves are relatively stable and, rather than migrating in one uniform direction, they are changing shape and eroding rather than migrating. Moreover, given the morphology of the sediment waves in this study, this indicates a loss in bedform mobility and therefore slower migration rates (Kubicki, 2008; Van Landeghem et al., 2012).

To investigate the hydrodynamics at the Tonn Nua site, I estimated the critical current velocity required for erosion using eARA derived mean grain size coupled with well-established formula, utilised bedforms and shipwrecks as indicators of the prevailing hydrodynamic regime to answer the following question: **What are the hydrodynamics of the site?** The estimated sediment derived current velocity of 11.22 cm s^{-1} to 71.84 cm s^{-1}, yielded an average of 40.58 cm s^{-1}, coincident with bedform flow velocities indicated by Stow et al. (2009), legacy current velocity measurements within close proximity to our study site and modelled near bed current speeds (Venterra, 2025). The orientation of bedforms, indicates a prevailing current direction of northeast to southwest, coincident with legacy current meter measurements, with a stronger southwest flow velocity, corresponding to the sandwaves asymmetrical shape, indicative of tidal asymmetry (Stride, 1963). As scour was primarily observed towards the northern sides of the wrecks, and deposition towards the southern side of the wrecks, this may be further indicative of the stronger south westerly flow.

To investigate the seabed stability and its implications for ORE development at Tonn Nua, based on eARA derived mean grain size, I calculated threshold bed shear stress and bed shear stress for each eARA segment across the site using well-established formulae. In addition, I compared our results to national and regional scale studies, particularly at an operational windfarm in the Irish Sea, to answer the following research question: **What is the seabed stability of Tonn Nua and therefore what are the implications for the development of ORE?** The highest threshold bed shear stress values can be seen towards the west of the site, with the centre of the site displaying the lowest values. The highest bed shear stress values are observed in areas with gravelly sediments, particularly in the western portion of the site. The central portion of the site typically exhibits lower shear bed stress values. In the central and eastern part of the site, the bed shear stress exceeds the threshold bed shear stress, therefore indicating the mobilisation of sediments (Coughlan et al., 2021). Whilst the western part of the seabed is relatively stable, as the bed shear stress does not exceed the threshold bed shear stress. Bed shear stress values coincide with reported bed shear stress values for combined current and wave in previous literature reported by Coughlan et al. (2021). The Tonn Nua Site, overall displays lower bed shear stress values than those reported around the Arklow Bank (Coughlan et al., 2021), which is the location of Ireland’s only operating windfarm, at present. Moreover, Peters et al. (2020) reported relatively high seabed stability at the Tonn Nua site, albeit at a much lower resolution. In addition, in accordance with results reported in Coughlan et al. (2021), Tonn Nua presents relatively stable seabed conditions, particularly in comparison to the Irish Sea, which hosts several proposed offshore wind (OW) sites. Thus, based on these findings I consider the proposed Tonn Nua site to be suitable for development for fixed-foundation turbines. However, in order to de-risk OW sites, the results demonstrate that the seabed is relatively stable, but key considerations must be made for the burial of cables, cable route planning, foundation design, scour protections, and turbine layout.

This research has demonstrated the feasibility of eARA to be upscaled to large-scale mapping programmes, while also being applicable to local scale studies, primarily in the context of ORE. Moreover, demonstrating how eARA derived grain size can be used as a grain size input parameter for various theoretical formulae to provide a spatially comprehensive grain size estimate, compared to traditional point sample locations. In addition, segments provide substantial potential to include additional information within segments, such as critical erosional velocity threshold, threshold bed shear stress and bed shear stress, as in this study. Moreover, this is the first study within the region that utilises time-lapse bathymetry data to quantify the spatio-temporal seabed change. Given the timely nature of this research, it provides a preliminary assessment of the seabed conditions and dynamics at Tonn Nua, which is critical to preliminary foundation design and cable route planning for ORE development.

4.1 Limitations

It is important to note that this research may be subject to limitations.

- **L1.** Given the importance of segmentation in OBIA approaches, the effectiveness of eARA may be limited in regions with gradational sedimentary boundaries, as it relies on the spectral properties of the backscatter mosaic. In such environments, the segmentation algorithm may struggle to accurately delineate sedimentary boundaries.
- **L2.** The method outlined in Chapter 2 may not be applicable to INSS datasets that exhibit poorer backscatter data quality, such as those in the Porcupine Seabight. This is partly due to the acquisition of multibeam bathymetry datasets, which are often prioritised over backscatter datasets i.e., acquisition parameters are optimised for bathymetry datasets rather than backscatter. Consequently, due to the latter, along with the deeper waters (>400 m) seen in many INSS areas, these datasets are often constrained by artefacts, low spatial resolution, and inconsistent backscatter results, which may impede the accuracy of ARA outputs. In addition, artefacts hinder the accurate segmentation of the backscatter mosaic by introducing false sedimentary boundaries.
- **L3.** Given the influence of other confounding factors (limited sediment samples; sediment sampling instrument; temporal offset between hydrographic and sampling surveys; and poor data quality), it was difficult to conclusively discern the impact of depth and operating frequency on eARA. Such factors likely introduce errors, lowering accuracy.
- **L4.** In terms of assessing change in sandwaves, the time-lapse aspect of Chapter 3 is limited by spatial resolution and only two data points due to a lack of appropriate

data. This limits the analysis to two time analysis periods, assumes a linear rate of change and is restricted to a relatively small portion of the site. Thereby may not be representative of broader temporal or spatial variability.

L5. Moreover, given the resolution and IHO standard of the bathymetric datasets used in Chapter 3, sandwave migration rates in some cases may be within the horizontal order of error of the acquisition systems, as I was limited by available datasets.

L6. In Chapter 3, the analysis focused on surface conditions, thereby not accounting for subsurface hazards and constraints. Similarly, as metocean variables were not incorporated, this research could not determine primary hydrodynamic forcings in the region.

4.2 Future Work

As a result of Limitation 1 (**L1**), which may impact the effectiveness of eARA in environments with gradational sediment e.g., contourites, and thus, to broaden the effectiveness of this method in a wider range of settings, the integration of additional layers such as bathymetry, bathymetric derivatives, and other ARA layers may provide meaningful information to aid the optimal segmentation in these settings.

In relation to Limitation 2 (**L2**), which highlights the impact of poor backscatter data quality on eARA results, as mentioned in the previous paragraph, the inclusion of additional layers may improve the segmentation of the backscatter mosaic and mitigate the impact of poor backscatter data quality. However, this will not mitigate poor ARA classifications, thus, additional MBES datasets are required in these INSS areas. These surveys should prioritise the well-calibrated acquisition of backscatter datasets to effectively manage these regions.

To overcome Limitation 3 (**L3**), which presented challenges to isolate the impact of depth and operating frequency on eARA, future research could exploit multifrequency backscatter, acquired at a singular site. As outlined in a review by Menandro et al. (2025), multifrequency MBES may have the ability to improve seabed characterisation techniques. Such multifrequency MBES workflows have been exploited in academic research (C. J. Brown et al., 2019; Runya et al., 2021), providing promising results. This approach may eliminate the influence of additional variables, providing a clearer insight regarding the influence of depth and operating frequency. Additionally, through utilising well-calibrated multibeam backscatter (Roche et al., 2018; Weber et al., 2018), this may improve eARA as a whole.

As a result of Limitation 4 (L4), this research was constrained by limited time-lapse bathymetry datasets at the Tonn Nua site, thereby more frequent and higher resolution MBES datasets are required in this region. This will enable sandwave migration analysis to be assessed over a larger timeframe and detect finer-scale shifts. Future research should therefore focus on acquiring newer MBES datasets, while also seeking to utilise previously acquired datasets at the Tonn Nua site, collected by industry or scientific surveys, thereby building a more comprehensive time-lapse dataset. Autonomous vessels such as uncrewed surface vessels or autonomous underwater vehicles could be utilised to enable cost and time efficient data acquisition to reduce survey personal and carbon emissions, providing an opportunity for more-frequent data acquisition.

In regard to Limitation 5 (L5), which results in uncertainties in sandwave migration assessments, future research should aim to utilise higher resolution MBES datasets that meet a minimum of IHO S-44 Order 1a or Special Order standards. This will reduce both the horizontal and vertical uncertainties and improve confidence in the derived results.

Finally, to address Limitation 6 (L6) regarding the lack of subsurface and metocean datasets incorporated in this research, future research should focus on the inclusion of shallow, high resolution seismic data. In-turn capturing sub-surface features and the internal structure of these features (e.g. the presence of cross-bedding in sandwaves), that are not visible in MBES datasets. In-addition, the integration of geophysical, geotechnical and ground-truthed datasets, coupled with modelled metocean data will enable a holistic assessment of seabed conditions along and hydrodynamic drivers. Further research should aim to quantify yearly sediment mobilisation and identify the primary hydrodynamic forces in the region.

References

Albarracín, S., Alcántara-Carrió, J., Montoya-Montes, I., Fontán-Bouzas, Á., Somoza, L., Amos, C.L., Salgado, J.R., 2014. Relict sand waves in the continental shelf of the Gulf of Valencia (Western Mediterranean). Journal of Sea Research.

Alevizos, E., Greinert, J., 2018. The Hyper-Angular Cube Concept for Improving the Spatial and Acoustic Resolution of MBES Backscatter Angular Response Analysis. Geosciences 8, 446. https://doi.org/10.3390/geosciences8120446

Anderson, J.T., Van Holliday, D., Kloser, R., Reid, D.G., Simard, Y., 2008. Acoustic seabed classification: current practice and future directions. ICES Journal of Marine Science 65, 1004–1011. https://doi.org/10.1093/icesjms/fsn061

Arosio, R., Gafeira, J., De Clippele, L.H., Wheeler, A.J., Huvenne, V.A.I., Sacchetti, F., Conti, L.A., Lim, A., 2024. CoMMa: A GIS geomorphometry toolbox to map and measure confined landforms. Geomorphology 458, 109227. https://doi.org/10.1016/j.geomorph.2024.109227

Arosio, R., Hobley, B., Wheeler, A.J., Sacchetti, F., Conti, L.A., Furey, T., Lim, A., 2023a. Fully convolutional neural networks applied to large-scale marine morphology mapping. Front. Mar. Sci. 10, 1228867. https://doi.org/10.3389/fmars.2023.1228867

Arosio, R., Wheeler, A.J., Sacchetti, F., Guinan, J., Benetti, S., O'Keeffe, E., Van Landeghem, K.J.J., Conti, L.A., Furey, T., Lim, A., 2023b. The geomorphology of Ireland's continental shelf. Journal of Maps 19, 2283192. https://doi.org/10.1080/17445647.2023.2283192

Ashley, G.M., 1990. Classification of Large-Scale Subaqueous Bedforms: A New Look at an Old Problem. SEPM JSR Vol. 60. https://doi.org/10.1306/212F9138-2B24-11D7-8648000102C1865D

Auguste, C., Marsh, P., Nader, J.-R., Penesis, I., Cossu, R., 2021. Modelling Morphological Changes and Migration of Large Sand Waves in a Very Energetic Tidal Environment: Banks Strait, Australia. Energies 14, 3943. https://doi.org/10.3390/en14133943

Bartholdy, J., Bartholomae, A., Flemming, B.W., 2002. Grain-size control of large compound flow-transverse bedforms in a tidal inlet of the Danish Wadden Sea. Marine Geology 188, 391–413. https://doi.org/10.1016/S0025-3227(02)00419-X

Beaudoin, J., 2010. Estimation of Sounding Uncertainty from Measurements of Water Mass Variability (PhD). Department of Geodesy and Geomatics Engineering, Technical Report No. 271, University of New Brunswick, Fredericton, New Brunswick, Canada.

Belderson, R.H., Johnson, M.A., Kenyon, N.H., 1982. Bedforms. In: Stride, A.H. (Ed.), Offshore Tidal Sands: Processess and Depositis. Chapman and Hall, London.

Bellec, V.K., Bøe, R., Bjarnadóttir, L.R., Albretsen, J., Dolan, M., Chand, S., Thorsnes, T., Jakobsen, F.W., Nixon, C., Plassen, L., Jensen, H., Baeten, N., Olsen, H., Elvenes, S., 2019. Sandbanks, sandwaves and megaripples on Spitsbergenbanken, Barents Sea. Marine Geology 416, 105998. https://doi.org/10.1016/j.margeo.2019.105998

Benz, U.C., Hofmann, P., Willhauck, G., Lingenfelder, I., Heynen, M., 2004. Multi-resolution, object-oriented fuzzy analysis of remote sensing data for GIS-ready information. ISPRS Journal of Photogrammetry and Remote Sensing 58, 239–258. https://doi.org/10.1016/j.isprsjprs.2003.10.002

Besio, G., Blondeaux, P., Brocchini, M., Vittori, G., 2004. On the modeling of sand wave migration. J. Geophys. Res. 109, 2002JC001622. https://doi.org/10.1029/2002JC001622

Besio, G., Blondeaux, P., Brocchini, M., Vittori, G., 2003. Migrating sand waves. Ocean Dynamics 53, 232–238. https://doi.org/10.1007/s10236-003-0043-x

Bhadouria, V., 2024. Pratt's Figure of Merit (https://www.mathworks.com/matlabcentral/fileexchange/60473-pratt-s-figure-of-merit), MATLAB Central File Exchange.

Blaschke, T., 2010. Object based image analysis for remote sensing. ISPRS Journal of Photogrammetry and Remote Sensing 65, 2–16. https://doi.org/10.1016/j.isprsjprs.2009.06.004

Blaschke, T., Hay, G.J., Kelly, M., Lang, S., Hofmann, P., Addink, E., Queiroz Feitosa, R., Van Der Meer, F., Van Der Werff, H., Van Coillie, F., Tiede, D., 2014. Geographic Object-Based Image Analysis – Towards a new paradigm. ISPRS Journal of Photogrammetry and Remote Sensing 87, 180–191. https://doi.org/10.1016/j.isprsjprs.2013.09.014

Blott, S.J., Pye, K., 2001. GRADISTAT: a grain size distribution and statistics package for the analysis of unconsolidated sediments. Earth Surf Processes Landf 26, 1237–1248. https://doi.org/10.1002/esp.261

Boggild, K., Li, M.Z., Eamer, J.B.R., Stacey, C.D., 2024. Geomorphology and sediment mobility on sand banks: A study of Dogfish Bank, Hecate Strait, Northeast Pacific Ocean. Earth Surf Processes Landf 49, 4485–4505. https://doi.org/10.1002/esp.5925

Brennan, C., Summers, G., De Oliveira, L.M.C., Lim, A., 2025. Enhanced angular range analysis: a novel object-based image analysis approach for seafloor characterisation. Mar Geophys Res 46, 12. https://doi.org/10.1007/s11001-025-09574-7

Brown, C., Beaudoin, J., Brissette, M., Gazzola, V., 2019. Multispectral Multibeam Echo Sounder Backscatter as a Tool for Improved Seafloor Characterization. Geosciences 9, 126. https://doi.org/10.3390/geosciences9030126

Brown, C.J., Beaudoin, J., Brissette, M., Gazzola, V., 2019. Multispectral Multibeam Echo Sounder Backscatter as a Tool for Improved Seafloor Characterization. Geosciences 9, 126. https://doi.org/10.3390/geosciences9030126

Brown, C.J., Smith, S.J., Lawton, P., Anderson, J.T., 2011. Benthic habitat mapping: A review of progress towards improved understanding of the spatial ecology of the seafloor using acoustic techniques. Estuarine, Coastal and Shelf Science 92, 502–520. https://doi.org/10.1016/j.ecss.2011.02.007

Buscombe, D., Grams, P.E., Kaplinski, M.A., 2017. Compositional Signatures in Acoustic Backscatter Over Vegetated and Unvegetated Mixed Sand-Gravel Riverbeds. JGR Earth Surface 122, 1771–1793. https://doi.org/10.1002/2017JF004302

Buscombe, D., Grams, P.E., Kaplinski, M.A., 2014. Characterizing riverbed sediment using high-frequency acoustics: 1. Spectral properties of scattering. J. Geophys. Res. Earth Surf. 119, 2674–2691. https://doi.org/10.1002/2014JF003189

BVG Associates, 2019. Guide to an offshore wind farm.

Camargo, J.M.R., Silva, M.V.B., Ferreira Júnior, A.V., Araújo, T.C.M., 2019. Marine Geohazards: A Bibliometric-Based Review. Geosciences 9, 100. https://doi.org/10.3390/geosciences9020100

Carrillo, L., Souza, A.J., Hill, A.E., Brown, J., Fernand, L., Candela, J., 2005. Detiding ADCP Data in a Highly Variable Shelf Sea: The Celtic Sea. Journal of Atmospheric and Oceanic Technology 22, 84–97. https://doi.org/10.1175/JTECH-1687.1

Casas, D., Chiocci, F., Casalbore, D., Ercilla, G., De Urbina, J.O., 2016. Magnitude-frequency distribution of submarine landslides in the Gioia Basin (southern Tyrrhenian Sea). Geo-Mar Lett 36, 405–414. https://doi.org/10.1007/s00367-016-0458-2

Castilla, G., Hay, G. J., 2008. Image objects and geographic objects, in: Blaschke, T., Lang, S., Hay, Geoffrey J. (Eds.), Object-Based Image Analysis, Lecture Notes in Geoinformation and Cartography. Springer Berlin Heidelberg, Berlin, Heidelberg, pp. 91–110. https://doi.org/10.1007/978-3-540-77058-9_5

Che Hasan, R., Ierodiaconou, D., Laurenson, L., 2012. Combining angular response classification and backscatter imagery segmentation for benthic biological habitat mapping. Estuarine, Coastal and Shelf Science 97, 1–9. https://doi.org/10.1016/j.ecss.2011.10.004

Che Hasan, R., Ierodiaconou, D., Laurenson, L., Schimel, A., 2014. Integrating Multibeam Backscatter Angular Response, Mosaic and Bathymetry Data for Benthic Habitat Mapping. PLoS ONE 9, e97339. https://doi.org/10.1371/journal.pone.0097339

Cohen, J., 1960. A Coefficient of Agreement for Nominal Scales. Educational and Psychological Measurement 20, 37–46. https://doi.org/10.1177/001316446002000104

Comaniciu, D., Meer, P., 2002. Mean shift: a robust approach toward feature space analysis. IEEE Trans. Pattern Anal. Machine Intell. 24, 603–619. https://doi.org/10.1109/34.1000236

Conti, L.A., Lim, A., Wheeler, A.J., 2019. High resolution mapping of a cold water coral mound. Sci Rep 9, 1016. https://doi.org/10.1038/s41598-018-37725-x

Coughlan, M., Guerrini, M., Creane, S., O’Shea, M., Ward, S.L., Van Landeghem, K.J.J., Murphy, J., Doherty, P., 2021. A new seabed mobility index for the Irish Sea: Modelling seabed shear stress and classifying sediment mobilisation to help predict erosion, deposition, and sediment distribution. Continental Shelf Research 229, 104574. https://doi.org/10.1016/j.csr.2021.104574

Coughlan, M., Long, M., Doherty, P., 2020a. Geological and geotechnical constraints in the Irish Sea for offshore renewable energy. Journal of Maps 16, 420–431. https://doi.org/10.1080/17445647.2020.1758811

Coughlan, M., Long, M., Doherty, P., 2020b. Geological and geotechnical constraints in the Irish Sea for offshore renewable energy. Journal of Maps 16, 420–431. https://doi.org/10.1080/17445647.2020.1758811

Creane, S., Coughlan, M., O'Shea, M., Murphy, J., 2022. Development and Dynamics of Sediment Waves in a Complex Morphological and Tidal Dominant System: Southern Irish Sea. Geosciences 12, 431. https://doi.org/10.3390/geosciences12120431

Creane, S., O'Shea, M., Coughlan, M., Murphy, J., 2023. Morphological Modelling to Investigate the Role of External Sediment Sources and Wind and Wave-Induced Flow on Sand Bank Sustainability: An Arklow Bank Case Study. JMSE 11, 2027. https://doi.org/10.3390/jmse11102027

Cummins, V., McKeogh, E., 2020. Blueprint for offshore wind in Ireland 2020-2050: A Research Synthesis. Zenodo. https://doi.org/10.5281/ZENODO.3958261

De Falco, G., Tonielli, R., Di Martino, G., Innangi, S., Simeone, S., Michael Parnum, I., 2010. Relationships between multibeam backscatter, sediment grain size and Posidonia oceanica seagrass distribution. Continental Shelf Research 30, 1941–1950. https://doi.org/10.1016/j.csr.2010.09.006

De Oliveira, N., Bastos, A.C., Da Silva Quaresma, V., Vieira, F.V., 2020. The use of Benthic Terrain Modeler (BTM) in the characterization of continental shelf habitats. Geo-Mar Lett 40, 1087–1097. https://doi.org/10.1007/s00367-020-00642-y

DECC, 2024. South Coast Designated Maritime Area Plan for Offshore Renewable Energy.

Di Stefano, M., Mirelis, G.G., Mayer, L., 2024. Groundtruther: A QGIS plug-in for seafloor characterization. Environmental Modelling & Software 171, 105861. https://doi.org/10.1016/j.envsoft.2023.105861

Díaz, J.V.M., n.d. Analysis of Multibeam Sonar Data for the Characterization of Seafloor Habitats.

Diesing, M., Green, S.L., Stephens, D., Lark, R.M., Stewart, H.A., Dove, D., 2014. Mapping seabed sediments: Comparison of manual, geostatistical, object-based image analysis and machine learning approaches. Continental Shelf Research 84, 107–119. https://doi.org/10.1016/j.csr.2014.05.004

Diesing, M., Mitchell, P., Stephens, D., 2016. Image-based seabed classification: what can we learn from terrestrial remote sensing? ICES J. Mar. Sci. 73, 2425–2441. https://doi.org/10.1093/icesjms/fsw118

Diesing, M., Mitchell, P.J., O’Keeffe, E., Gavazzi, G.O.A.M., Bas, T.L., 2020. Limitations of Predicting Substrate Classes on a Sedimentary Complex but Morphologically Simple Seabed. Remote Sensing 12, 3398. https://doi.org/10.3390/rs12203398

Diesing, M., Stephens, D., 2015a. A multi-model ensemble approach to seabed mapping. Journal of Sea Research 100, 62–69. https://doi.org/10.1016/j.seares.2014.10.013

Diesing, M., Stephens, D., 2015b. A multi-model ensemble approach to seabed mapping. Journal of Sea Research 100, 62–69. https://doi.org/10.1016/j.seares.2014.10.013

Dinh, V.N., Leahy, P., McKeogh, E., Murphy, J., Cummins, V., 2021. Development of a viability assessment model for hydrogen production from dedicated offshore wind farms. International Journal of Hydrogen Energy 46, 24620–24631. https://doi.org/10.1016/j.ijhydene.2020.04.232

Dorschel, B., Hebbeln, D., Foubert, A., White, M., Wheeler, A.J., 2007. Hydrodynamics and cold-water coral facies distribution related to recent sedimentary processes at Galway Mound west of Ireland. Marine Geology 244, 184–195. https://doi.org/10.1016/j.margeo.2007.06.010

Downing, E., O’Reilly, L., Majcher, J., O’Mahony, E., Peters, J., 2025. A Semi-Automated, Hybrid GIS-AI Approach to Seabed Boulder Detection Using High Resolution Multibeam Echosounder. Remote Sensing 17, 2711. https://doi.org/10.3390/rs17152711

Dunn, O.J., 1964. Multiple Comparisons Using Rank Sums. Technometrics 6, 241–252. https://doi.org/10.1080/00401706.1964.10490181

Eleftherakis, D., Snellen, M., Amiri-Simkooei, A., Simons, D.G., Siemes, K., 2014. Observations regarding coarse sediment classification based on multi-beam echo-sounder’s backscatter strength and depth residuals in Dutch rivers. The Journal of the Acoustical Society of America 135, 3305–3315. https://doi.org/10.1121/1.4875236

Emeana, C.J., Hughes, T.J., Dix, J.K., Gernon, T.M., Henstock, T.J., Thompson, C.E.L., Pilgrim, J.A., 2016. The thermal regime around buried submarine high-voltage cables. Geophysical Journal International 206, 1051–1064. https://doi.org/10.1093/gji/ggw195

Esmaeili, M., Dennehy, E., Flynn, D., 2024. Temporal and spatial assessment of offshore wind energy: system benefits for Ireland. IET Conf. Proc. 2024, 1–6. https://doi.org/10.1049/icp.2024.4496

Evans, W., 2018. Hydrodynamic modelling of sediment transport and bedform formation on the NW Irish shelf (PhD). University of Ulster.

Evans, W., Benetti, S., Sacchetti, F., Jackson, D.W.T., Dunlop, P., Monteys, X., 2015. Bedforms on the northwest Irish Shelf: indication of modern active sediment transport and over printing of paleo-glacial sedimentary deposits. Journal of Maps 11, 561–574. https://doi.org/10.1080/17445647.2014.956820

Ferrini, V.L., Flood, R.D., 2006. The effects of fine-scale surface roughness and grain size on 300 kHz multibeam backscatter intensity in sandy marine sedimentary environments. Marine Geology.

Flood, R.D., 1983. Classification of sedimentary furrows and a model for furrow initiation and evolution. Geol Soc America Bull 94, 630. https://doi.org/10.1130/0016-7606(1983)94<630:COSFAA>2.0.CO;2

Folk, R.L., 1954. The Distinction between Grain Size and Mineral Composition in Sedimentary-Rock Nomenclature. The Journal of Geology 62, 344–359.

Fonseca, L., Brown, C., Calder, B., Mayer, L., Rzhanov, Y., 2009. Angular range analysis of acoustic themes from Stanton Banks Ireland: A link between visual interpretation and multibeam echosounder angular signatures. Applied Acoustics 70, 1298–1304. https://doi.org/10.1016/j.apacoust.2008.09.008

Fonseca, L., Mayer, L., 2007a. Remote estimation of surficial seafloor properties through the application Angular Range Analysis to multibeam sonar data. Mar Geophys Res 28, 119–126. https://doi.org/10.1007/s11001-007-9019-4

Fonseca, L., Mayer, L., 2007b. Remote estimation of surficial seafloor properties through the application Angular Range Analysis to multibeam sonar data. Mar Geophys Res 28, 119–126. https://doi.org/10.1007/s11001-007-9019-4

Fonseca, L., Mayer, L., 2007c. Remote estimation of surficial seafloor properties through the application Angular Range Analysis to multibeam sonar data. Mar Geophys Res 28, 119–126. https://doi.org/10.1007/s11001-007-9019-4

Fonseca, L., Mayer, L., Orange, D., Driscoll, N., 2002. The high-frequency backscattering angular response of gassy sediments: Model/data comparison from the Eel River Margin, California. The Journal of the Acoustical Society of America 111, 2621–2631. https://doi.org/10.1121/1.1471911

Fonseca, L.E., Calder, B.R., n.d. Geocoder: An Efficient Backscatter Map Constructor.

Fonseca, L.E., Mayer, L.A., Kraft, B.J., 2005. Seafloor Characterization Through the Application of AVO Analysis to Multibeam Sonar Data. Boundary Influences in High Frequency Shallow Water Acoustics.

Foubert, A., Beck, T., Wheeler, A.J., Opderbecke, J., Grehan, A., Klages, M., Thiede, J., Henriet, J.-P., Polarstern ARK-XIX/3a Shipboard Party, 2005. New view of the Belgica Mounds, Porcupine Seabight, NE Atlantic: preliminary results from the Polarstern ARK-XIX/3a ROV cruise, in: Freiwald, A., Roberts, J.M. (Eds.), Cold-Water Corals and Ecosystems. Springer Berlin Heidelberg, Berlin, Heidelberg, pp. 403–415. https://doi.org/10.1007/3-540-27673-4_20

Foubert, A., Huvenne, V.A.I., Wheeler, A., Kozachenko, M., Opderbecke, J., Henriet, J.-P., 2011. The Moira Mounds, small cold-water coral mounds in the Porcupine Seabight, NE Atlantic: Part B—Evaluating the impact of sediment dynamics through high-resolution ROV-borne bathymetric mapping. Marine Geology 282, 65–78. https://doi.org/10.1016/j.margeo.2011.02.008

Frey, D., Borisov, D., Fomin, V., Morozov, E., Levchenko, O., 2022. Modeling of bottom currents for estimating their erosional-depositional potential in the Southwest Atlantic. Journal of Marine Systems 230, 103736. https://doi.org/10.1016/j.jmarsys.2022.103736

Gafeira, J., Dolan, M.F.J., Monteys, X., 2018. Geomorphometric Characterization of Pockmarks by Using a GIS-Based Semi-Automated Toolbox. Geosciences 8, 154. https://doi.org/10.3390/geosciences8050154

Gaida, T., Tengku Ali, T., Snellen, M., Amiri-Simkooei, A., Van Dijk, T., Simons, D., 2018. A Multispectral Bayesian Classification Method for Increased Acoustic Discrimination of Seabed Sediments Using Multi-Frequency Multibeam Backscatter Data. Geosciences 8, 455. https://doi.org/10.3390/geosciences8120455

Gaida, T.C., Mohammadloo, T.H., Snellen, M., Simons, D.G., 2019a. Mapping the Seabed and Shallow Subsurface with Multi-Frequency Multibeam Echosounders. Remote Sensing 12, 52. https://doi.org/10.3390/rs12010052

Gaida, T.C., Snellen, M., Van Dijk, T.A.G.P., Simons, D.G., 2019b. Geostatistical modelling of multibeam backscatter for full-coverage seabed sediment maps. Hydrobiologia 845, 55–79. https://doi.org/10.1007/s10750-018-3751-4

Gallagher, C., 2002. The morphology and palaeohydrology of a submerged glaciofluvial channel emerging from Waterford Harbour onto the nearshore continental shelf of the Celtic Sea. Irish Geography 35, 111–132.

Gallagher, C., Sutton, G., Bell, T., 2004. Submerged ice marginal forms in the Celtic sea off Waterford Harbour, Ireland: Implications for understanding regional glaciation and sea level changes following the last glacial maximum in Ireland. Irish Geography 37, 145–165. https://doi.org/10.1080/00750770409555839

Garlan, T., Marches, E., Brenon, E., 2015. A CLASSIFICATION OF SCOURING MARKS IN MACROTIDAL ENVIRONMENTS FROM ANALYSIS OF LONG TERM WRECK MARKS, in: The Proceedings of the Coastal Sediments 2015. Presented at the Coastal Sediments 2015, WORLD SCIENTIFIC, San Diego, USA. https://doi.org/10.1142/9789814689977_0202

Gaughan, E., 2020. An assessment of the potential for Co-located offshore wind and wave farms in Ireland.

Gavin & Doherty Geosolutions (GDG), 2021. A review of the Irish Offshore Renewable Energy (ORE) Sector's data and information requirements in the context of the INFOMAR Seabed Mapping Programme Review report.

Giglio, C., Benetti, S., Plets, R.M.K., Dunlop, P., Ó Cofaigh, C., Sacchetti, F., Salomon, E., 2022a. Character of advance and retreat of the southwest sector of the British-Irish Ice Sheet during the last glaciation. Quaternary Science Reviews 291, 107655. https://doi.org/10.1016/j.quascirev.2022.107655

Giglio, C., Benetti, S., Sacchetti, F., Lockhart, E., Hughes Clarke, J., Plets, R., Van Landeghem, K., Ó Cofaigh, C., Scourse, J., Dunlop, P., 2022b. A Late Pleistocene channelized subglacial meltwater system on the Atlantic continental shelf south of Ireland. Boreas 51, 118–135. https://doi.org/10.1111/bor.12536

Goff, J.A., Kraft, B.J., Mayer, L.A., Schock, S.G., Sommerfield, C.K., Olson, H.C., Gulick, S.P.S., Nordfjord, S., 2004. Seabed characterization on the New Jersey middle and outer shelf: correlatability and spatial variability of seafloor sediment properties. Marine Geology 209, 147–172. https://doi.org/10.1016/j.margeo.2004.05.030

Goff, J.A., Swift, D.J.P., Duncan, C.S., Mayer, L.A., Hughes-Clarke, J., 1999. High-resolution swath sonar investigation of sand ridge, dune and ribbon morphology in the offshore environment of the New Jersey margin. Marine Geology 161, 307–337. https://doi.org/10.1016/S0025-3227(99)00073-0

Griffin, J.D., Hemer, M.A., Jones, B.G., 2008. Mobility of sediment grain size distributions on a wave dominated continental shelf, southeastern Australia. Marine Geology 252, 13–23. https://doi.org/10.1016/j.margeo.2008.03.005

Guinan, J., McKeon, C., O'Keeffe, E., Monteys, X., Sacchetti, F., Coughlan, M., Nic Aonghusa, C., 2021. INFOMAR data supports offshore energy development and marine spatial planning in the Irish offshore via the EMODnet Geology portal. QJEGH 54, qjegh2020-033. https://doi.org/10.1144/qjegh2020-033

Hamilton, D., Sommerville, J.H., Stanford, P.N., 1980. Bottom currents and shelf sediments, southwest of Britain. Sedimentary Geology 26, 115–138. https://doi.org/10.1016/0037-0738(80)90008-1

Hamilton, E.L., 1974. Prediction of Deep-Sea Sediment Properties: State-of-the-Art, in: Inderbitzen, A.L. (Ed.), Deep-Sea Sediments. Springer US, Boston, MA, pp. 1–43. https://doi.org/10.1007/978-1-4684-2754-7_1

Hamilton, L.J., Parnum, I., 2011. Acoustic seabed segmentation from direct statistical clustering of entire multibeam sonar backscatter curves. Continental Shelf Research 31, 138–148. https://doi.org/10.1016/j.csr.2010.12.002

Hasan, R., Ierodiaconou, D., Monk, J., 2012. Evaluation of Four Supervised Learning Methods for Benthic Habitat Mapping Using Backscatter from Multi-Beam Sonar. Remote Sensing 4, 3427–3443. https://doi.org/10.3390/rs4113427

Hassan, Q., Viktor, P., J. Al-Musawi, T., Mahmood Ali, B., Algburi, S., Alzoubi, H.M., Khudhair Al-Jiboory, A., Zuhair Sameen, A., Salman, H.M., Jaszczur, M., 2024. The renewable energy role in the global energy Transformations. Renewable Energy Focus 48, 100545. https://doi.org/10.1016/j.ref.2024.100545

Hay, G.J., Castilla, G., n.d. OBJECT-BASED IMAGE ANALYSIS: STRENGTHS, WEAKNESSES, OPPORTUNITIES AND THREATS (SWOT).

Hidayat, A.R.T., Hasyim, A.W., Prayitno, G., Harisandy, J.D., 2021. Farm Owners' Perception toward Farmland Conversion: An Empirical Study from Indonesian Municipality. EREM 77, 109–124. https://doi.org/10.5755/j01.erem.77.1.27471

Hildebrand, J., 2004. Sources of anthropogenic sound in the marine environment. In Report to the policy on sound and marine mammals: an international workshop. US Marine Mammal Commission and Joint Nature Conservation Committee, UK. London, England.

Hodge, R.A., Voepel, H.E., Yager, E.M., Leyland, J., Johnson, J.P.L., Sear, D.A., Ahmed, S., 2024. Improving predictions of critical shear stress in gravel bed rivers: Identifying the onset of sediment transport and quantifying sediment structure. Earth Surf Processes Landf 49, 2517–2537. https://doi.org/10.1002/esp.5842

Hopkins, A., 2007. MESH Recommended operating guidelines (ROG) for swath bathymetry.

Hossain, M.D., 2019. Segmentation for Object-Based Image Analysis (OBIA)_ A review of algorithms and challenges from remote sensing perspective. ISPRS Journal of Photogrammetry and Remote Sensing.

Hossain, M.D., Chen, D., 2019. Segmentation for Object-Based Image Analysis (OBIA): A review of algorithms and challenges from remote sensing perspective. ISPRS Journal of Photogrammetry and Remote Sensing 150, 115–134. https://doi.org/10.1016/j.isprsjprs.2019.02.009

Howe, J.A., Stoker, M.S., Masson, D.G., Pudsey, C.J., Morris, P., Larter, R.D., Bulat, J., 2006. Seabed morphology and the bottom-current pathways around Rosemary Bank seamount, northern Rockall Trough, North Atlantic. Marine and Petroleum Geology 23, 165–181. https://doi.org/10.1016/j.marpetgeo.2005.08.003

Huang, Z., Siwabessy, J., Cheng, H., Nichol, S., 2018. Using Multibeam Backscatter Data to Investigate Sediment-Acoustic Relationships. JGR Oceans 123, 4649–4665. https://doi.org/10.1029/2017JC013638

Huang, Z., Siwabessy, J., Nichol, S., Anderson, T., Brooke, B., 2013. Predictive mapping of seabed cover types using angular response curves of multibeam backscatter data: Testing different feature analysis approaches. Continental Shelf Research 61–62, 12–22. https://doi.org/10.1016/j.csr.2013.04.024

Huang, Z., Siwabessy, J., Nichol, S.L., Brooke, B.P., 2014. Predictive mapping of seabed substrata using high-resolution multibeam sonar data: A case study from a shelf with complex geomorphology. Marine Geology 357, 37–52. https://doi.org/10.1016/j.margeo.2014.07.012

Huang Zhi, Justy Siwabessy, Scott L. Nichol, Brendan P. Brooke, 2014. Predictive mapping of seabed substrata using high-resolution multibeam sonar data: A case study from a shelf with complex geomorphology. Marine Geology 357, 37–52. https://doi.org/10.1016/j.margeo.2014.07.012

Hughes Clarke, J., 1994a. Toward remote seafloor classification using the angular response of acoustic backscattering: a case study from multiple overlapping GLORIA data. IEEE J. Oceanic Eng. 19, 112–127. https://doi.org/10.1109/48.289456

Hughes Clarke, J., 1994b. Toward remote seafloor classification using the angular response of acoustic backscattering: a case study from multiple overlapping GLORIA data. IEEE J. Oceanic Eng. 19, 112–127. https://doi.org/10.1109/48.289456

Hughes Clarke, J.E., Mayer, L.A., Wells, D.E., 1996. Shallow-water imaging multibeam sonars: A new tool for investigating seafloor processes in the coastal zone and on the continental shelf. Marine Geophysical Researches 18, 607–629. https://doi.org/10.1007/BF00313877

Huntley, D.A., Nicholls, R.J., Liu, C., Dyer, K.R., 1994. Measurements of the semi-diurnal drag coefficient over sand waves. Continental Shelf Research 14, 437–456. https://doi.org/10.1016/0278-4343(94)90097-3

Huvenne, V.A.I., Beyer, A., De Haas, H., Dekindt, K., Henriet, J.-P., Kozachenko, M., Olu-Le Roy, K., Wheeler, A.J., TOBI/Pelagia 197, CARACOLE cruise participants, 2005. The seabed appearance of different coral bank provinces in the Porcupine Seabight, NE Atlantic: results from sidescan sonar and ROV seabed mapping, in: Freiwald, A., Roberts, J.M. (Eds.), Cold-Water Corals and Ecosystems. Springer Berlin Heidelberg, Berlin, Heidelberg, pp. 535–569. https://doi.org/10.1007/3-540-27673-4_27

Huvenne, V.A.I., Masson, D.G., Wheeler, A.J., 2009. Sediment dynamics of a sandy contourite: the sedimentary context of the Darwin cold-water coral mounds, Northern Rockall Trough. Int J Earth Sci (Geol Rundsch) 98, 865–884. https://doi.org/10.1007/s00531-008-0312-5

Ierodiaconou, D., Schimel, A.C.G., Kennedy, D., Monk, J., Gaylard, G., Young, M., Diesing, M., Rattray, A., 2018a. Combining pixel and object based image analysis of ultra-high resolution multibeam bathymetry and backscatter for habitat mapping in shallow marine waters. Mar Geophys Res 39, 271–288. https://doi.org/10.1007/s11001-017-9338-z

Ierodiaconou, D., Schimel, A.C.G., Kennedy, D., Monk, J., Gaylard, G., Young, M., Diesing, M., Rattray, A., 2018b. Combining pixel and object based image analysis of ultra-high resolution multibeam bathymetry and backscatter for habitat mapping in shallow marine waters. Mar Geophys Res 39, 271–288. https://doi.org/10.1007/s11001-017-9338-z

INFOMAR, 2007. Ground Truthing and Sampling Strategy.

Ivakin, A.N., Sessarego, J.-P., 2007. High frequency broad band scattering from water-saturated granular sediments: Scaling effects. The Journal of the Acoustical Society of America 122, EL165–EL171. https://doi.org/10.1121/1.2784534

Jackson, D.R., Baird, A.M., Crisp, J.J., Thomson, P.A.G., 1986a. High-frequency bottom backscatter measurements in shallow water. The Journal of the Acoustical Society of America 80, 1188–1199. https://doi.org/10.1121/1.393809

Jackson, D.R., Richardson, M.D., 2007. Seafloor Roughness, in: High-Frequency Seafloor Acoustics. Springer New York, New York, NY, pp. 171–200. https://doi.org/10.1007/978-0-387-36945-7_6

Jackson, D.R., Winebrenner, D.P., Ishimaru, A., 1986b. Application of the composite roughness model to high-frequency bottom backscattering. The Journal of the Acoustical Society of America 79, 1410–1422. https://doi.org/10.1121/1.393669

Jakeman, E., Tough, R.J.A., 1988. Non-Gaussian models for the statistics of scattered waves. Advances in Physics 37, 471–529. https://doi.org/10.1080/00018738800101419

Jakobsson, M., Graham, G., Carbotte, S., Falconer, R., Ferrini, V., Marks, K., Mayer, L., Rovere, M., Schmitt, T., Weatherall, P., Wigley, R., 2020. The Nippon Foundation – GEBCO – Seabed 2030: Roadmap for Future Ocean Floor Mappig.

Janowski, Ł., Tęgowski, J., Nowak, J., 2018. Seafloor mapping based on multibeam echosounder bathymetry and backscatter data using Object-Based Image Analysis: a case study from the Rewal site, the Southern Baltic. Oceanological and Hydrobiological Studies 47, 248–259. https://doi.org/10.1515/ohs-2018-0024

Jasiewicz, J., Stepinski, T.F., 2013. Geomorphons — a pattern recognition approach to classification and mapping of landforms. Geomorphology 182, 147–156. https://doi.org/10.1016/j.geomorph.2012.11.005

Jiang, S., Dong, C., Feng, J., Cheng, H., Yang, J., Li, M., Wang, J., Chen, X., Zhou, Y., 2023. Geological hazards in the Oujiang estuary in the Zhejiang Province, China: type, distribution, and origin. Front. Earth Sci. 11, 1237831. https://doi.org/10.3389/feart.2023.1237831

Keer, F.R., Cardinell, A.P., 1981. "Potential Geologic Hazards and Constraints for Blocks in Proposed Mid-Atlantic OCS Oil and Gas Lease Sale 59,." United States Department of the Interior, Geological Survey, Open-File Report 81-725.

Kenyon, N.H., 1970. Sand ribbons of European tidal seas. Marine Geology 9, 25–39. https://doi.org/10.1016/0025-3227(70)90078-2

Kenyon, N.H., Belderson, R.H., 1973. Bed forms of the Mediterranean undercurrent observed with side-scan sonar. Sedimentary Geology 9, 77–99. https://doi.org/10.1016/0037-0738(73)90027-4

Knaapen, M.A.F., 2005. Sandwave migration predictor based on shape information. J. Geophys. Res. 110, 2004JF000195. https://doi.org/10.1029/2004JF000195

Kopp, H., Chiocci, F.L., Berndt, C., Namık Çağatay, Ferreira, T., Fortes, J., Eulàlia Gràcia, Vega, A.G., Kopf, A., Sørensen, M., Sultan, N., Yeo, I., 2021. Marine geohazards: Safeguarding society and the Blue Economy from a hidden threat. Zenodo. https://doi.org/10.5281/ZENODO.5591938

Kubicki, A., 2008. Large and very large subaqueous dunes on the continental shelf off southern Vietnam, South China Sea. Geo-Mar Lett 28, 229–238. https://doi.org/10.1007/s00367-008-0103-9

Kucharczyk, M., Hay, G.J., Ghaffarian, S., Hugenholtz, C.H., 2020. Geographic Object-Based Image Analysis: A Primer and Future Directions. Remote Sensing 12, 2012. https://doi.org/10.3390/rs12122012

Lamarche, G., Lurton, X., 2018. Recommendations for improved and coherent acquisition and processing of backscatter data from seafloor-mapping sonars. Mar Geophys Res 39, 5–22. https://doi.org/10.1007/s11001-017-9315-6

Landero Figueroa, M.M., Parsons, M.J.G., Saunders, B.J., Radford, B., Salgado-Kent, C., Parnum, I.M., 2021. The use of singlebeam echo-sounder depth data to produce demersal fish distribution models that are comparable to models produced using multibeam echo-sounder depth. Ecology and Evolution 11, 17873–17884. https://doi.org/10.1002/ece3.8351

Langhorne, D.N., 1978. Offshore Engineering and Navigational Problems - The Relevance of Sandwave Research. Published by the Society for Underwater Technology in Conjunction with the Institute of Oceanographic Sciences.

Leenders, S., Damveld, J.H., Schouten, J., Hoekstra, R., Roetert, T.J., Borsje, B.W., 2021. Numerical modelling of the migration direction of tidal sand waves over sand banks. Coastal Engineering 163, 103790. https://doi.org/10.1016/j.coastaleng.2020.103790

Legere, C., n.d. QPS Angular Range Analysis Documentation.

Li, D., Tang, C., Xia, C., Zhang, H., 2017. Acoustic mapping and classification of benthic habitat using unsupervised learning in artificial reef water. Estuarine, Coastal and Shelf Science 185, 11–21. https://doi.org/10.1016/j.ecss.2016.12.001

Li, M.Z., Hannah, C.G., Perrie, W.A., Tang, C.C.L., Prescott, R.H., Greenberg, D.A., 2015. Modelling seabed shear stress, sediment mobility, and sediment transport in the Bay of Fundy. Can. J. Earth Sci. 52, 757–775. https://doi.org/10.1139/cjes-2014-0211

Li, Z., Yin, Z., Yan, X., Yang, X., Huang, X., Han, Z., 2025. Safety assessment of wellhead devices on the offshore platform in a shallow gas blowout accident. Process Safety Progress 44, 57–69. https://doi.org/10.1002/prs.12653

Lichtman, I.D., Baas, J.H., Amoudry, L.O., Thorne, P.D., Malarkey, J., Hope, J.A., Peakall, J., Paterson, D.M., Bass, S.J., Cooke, R.D., Manning, A.J., Davies, A.G., Parsons, D.R., Ye, L., 2018. Bedform migration in a mixed sand and cohesive clay intertidal environment and implications for bed material transport predictions. Geomorphology 315, 17–32. https://doi.org/10.1016/j.geomorph.2018.04.016

Lim, A., Huvenne, V.A.I., Vertino, A., Spezzaferri, S., Wheeler, A.J., 2018. New insights on coral mound development from groundtruthed high-resolution ROV-mounted multibeam imaging. Marine Geology 403, 225–237. https://doi.org/10.1016/j.margeo.2018.06.006

Lim, A., Wheeler, A.J., Price, D.M., O'Reilly, L., Harris, K., Conti, L., 2020. Influence of benthic currents on cold-water coral habitats: a combined benthic monitoring and 3D photogrammetric investigation. Sci Rep 10, 19433. https://doi.org/10.1038/s41598-020-76446-y

Lockhart, E.A., 2019. Glacial sculpting and post-glacial drowning of the Celtic Sea (PhD). Bangor University.

Lockhart, E.A., Scourse, J.D., Praeg, D., Van Landeghem, K.J.J., Mellett, C., Saher, M., Callard, L., Chiverrell, R.C., Benetti, S., Cofaigh, C.Ó., Clark, C.D., 2018. A stratigraphic investigation of the Celtic Sea megaridges based on seismic and core data from the Irish-UK sectors. Quaternary Science Reviews 198, 156–170. https://doi.org/10.1016/j.quascirev.2018.08.029

Lu, D., Weng, Q., 2007. A survey of image classification methods and techniques for improving classification performance. International Journal of Remote Sensing 28, 823–870. https://doi.org/10.1080/01431160600746456

Lucieer, V., Roche, M., Degrendele, K., Malik, M., Dolan, M., Lamarche, G., 2018. User expectations for multibeam echo sounders backscatter strength data-looking back into the future. Mar Geophys Res 39, 23–40. https://doi.org/10.1007/s11001-017-9316-5

Lurton, X., Lamarche, G., 2015. Chapter 1: introduction to backscat ter measurements by seafloor-mapping sonars., in: Lurton X, Lamarche G (Eds) Backscatter Measurements by Seafloor-Mapping Sonars: Guidelines and Recommendations. GeoHab Backscatter Working Group.

Majcher, J., Quinn, R., Smyth, T., Plets, R., McGonigle, C., Westley, K., Sacchetti, F., Coughlan, M., 2022. Using difference modelling and computational fluid dynamics to investigate the evolution of complex, tidally influenced shipwreck sites. Ocean Engineering 246, 110625. https://doi.org/10.1016/j.oceaneng.2022.110625

Marine Institute, 2024. Data delivery technical note TC24016.

Martinez, A., Iglesias, G., 2022. Site selection of floating offshore wind through the levelised cost of energy: A case study in Ireland. Energy Conversion and Management 266, 115802. https://doi.org/10.1016/j.enconman.2022.115802

May, J.-H., 2015. Parabolic Dune, in: Hargitai, H., Kereszturi, Á. (Eds.), Encyclopedia of Planetary Landforms. Springer New York, New York, NY, pp. 1515–1518. https://doi.org/10.1007/978-1-4614-3134-3_251

Mayer, L., Jakobsson, M., Allen, G., Dorschel, B., Falconer, R., Ferrini, V., Lamarche, G., Snaith, H., Weatherall, P., 2018a. The Nippon Foundation—GEBCO Seabed 2030 Project: The Quest to See the World’s Oceans Completely Mapped by 2030. Geosciences 8, 63. https://doi.org/10.3390/geosciences8020063

Mayer, L., Jakobsson, M., Allen, G., Dorschel, B., Falconer, R., Ferrini, V., Lamarche, G., Snaith, H., Weatherall, P., 2018b. The Nippon Foundation—GEBCO Seabed 2030 Project: The Quest to See the World’s Oceans Completely Mapped by 2030. Geosciences 8, 63. https://doi.org/10.3390/geosciences8020063

McGonigle, C., Brown, C., Quinn, R., Grabowski, J., 2009. Evaluation of image-based multibeam sonar backscatter classification for benthic habitat discrimination and mapping at Stanton Banks, UK. Estuarine, Coastal and Shelf Science 81, 423–437. https://doi.org/10.1016/j.ecss.2008.11.017

McGonigle, C., Collier, J.S., 2014a. Interlinking backscatter, grain size and benthic community structure. Estuarine, Coastal and Shelf Science 147, 123–136. https://doi.org/10.1016/j.ecss.2014.05.025

McGonigle, C., Collier, J.S., 2014b. Interlinking backscatter, grain size and benthic community structure. Estuarine, Coastal and Shelf Science 147, 123–136. https://doi.org/10.1016/j.ecss.2014.05.025

Mellett, C., Long, D., Carter, G., Chiverell, R., Van Landeghem, K., 2015. Geology of the seabed and shallow subsurface: The Irish Sea. British Geological Survey Commissioned Report (No. CR/15/057).

Menandro, P.S., Misiuk, B., Schneider Von Deimling, J., Bastos, A.C., Brown, C.J., 2025. Multifrequency seafloor acoustic backscatter as a tool for improved biological and geological assessments – updating knowledge, prospects, and challenges. Front. Remote Sens. 6, 1546280. https://doi.org/10.3389/frsen.2025.1546280

Misiuk, B., Brown, C.J., 2022. Multiple imputation of multibeam angular response data for high resolution full coverage seabed mapping. Mar Geophys Res 43, 7. https://doi.org/10.1007/s11001-022-09471-3

Misiuk, B., Brown, C.J., Robert, K., Lacharité, M., 2020. Harmonizing Multi-Source Sonar Backscatter Datasets for Seabed Mapping Using Bulk Shift Approaches. Remote Sensing 12, 601. https://doi.org/10.3390/rs12040601

Mulrooney, T., Akinnusi, S., McGinn, C., Okoli, C., Esimaje, T., 2024. A comparison of raster-based point density calculations to vector-based counterparts as applied to the study of food availability. Agric & Food Secur 13, 4. https://doi.org/10.1186/s40066-023-00455-z

Nanson, R., Arosio, R., Gafeira, J., McNeil, M., Dove, D., Bjarnadóttir, L., Dolan, M., Guinan, J., Post, A., Webb, J., Nichol, S., 2023. A two-part seabed geomorphology classification scheme; Part 2: Geomorphology classification framework and glossary (Version 1.0). Zenodo. https://doi.org/10.5281/ZENODO.7804019

Negro, V., López-Gutiérrez, J.-S., Esteban, M.D., Matutano, C., 2014. Uncertainties in the design of support structures and foundations for offshore wind turbines. Renewable Energy 63, 125–132. https://doi.org/10.1016/j.renene.2013.08.041

Nemeth, A., Hulscher, S.J.M.H., De Vriend, H.J., 2003. Offshore sand wave dynamics, engineering problems and future solutions. Pipeline Gas J 230, 67–69.

Németh, A.A., Hulscher, S.J.M.H., De Vriend, H.J., 2002. Modelling sand wave migration in shallow shelf seas. Continental Shelf Research 22, 2795–2806. https://doi.org/10.1016/S0278-4343(02)00127-9

O'Hanlon, Z., Cummins, V., 2020. A comparative insight of Irish and Scottish regulatory frameworks for offshore wind energy – An expert perspective. Marine Policy 117, 103934. https://doi.org/10.1016/j.marpol.2020.103934

O'Toole, R., Judge, M., Sacchetti, F., Furey, T., Mac Craith, E., Sheehan, K., Kelly, S., Cullen, S., McGrath, F., Monteys, X., 2022. Mapping Ireland's coastal, shelf and deep-water environments using illustrative case studies to highlight the impact of seabed mapping on the generation of blue knowledge. SP 505, 71–96. https://doi.org/10.1144/SP505-2019-207

Pantin, H.M., Evans, C.D.R., 1984. The Quaternary history of the central and southwestern Celtic Sea. Marine Geology 57, 259–293. https://doi.org/10.1016/0025-3227(84)90202-0

Parnum, I.M., 2007. Benthic Habitat Mapping using Multibeam Sonar Systems.

Peters, J.L., Butschek, F., O'Connell, R., Cummins, V., Murphy, J., Wheeler, A.J., 2020. Geological seabed stability model for informing Irish offshore renewable energy opportunities. Adv. Geosci. 54, 55–65. https://doi.org/10.5194/adgeo-54-55-2020

Peters, J.L., Wheeler, A.J., Cummins, V., 2019. Data Resources Assessment—Phase 2. Zenodo. https://doi.org/10.5281/ZENODO.3948330

Phinn, S.R., Roelfsema, C.M., Mumby, P.J., 2012. Multi-scale, object-based image analysis for mapping geomorphic and ecological zones on coral reefs. International Journal of Remote Sensing 33, 3768–3797. https://doi.org/10.1080/01431161.2011.633122

Pingree, R.D., 1980. Chapter 13 Physical Oceanography of the Celtic Sea and English Channel, in: Elsevier Oceanography Series. Elsevier, pp. 415–465. https://doi.org/10.1016/S0422-9894(08)71358-8

Pratt, W.K., 2001. Digital Image Processing (Third Edition): PIKS Inside, 3rd ed. ed. Wiley-Interscience, S.l.

Quality Positioning Services (QPS), 2022. Fledermaus 7.8 Documentation FMGT 7.10/FMMidwater 7.9.

Quinn, R., 2006. The role of scour in shipwreck site formation processes and the preservation of wreck-associated scour signatures in the sedimentary record – evidence from seabed and sub-surface data. Journal of Archaeological Science 33, 1419–1432. https://doi.org/10.1016/j.jas.2006.01.011

Quinn, R.., Smyth, T.A.G., 2018. Processes and patterns of flow, erosion, and deposition at shipwreck sites: a computational fluid dynamic simulation. Archaeol Anthropol Sci 10, 1429–1442. https://doi.org/10.1007/s12520-017-0468-7

Rebesco, M., Hernández-Molina, F.J., Van Rooij, D., Wåhlin, A., 2014. Contourites and associated sediments controlled by deep-water circulation processes: State-of-the-art and future considerations. Marine Geology 352, 111–154. https://doi.org/10.1016/j.margeo.2014.03.011

Roberts, J.M., Peppe, O.C., Dodds, L.A., Mercer, D.J., Thomson, W.T., Gage, J.D., Meldrum, D.T., 2005. Monitoring environmental variability around cold-water coral reefs: the use of a benthic photolander and the potential of seafloor observatories, in: Freiwald, A., Roberts, J.M. (Eds.), Cold-Water Corals and Ecosystems. Springer Berlin Heidelberg, Berlin, Heidelberg, pp. 483–502. https://doi.org/10.1007/3-540-27673-4_24

Roche, M., Degrendele, K., Vrignaud, C., Loyer, S., Le Bas, T., Augustin, J.-M., Lurton, X., 2018. Control of the repeatability of high frequency multibeam echosounder backscatter by using natural reference areas. Mar Geophys Res 39, 89–104. https://doi.org/10.1007/s11001-018-9343-x

Roetert, T., Raaijmakers, T., Borsje, B., 2017. Cable route optimization for offshore wind farms in morphodynamic areas.

Runya, R.M., McGonigle, C., Quinn, R., Howe, J., Collier, J., Fox, C., Dooley, J., O'Loughlin, R., Calvert, J., Scott, L., Abernethy, C., Evans, W., 2021. Examining the Links between Multi-Frequency Multibeam Backscatter Data and Sediment Grain Size. Remote Sensing 13, 1539. https://doi.org/10.3390/rs13081539

Rzhanov, Y., Fonseca, L., Mayer, L., 2012. Construction of seafloor thematic maps from multibeam acoustic backscatter angular response data. Computers & Geosciences 41, 181–187. https://doi.org/10.1016/j.cageo.2011.09.001

Sacchetti, F., Benetti, S., Ó Cofaigh, C., Georgiopoulou, A., 2012. Geophysical evidence of deep-keeled icebergs on the Rockall Bank, Northeast Atlantic Ocean. Geomorphology 159–160, 63–72. https://doi.org/10.1016/j.geomorph.2012.03.005

Samsudin, S.A., Hasan, R.C., 2017. ASSESSMENT OF MULTIBEAM BACKSCATTER TEXTURE ANALYSIS FOR SEAFLOOR SEDIMENT CLASSIFICATION. Int. Arch. Photogramm. Remote Sens. Spatial Inf. Sci. XLII-4/W5, 177–183. https://doi.org/10.5194/isprs-archives-XLII-4-W5-177-2017

Santos, R., Rodrigues, A., Quartau, R., 2018. Acoustic remote characterization of seabed sediments using the Angular Range Analysis technique: The inlet channel of Tagus

River estuary (Portugal). Marine Geology 400, 60–75. https://doi.org/10.1016/j.margeo.2018.03.005

Schimel, A.C.G., Beaudoin, J., Parnum, I.M., Le Bas, T., Schmidt, V., Keith, G., Ierodiaconou, D., 2018. Multibeam sonar backscatter data processing. Mar Geophys Res 39, 121–137. https://doi.org/10.1007/s11001-018-9341-z

Schimel, A.C.G., Healy, T.R., Johnson, D., Immenga, D., 2010. Quantitative experimental comparison of single-beam, sidescan, and multibeam benthic habitat maps. ICES Journal of Marine Science 67, 1766–1779. https://doi.org/10.1093/icesjms/fsq102

Schimel, A.C.G., Ierodiaconou, D., Hulands, L., Kennedy, D.M., 2015. Accounting for uncertainty in volumes of seabed change measured with repeat multibeam sonar surveys. Continental Shelf Research 111, 52–68. https://doi.org/10.1016/j.csr.2015.10.019

Schneider Von Deimling, J., Weinrebe, W., Tóth, Zs., Fossing, H., Endler, R., Rehder, G., Spieß, V., 2013. A low frequency multibeam assessment: Spatial mapping of shallow gas by enhanced penetration and angular response anomaly. Marine and Petroleum Geology 44, 217–222. https://doi.org/10.1016/j.marpetgeo.2013.02.013

Scourse, J.D., Austin, W.E.N., Bateman, R.M., Catt, J.A., Evans, C.D.R., Robinson, J.E., Young, J.R., 1990. Sedimentology and micropalaeontology of glacimarine sediments from the Central and Southwestern Celtic Sea. SP 53, 329–347. https://doi.org/10.1144/GSL.SP.1990.053.01.19

Seabed 2030 announces millions of square kilometers of new seafloor data on World Hydrography Day [WWW Document], 2025. . Seabed 2030. URL https://seabed2030.org/2025/06/21/seabed-2030-announces-millions-of-square-kilometers-of-new-seafloor-data-on-world-hydrography-day/ (accessed 9.10.25).

Sheehan, K., 2013. Survey Report: CV13_01. Marine Institute & Geological Survey of Ireland.

Sheehan, P.K., Borovik, A., 2007. Survey Report: Leg CV07_02. Marine Institute & Geological Survey of Ireland.

Song, B., Cummins, C., Zou, Q., 2023. Coupled stability of offshore wind monopile foundations and submarine slopes under periodic loads. Applied Ocean Research 140, 103714. https://doi.org/10.1016/j.apor.2023.103714

Soulsby, R., 1997. Dynamics of marine sands, a manual for practical applications. Thomas Telford, London.

Soulsby, R.L., Clarke, S., 2005. Bed shear-stresses under combined waves and currents on smooth and rough beds.

Stephens, D., Diesing, M., 2014. A Comparison of Supervised Classification Methods for the Prediction of Substrate Type Using Multibeam Acoustic and Legacy Grain-Size Data. PLoS ONE 9, e93950. https://doi.org/10.1371/journal.pone.0093950

Stone, A., Hickey, S., Radford, B., Wakeford, M., 2024. Mapping emergent coral reefs: a comparison of pixel- and object-based methods. Remote Sens Ecol Conserv rse2.401. https://doi.org/10.1002/rse2.401

Stow, D.A.V., Hernández-Molina, F.J., Llave, E., Sayago-Gil, M., Díaz Del Río, V., Branson, A., 2009. Bedform-velocity matrix: The estimation of bottom current velocity from bedform observations. Geology 37, 327–330. https://doi.org/10.1130/G25259A.1

Strachan, R., 2021. Bedrock target analysis for ROV rockdrill sampling and existing sample stratigraphic and mineralogical verification (BeTar_drill) (MRes Thesis). University College Cork.

Stride, A.H., 1963. Current-swept sea floors near the southern half of Great Britain. QJGS 119, 175–197. https://doi.org/10.1144/gsjgs.119.1.0175

Summers, G., Lim, A., Wheeler, A.J., 2023. Multi resolution appraisal of Cork Harbour estuary: An object based image analysis approach. Geomorphology 439, 108851. https://doi.org/10.1016/j.geomorph.2023.108851

Summers, G., Lim, A., Wheeler, A.J., 2022. A Characterisation of Benthic Currents from Seabed Bathymetry: An Object-Based Image Analysis of Cold-Water Coral Mounds. Remote Sensing 14, 4731. https://doi.org/10.3390/rs14194731

Summers, G., Lim, A., Wheeler, A.J., 2021. A Scalable, Supervised Classification of Seabed Sediment Waves Using an Object-Based Image Analysis Approach. Remote Sensing 13, 2317. https://doi.org/10.3390/rs13122317

Survarachakan, S., Prasad, P.J.R., Naseem, R., Pérez De Frutos, J., Kumar, R.P., Langø, T., Alaya Cheikh, F., Elle, O.J., Lindseth, F., 2022. Deep learning for image-based liver analysis — A comprehensive review focusing on malignant lesions. Artificial Intelligence in Medicine 130, 102331. https://doi.org/10.1016/j.artmed.2022.102331

Thébaudeau, B., Monteys, X., McCarron, S., O'Toole, R., Caloca, S., 2016. Seabed geomorphology of the Porcupine Bank, West of Ireland. Journal of Maps 12, 947–958. https://doi.org/10.1080/17445647.2015.1099573

Thompson, C.E.L., Silburn, B., Williams, M.E., Hull, T., Sivyer, D., Amoudry, L.O., Widdicombe, S., Ingels, J., Carnovale, G., McNeill, C.L., Hale, R., Marchais, C.L., Hicks, N., Smith, H.E.K., Klar, J.K., Hiddink, J.G., Kowalik, J., Kitidis, V., Reynolds, S., Woodward, E.M.S., Tait, K., Homoky, W.B., Kröger, S., Bolam, S., Godbold, J.A., Aldridge, J., Mayor, D.J., Benoist, N.M.A., Bett, B.J., Morris, K.J., Parker, E.R., Ruhl, H.A., Statham, P.J., Solan, M., 2017. An approach for the identification of exemplar sites for scaling up targeted field observations of benthic biogeochemistry in heterogeneous environments. Biogeochemistry 135, 1–34. https://doi.org/10.1007/s10533-017-0366-1

Tóth, Z., McCarron, S., Wheeler, A.J., Wenau, S., Davis, S., Lim, A., Spiess, V., 2020. Geomorphological and seismostratigraphic evidence for multidirectional polyphase glaciation of the northern Celtic Sea. J Quaternary Science 35, 465–478. https://doi.org/10.1002/jqs.3189

Urick, R.J., 1983. Principles of Underwater Sound, 3rd ed. McGraw-Hill, New York.

Van Dijk, T.A.G.P., Kleinhans, M.G., 2005. Processes controlling the dynamics of compound sand waves in the North Sea, Netherlands. J. Geophys. Res. 110, 2004JF000173. https://doi.org/10.1029/2004JF000173

Van Landeghem, K.J.J., Baas, J.H., Mitchell, N.C., Wilcockson, D., Wheeler, A.J., 2012. Reversed sediment wave migration in the Irish Sea, NW Europe: A reappraisal of the validity of geometry-based predictive modelling and assumptions. Marine Geology 295–298, 95–112. https://doi.org/10.1016/j.margeo.2011.12.004

Venterra, 2025. SC-DMAP METOCEAN STUDY.

W. C. Krumbein, 1938. Size Frequency Distributions of Sediments and the Normal Phi Curve. SEPM JSR Vol. 8. https://doi.org/10.1306/D4269008-2B26-11D7-8648000102C1865D

Walbridge, S., Slocum, N., Pobuda, M., Wright, D., 2018. Unified Geomorphological Analysis Workflows with Benthic Terrain Modeler. Geosciences 8, 94. https://doi.org/10.3390/geosciences8030094

Walsh, K., Holloway, P., Lim, A., 2024. Optimising Submarine Cable Routes from Offshore Wind Farms. https://doi.org/10.2139/ssrn.5015435

Weber, T.C., Rice, G., Smith, M., 2018. Toward a standard line for use in multibeam echo sounder calibration. Mar Geophys Res 39, 75–87. https://doi.org/10.1007/s11001-017-9334-3

Wei, W., Malekjafarian, A., Salauddin, M., 2024. Scour Protection Measures for Offshore Wind Turbines: A Systematic Literature Review on Recent Developments. Energies 17, 1068. https://doi.org/10.3390/en17051068

Weiss, A.D., 2000. Topographic Position and Landforms Analysis, in: In Proceedings of the Esri User Conference. Presented at the Esri User Conference, San Diego, CA, USA, p. 1.

Wheeler, A.J., Kozachenko, M., Beyer, A., Foubert, A., Huvenne, V.A.I., Klages, M., Masson, D.G., Olu-Le Roy, K., Thiede, J., 2005. Sedimentary processes and carbonate mounds in the Belgica Mound province, Porcupine Seabight, NE Atlantic, in: Freiwald, A., Roberts, J.M. (Eds.), Cold-Water Corals and Ecosystems. Springer Berlin Heidelberg, Berlin, Heidelberg, pp. 571–603. https://doi.org/10.1007/3-540-27673-4_28

Whitehouse, R.J.S., Damgaard, J.S., Langhorne, D.N., 2000. Sand waves and seabed engineering: application to submarine cables, in: Trentesaux, A., Garlan, T (Eds.), . Presented at the Marine Sandwave Dynamics, International Workshop, March 23-24 2000, University of Lille 1, France. Proceedings, pp. 228–234.

Whitehouse, R.J.S., Damgaard, J.S., Langhorne, D.N., n.d. Sandwaves and seabed engineering; the application to submarine cables.

Whitehouse, R.J.S., Harris, J.M., Sutherland, J., Rees, J., 2011. The nature of scour development and scour protection at offshore windfarm foundations. Marine Pollution Bulletin 62, 73–88. https://doi.org/10.1016/j.marpolbul.2010.09.007

Wilson, M.F.J., O'Connell, B., Brown, C., Guinan, J.C., Grehan, A.J., 2007. Multiscale Terrain Analysis of Multibeam Bathymetry Data for Habitat Mapping on the Continental Slope. Marine Geodesy 30, 3–35. https://doi.org/10.1080/01490410701295962

Wölfl, A.-C., Snaith, H., Amirebrahimi, S., Devey, C.W., Dorschel, B., Ferrini, V., Huvenne, V.A.I., Jakobsson, M., Jencks, J., Johnston, G., Lamarche, G., Mayer, L., Millar, D., Pedersen, T.H., Picard, K., Reitz, A., Schmitt, T., Visbeck, M., Weatherall, P., Wigley, R., 2019. Seafloor Mapping – The Challenge of a Truly Global Ocean Bathymetry. Front. Mar. Sci. 6, 283. https://doi.org/10.3389/fmars.2019.00283

Yang, Y., Liu, M., Xu, J., Xu, W., 2022. Migrating sandwaves riding on relict dunes of Taiwan shoal, northern South China Sea. Front. Earth Sci. 10. https://doi.org/10.3389/feart.2022.975220

Zimmer, M.A., Bibee, L.D., Richardson, M.D., 2010. Measurement of the frequency dependence of the sound speed and attenuation of seafloor sands from 1 to 400 kHz. IEEE J. Oceanic Eng. 35, 538–557. https://doi.org/10.1109/JOE.2010.2056230

Appendices

Appendix A: Supplementary Materials

Appendix B: Courses Completed

Appendix C: Publications

Appendix D: Research Cruises/Fieldwork

Appendix E: Conference Presentations

Appendix F: Teaching

Appendix A: Supplementary Materials

Chapter 2. Enhanced Angular Range Analysis: A Novel Object-based Image Analysis Approach for Seafloor Characterisation

Table A. 1. Descriptions of data available in particle size analysis (PSA) sediment samples attributes table including field and description.

Field	Description
FID	Feature identification (assigned to each point)
Shape *	Point
Date	Date of acquisition
Lat	y-coordinate
Long	x-coordinate
Instrument	Sediment sampling instrument
Sample_ID	Name assigned to the sample
Folk	Substrate material based on Folk classification
MEAN	Sediment type
SORTING	Sorting of sediments
MODE_1	Mode grain size
MODE_2	Mode grain size
MODE_3	Mode grain size
D10	10^{th} percentile
D50	Median grain size
D90	90^{th} percentile
GRAVEL	Gravel (%)
SAND	Sand (%)
MUD	Mud (%)
VC_GRAVEL	Very coarse gravel (%)
C_GRAVEL	Coarse gravel (%)
MED_GRAVEL	Medium gravel (%)
F_GRAVEL	Fine gravel (%)
VF_GRAVEL	Very fine gravel (%)

VC_SAND	Very coarse gravel (%)
C_SAND	Coarse sand (%)
MED_SAND	Medium sand (%)
F_SAND	Fine sand (%)
VF_SAND	Very fine sand (%)
VC_SILT	Very coarse silt (%)
C_SILT	Coarse silt (%)
MED_SILT	Medium silt (%)
F_SILT	Fine silt (%)
VF_SILT	Very fine silt (%)
CLAY	Clay (%)

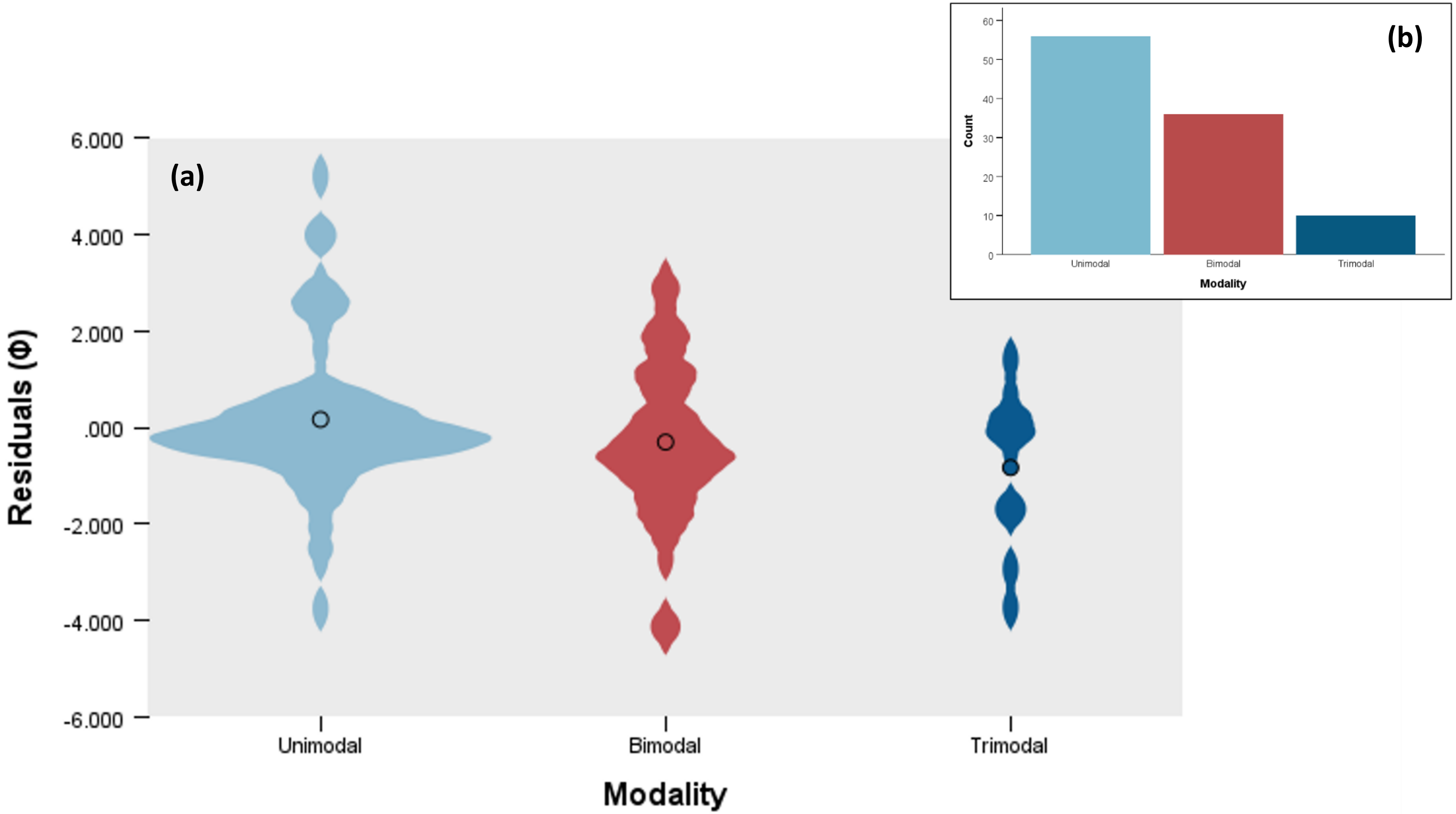

Figure A. 1. (a) Violin plots displaying the distribution of residuals based on modality; and (b) bar charts showing the distribution of samples based on modality.

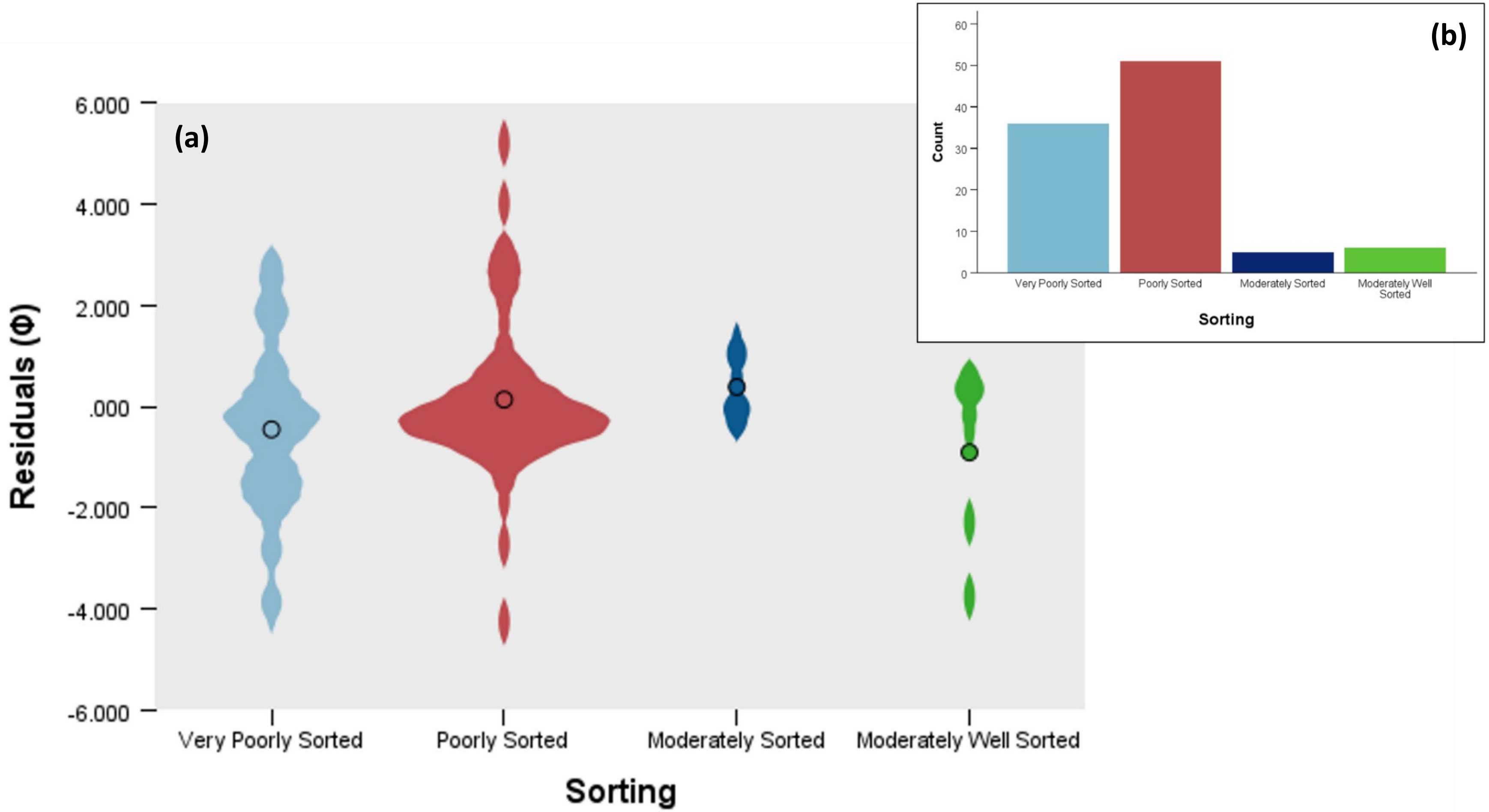

Figure A. 2. (a) Violin plots displaying the distribution of residuals based on sorting; and (b) bar charts showing the distribution of samples based on sorting.

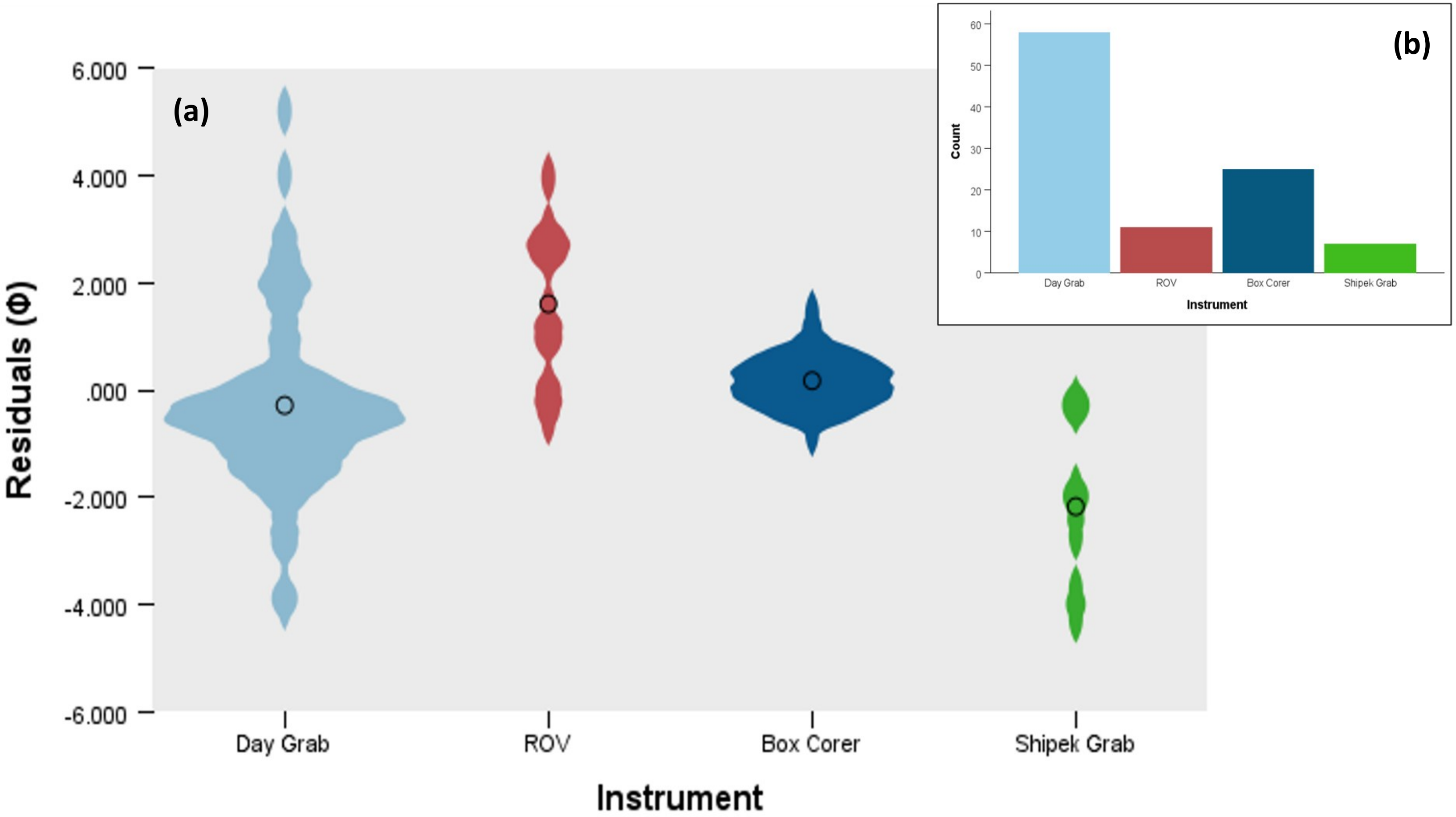

Figure A. 3. (a) Violin plots displaying the distribution of residuals based on instrument; and (b) bar charts showing the distribution of samples based on instrument.

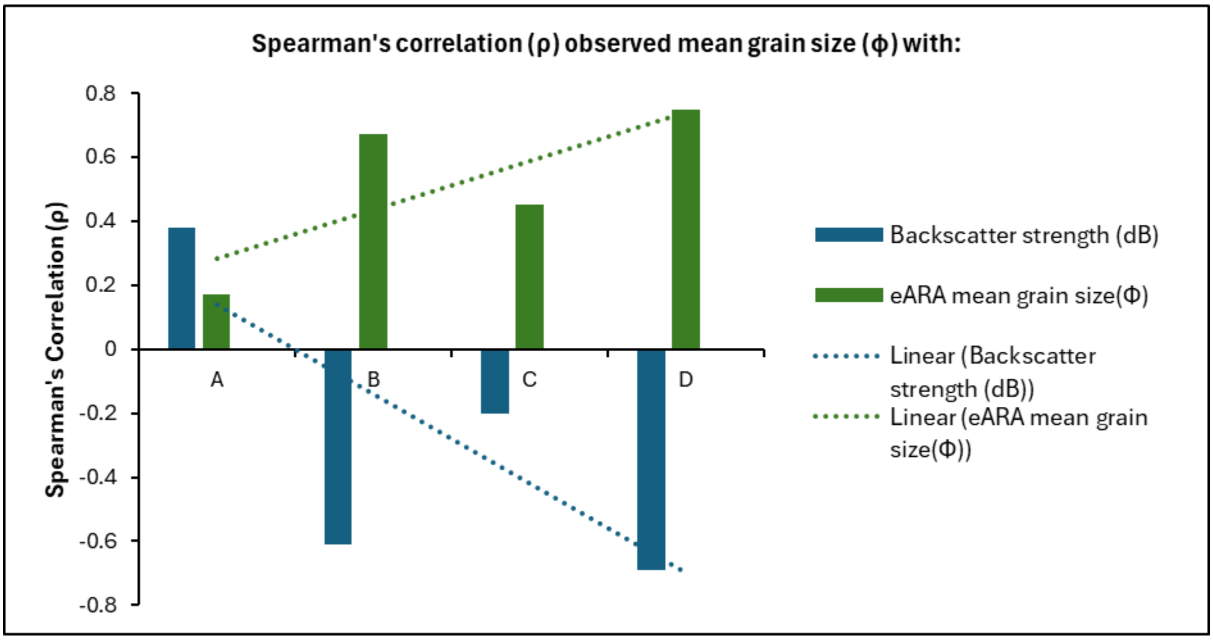

Figure A. 4. Spearman's Rank correlation between: eARA mean grain size (Φ) and observed mean grain size (Φ); and backscatter strength (dB) and observed mean grain size (Φ).

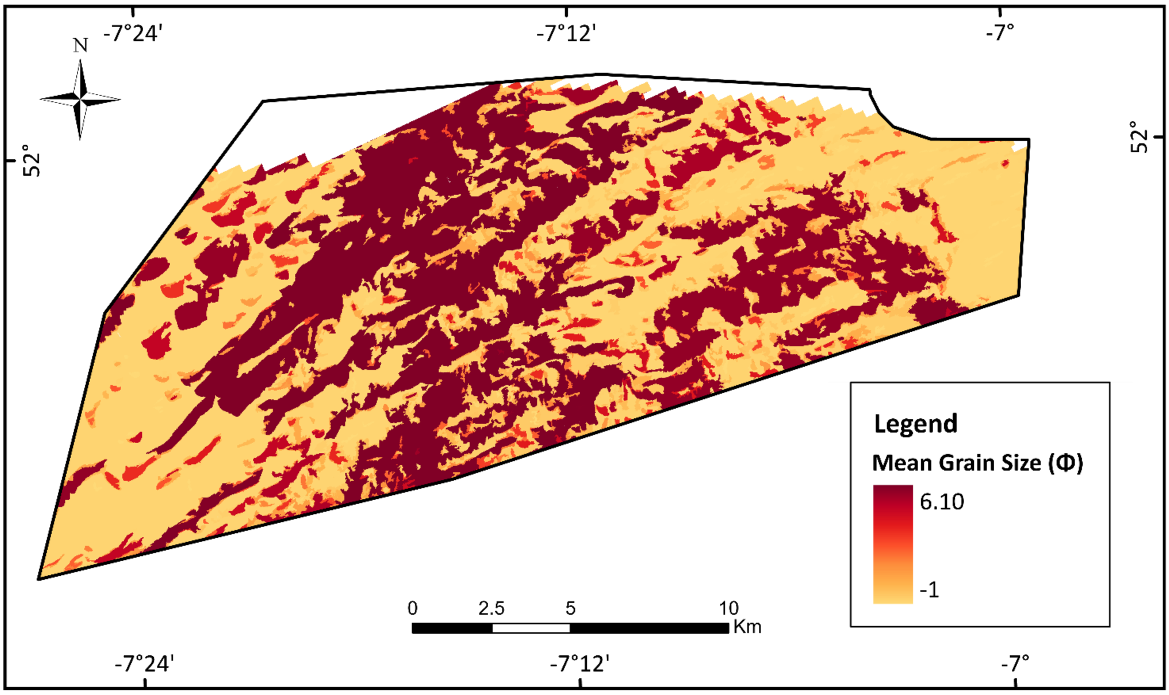

Figure A. 5. Spatial distribution of sediments in terms of mean grain size (Φ), based on the CV13_01 dataset.

Table A. 2. Legacy current meter dataset information.

Reference Number	Instrument Type	Instrument Mounting	Latitude	Longitude	Source
23521	Aanderaa RCM 4/5 Recording Current Meter	fixed benthic node	51.75500 N (51° 45.3' N)	6.63000 W (6° 37.8' W)	National Oceanography Centre https://www.bodc.ac.uk/data/documents/series/23521/

Appendix B: Courses Completed

2023

GG6540: Applied Seafloor Mapping (2023/2024), University College Cork (Grade: 80%)

Offshore Security Awareness Training (2023), Secure West (Grade: Pass)

Appendix C: Publications

Brennan, C., Summers, G., de Oliveira, L.M.C. and Lim, A. (2025) Enhanced angular range analysis: a novel object-based image analysis approach for seafloor characterisation. *Mar Geophys Res* 46, 12. https://doi.org/10.1007/s11001-025-09574-7

Brennan, C., Summers, G., de Oliveira, L.M.C. and Lim, A. *Seabed Dynamics and Geological Constraint Mapping for Offshore Renewable Energy: Insights from Tonn Nua, North Celtic Sea, NE Atlantic* (Under Review Applied Ocean Research).

Lim, A., Macedo Cruz de Oliveira, L., Boolukos, C., Strachan, R., Bush, D., Summers, G., Kevin, W., Brennan, C., Luca, C., Loriga, I., Bonnie, Y., & Julian, O. M. (2025). CE25006 – ROV Monitoring Survey (Version 1). Zenodo. https://doi.org/10.5281/zenodo.17036804

Appendix D: Research Cruises/Fieldwork

2025

ROV Monitoring Survey, Celtic Sea and North Atlantic Ocean aboard RV Celtic Explorer (May 2025)

SEAMANS_Carbon Fieldwork, Turnaffe Atoll, Belize (January 2025)

2024

SMART Sea School Offshore Training, Cork Habour (February 2024)

2023

QUEST CE23_016 Survey, Irish Sea aboard aboard RV Celtic Explorer (September/October 2023)

Appendix E: Conference Presentations

2025

"Enhanced Angular Range Analysis: A Novel Object-based Image Analysis Approach for Seafloor Characterisation" at the Geohab 2025 Conference, Florida Keys, USA (Oral Presentation)

"Enhanced Angular Range Analysis: A Novel Object-based Image Analysis Approach for Seafloor Characterisation" at the Geomorphology Association of Ireland's Annual Workshop 2025, Dublin City University, Dublin (Oral Presentation)

"Enhanced Angular Range Analysis: A Novel Object-based Image Analysis Approach for Seafloor Characterisation" at Irish Geological Research Meeting (IGRM) 2025 Conference, Trinity University, Dublin (Poster Presentation)

2024

"An Enhanced ARA workflow for wider industrial impact and uptake of INFOMAR data" at Geoscience 2024 Conference, Dublin Castle (Poster Presentation)

"An Enhanced ARA workflow for wider industrial impact and uptake of INFOMAR data" at Irish Geological Research Meeting (IGRM) 2024 Conference, University of Galway (Oral Presentation)

2023

"An Enhanced ARA workflow for wider industrial impact and uptake of INFOMAR data" at the Geoscience 2023 Conference, Dublin Castle (Poster Presentation)

Appendix F: Teaching

2025: GS2003 Paleo-Environments/ Coastal Processes – Field day demonstrator

2024: GG1015 Geographies in Action - Tutor

2023: GG1015 Geographies in Action - Tutor